Queuosine modification of tRNA-Tyrosine elicits translational reprogramming and enhances growth of *Vibrio cholerae* with aminoglycosides.

Louna Fruchard [1,2,#], Anamaria Babosan [1,#], Andre Carvalho [1], Manon Lang [1,2], Blaise Li [3], Magalie Duchateau [4], Quentin Giai-Gianetto [4,5], Mariette Matondo [4], Frédéric Bonhomme [6], Céline Fabret [7], Olivier Namy [7], Valérie de Crécy-Lagard [8,9], Didier Mazel [1,*], Zeynep Baharoglu [1,*].

# equal contribution
*Corresponding authors: baharogl@pasteur.fr, mazel@pasteur.fr

1. Institut Pasteur, Université de Paris Cité, Unité Plasticité du Génome Bactérien, UMR3525, CNRS, 75015, Paris, France
2. Sorbonne Université, Collège Doctoral, F-75005, Paris, France
3. Institut Pasteur, Université Paris Cité, Bioinformatics and Biostatistics Hub, F-75015 Paris, France
4. Institut Pasteur, Université de Paris, Proteomics Platform, Mass Spectrometry for Biology Unit, UAR2024, CNRS 2000, Paris, France.
5. Institut Pasteur, Université de Paris, Department of Computation Biology, Bioinformatics and Biostatistics Hub, Paris, France.
6. Institut Pasteur, Université Paris cité, Epigenetic Chemical Biology Unit, UMR 3523, CNRS, 75015, Paris, France
7. Université Paris-Saclay, CEA, CNRS, Institute for Integrative Biology of the Cell (I2BC), F-91198, Gif-sur-Yvette, France
8. Department of Microbiology and Cell Science, University of Florida, Gainesville, Florida 32611, United States.
9. University of Florida Genetics Institute, Florida 32611, United States

Abstract

Tgt is the enzyme modifying the guanine (G) in tRNAs with GUN anti-codon to queuosine (Q). *tgt* is required for optimal growth of *Vibrio cholerae* in the presence of sub-lethal aminoglycoside concentrations. We further explored here the role of the Q in the efficiency of codon decoding upon tobramycin exposure. We characterized its impact on the overall bacterial proteome, and elucidated the molecular mechanisms underlying the effects of Q modification in antibiotic translational stress response. Using molecular reporters, we showed that Q impacts the efficiency of decoding at tyrosine TAT and TAC codons. Proteomics analyses revealed that the anti-SoxR factor RsxA is better translated in the absence of *tgt*. RsxA displays a codon bias towards tyrosine TAT and its overabundance leads to decreased expression of genes belonging to SoxR oxidative stress regulon. We also identified conditions that regulate *tgt* expression. We propose that regulation of Q modification in response to environmental cues leads to translational reprogramming of genes bearing a biased tyrosine codon usage. *In silico* analysis further identified candidate genes possibly subject to such translational regulation, among which DNA repair factors. Such transcripts, fitting the definition of modification tunable transcripts, are plausibly central in the bacterial response to antibiotics.

1

Introduction

Antimicrobial resistance is an increasingly serious threat to global public health. Our recent finding that many tRNA modification genes are involved in the response to antibiotics from different families (1) led to further investigate the links between environmental factors (e.g. traces of antibiotics), tRNA modifications and bacterial survival to antibiotics.

The regulatory roles of RNA modifications was first proposed for eukaryotes(2) and their importance in human diseases has recently emerged(3,4). In bacteria, while some tRNA modifications are essential(5), the absence of many shows no growth phenotype in unstressed cells(6). At the molecular level, the roles of tRNA modifications in differential codon decoding have been described in various species(7-10). At the phenotypic level, no growth phenotype was associated with these variations in decoding in bacteria in most cases. Recent studies, however, do highlight the links between tRNA modifications and stress responses in several bacterial species(6,11-17), and new modifications are still being discovered(18). Until recently, few tRNA modification factors have been clearly linked with resistance and persistence to antibiotics, via differential codon decoding in cell membrane and efflux proteins (TrmD(19), MiaA(8)). A link between stress and adaptation was described to occur via the existence of modification tunable transcripts, or MoTTs.

MoTTs were first (and mostly) defined in eukaryotes as transcripts that will be translated more or less efficiently depending on the presence or absence of tRNA modifications(20), namely upon stress(21). In bacteria, links between tRNA modifications and the response to several stresses, are highlighted by studies focusing on the following MoTT/codon and tRNA modification couples (reviewed in(6)): differential translation of RpoS/leucine codons via MiaA (*E. coli*)(12); Fur/serine codons via MiaB, in response to low iron (*E. coli*)(13); MgtA/proline codons via TrmD, in response to low magnesium(14); catalases/phenylalanine and aspartate codons via TrmB, during oxidative stress (*P. aeruginosa*)(11). Mycobacterial response to hypoxic stress(15) also features MoTTs. In this latter study, specific stress response genes were identified *in silico,* through their codon usage bias, and then experimentally confirmed for their differential translation. tRNA modification-dependent translational reprogramming in response to antibiotic stress has not been the focus of a study so far in bacteria.

During studies in *V. cholerae*, we recently discovered that t/rRNA modifications play a central role in response to stress caused by antibiotics with very different modes of action (1), not through resistance development, but by modulating tolerance. The identified RNA modification genes had not previously been associated with any antibiotic resistance phenotype. The fact that different tRNA modifications have opposite effects on tolerance to different antibiotics highlights the complexity of such a network, and shows that the observed phenotypes are not merely due to a general mistranslation effect. Since tRNA modifications affect codon decoding and accuracy, it is important to address how differential translation can generate proteome diversity, and eventually adaptation to antibiotics.

In particular, deletion of the *tgt* gene encoding tRNA-guanine transglycosylase (Tgt) in *V. cholerae* confers a strong growth defect in the presence of aminoglycosides at doses below the minimal inhibitory concentration (sub-MIC)(1). Tgt incorporates queuosine (Q) in the place of guanosine (G) in the wobble position of four tRNAs with G*UN anticodon (tRNA-Asp GUC, tRNA-Asn GUU, tRNA-Tyr GUA, tRNA-His GUG)(22). Each one of these four tRNAs decodes two synonymous codons (aspartate GAC/GAT, asparagine AAC/AAT, tyrosine TAC/TAT, histidine CAC/CAT) which differ in the third position. Q is known to increase or decrease translation error rates in eukaryotes in a codon and organism specific manner(22,23). Q was shown to induce mild oxidative stress resistance in the eukaryotic parasite *Entamoeba histolytica*, the causative agent of amebic dysentery, and to attenuate its virulence(24). In *E. coli*, the absence of Q modification was found to decrease mistranslation rates by tRNA-Tyr, while increasing it for tRNA-Asp(25,26). No significant biological difference was found in *E. coli Δtgt* mutant, except for a slight defect in stationary phase viability(27). Recent studies show that the *E. coli tgt* mutant is more sensitive to aminoglycosides but not to ampicillin nor spectinomycin and is more sensitive to oxidative stress but the molecular mechanisms were not elucidated(28).

We asked here, how queuosine (Q) modification by Tgt modulates the response to sub-MIC aminoglycosides. We find that *V. cholerae Δtgt* displays differential decoding of tyrosine TAC/TAT.

Molecular reporters, coupled to proteomics and *in silico* analysis reveal that several proteins with codon usage biased towards TAT (versus TAC) are more efficiently translated in Δ*tgt*. One of these proteins is RsxA, which prevents activation of SoxR oxidative stress response regulon. We propose that sub-MIC TOB treatment leads to increased expression of *tgt* and Q modification, which in turn allows for more efficient Sox regulon related oxidative stress response, and better response to sub-MIC TOB. Lastly, bioinformatic analysis identified DNA repair gene transcripts with TAT codon bias as transcripts modulated by Q modification, which was confirmed by decreased UV susceptibility of *V. cholerae* Δ*tgt*.

Results

Tobramycin tolerance is decreased in *Δtgt* without any difference in uptake.

We confirmed *V. cholerae Δtgt* strain's growth defect in sub-MIC tobramycin (TOB) (**Fig. 1A**) and that expression of *tgt* in trans restores growth in these conditions (**Fig. 1B**). We further tested tolerance to lethal antibiotic concentrations by measuring survival after antibiotic treatment during 15 minutes to 4 hours. As expected, *Δtgt* is less tolerant than WT to TOB (**Fig. 1CD**), but had no impact in ciprofloxacin (CIP) or carbenicillin (CRB) (**Fig. 1EF**). We asked whether the growth defect of *Δtgt* is due to increased aminoglycoside entry and/or a change in proton-motive force (PMF) (29,30). We used a *ΔtolA* strain as a positive control for disruption of outer membrane integrity and aminoglycoside uptake(31). No changes either in PMF (**Fig. 1G**), nor in uptake of the fluorescent aminoglycoside molecule Neo-cy5 (**Fig. 1H**)(32) were detected in the in *Δtgt* strain, indicating that the increased susceptibility of *Δtgt* to TOB is not due to increased aminoglycoside entry into the *V. cholerae* cell.

Q modification influences stop codon readthrough in *V. cholerae.*

To test whether a defect in Q modification influences the fidelity of translation in the presence and absence of sub-MIC TOB, previously developed reporter tools were used(33), to measure stop codons readthrough and ribosomal frameshifting in *V. cholerae Δtgt* and wild-type strains. The system consists of vectors containing readthrough or frameshift-promoting signals inserted between the *lacZ* and *luc* sequences, encoding β-galactosidase and luciferase, respectively. Luciferase activity reflects the readthrough or frameshifting efficiency, while β-galactosidase activity serves as an internal control of expression level, integrating a number of possible sources of variability (plasmid copy number, transcriptional activity, mRNA stability, and translation rate).

While no significant difference was observed in translational frameshifting (**Sup. fig. S1A**), we found increased readthrough at stop codons TAA and to a lesser extent at TAG for *Δtgt*, and this increase was amplified for TAG in presence of sub-MIC TOB (**Fig. 2A**). In the case of TAA, TOB appears to decrease readthrough, this may be artefactual, due to the toxic effect of TOB on *Δtgt.* A similar profile was obtained for TAA readthrough in *E. coli* (**Ext. fig. S1B**), although the differences were smaller than in *V. cholerae*. This supports the fact that tRNA Q modification is involved in translation fidelity during antibiotic stress.

Q modification influences amino-acid incorporation at tyrosine codons.

We next asked whether all four tRNAs modified by Tgt are equally important for the TOB sensitivity phenotype of the *Δtgt* mutant: Aspartate (Asp)/Asparagine (Asn)/Tyrosine (Tyr)/Histidine (His). We set out to measure the efficiency of amino-acid incorporation at corresponding codons in *Δtgt*. To do so, after having confirmed that Gfp fluorescence is not affected in *Δtgt* compared to WT (*gfpmut3* in **Fig. 2B to H**), we constructed *gfp* fluorescent reporters carrying within their coding sequence, stretches of repeated identical codons, for Asp/Asn/Tyr/His codons. This set of reporters revealed that the absence of Q leads to an increase of amino-acid incorporation at Tyr TAT codons (**Fig. 2B**), highlighting the importance of Q in decoding of Tyr codons but not Asp, His or Asn. No significant effect of *tgt* was observed for near-cognate codons obtained by changing 1 base of the triplet for TAC and TAT codons: 1st near cognate Asp GAC/GAT, His CAC/CAT, Asn AAC/AAT codons, and 2nd near-cognate Phe TTC/TTT, Cys TGT/TGC, Ser TCT/TCC (the 3rd near-cognate stop codons TAA and TAG were not tested in this setup).

In parallel, we adopted a tRNA overexpression strategy from a high copy plasmid. We cloned and constitutively expressed tRNAs decoding Tyr/Asp/His/Asn, for which the GUN anticodon is hypermodified to QUN by Tgt. The following tRNAs-$_{GUN}$ are the canonical tRNAs which are present in the genome: Tyr$_{GUA}$ (codon TAC), His$_{GUG}$ (codon CAC), Asn$_{GUU}$ (codon AAC), Asp$_{GUC}$ (codon GAT). The following tRNAs-$_{AUN}$ are synthetic tRNAs which are not present in the genome: Tyr$_{AUA}$, His$_{AUG}$, Asn$_{AUU}$, Asp$_{AUC}$. tRNA$^{Phe}_{GAA}$ was also used as non Tgt-modified control (**Sup. Fig. S2ABC**). Overexpression of tRNA$^{Tyr}_{GUA}$, but not tRNA$^{Tyr}_{AUA}$ rescues the *Δtgt* mutant's growth defect in sub-MIC TOB. We do not observe any major rescue of TOB sensitive phenotypes when the other tRNAs are overexpressed suggesting changes in Tyr codon decoding may mostly be responsible for the *Δtgt* mutant's TOB-susceptibility phenotype.

The absence of Q could have direct effects at the level of codon decoding but also indirect effects such as influencing tRNAs' degradation(34). qRT-PCR analysis of tRNA^{Tyr} levels showed no major differences between WT and *Δtgt* strains, making it unlikely that the effect of Q modification on codon decoding is caused by altered synthesis or degradation of tRNA^{Tyr} (**Sup. Fig. S2DEF**). The levels of the other three tRNAs modified by Tgt also remained unchanged (**Sup. Fig. S2DEF**). These results do not however exclude a more subtle or heterogeneous effect of Q modification on tRNA levels, which would be below the detection limits of the technique in a bacterial whole population.

In specific cases, the levels of a given tRNA modification can depend on the presence of other ones(35). One example is the m^{5}C38 modification of tRNA^{Asp} which is favored by the presence of Q in eukaryotes(22,36). However, bacterial tRNAs do not harbor m^{5}C and we confirmed this in *V. cholerae* tRNAs (unpublished data). In *E. coli*, tRNA^{Tyr} is modified by RluF which introduces a pseudouridine (Ψ) at position 35 of the anticodon, next to the G/Q at position 34 (37) . We tested whether the presence or absence of this second modification has an impact on Q-dependent fitness phenotypes. We constructed a simple *ΔrluF* and a double *ΔrluF Δtgt* mutant. Competition experiments showed no effect of the *rluF* deletion in any condition (**Sup. Fig. S3**), showing that the effect of *tgt* is not indirectly due to an effect of a Ψ modification possibly made by RluF in *V. cholerae*.

The absence of Q decreases misincorporation at Tyr TAT

We developed β-lactamase reporter tools to assess errors at sense codons using carbenicillin resistance/tolerance as a readout (**Fig. 3A**). The amino acids Tyr103 and Asp129 of the β-lactamase, were previously shown to be important for its function(38-40). We replaced the codons for either Tyr103 or Asp129 with a near-cognate codon. The expression of the resulting mutant β-lactamase is expected to yield a carbenicillin sensitive phenotype. In this system, increased amino-acid misincorporation (more mistakes) by tRNA^{Tyr} or tRNA^{Asp} which incorporate Tyr or Asp at the mutated codon leads to increased synthesis of active β-lactamase, which can be evaluated by carbenicillin tolerance tests. As such, amino-acid misincorporation leads here to phenotypic (transient) tolerance, while genetic reversion mutations result in resistance (growth on carbenicillin). The rationale is summarized in **Sup. Fig. S4AB**.

We first validated this tool by replacing the Tyr103-TAC codon with stop codons (**Sup. Fig. S4D: TAA/TGA/TAG**). Consistent with the readthrough reporter results, tolerance was increased in *Δtgt* compared to WT when Tyr codon was replaced with the stop codon TAA. This suggests an increased stop codon readthrough by tRNA^{Tyr} at TAA.

Next, to test decoding of sense codons in *Δtgt* (**Fig. 3A**), we replaced Tyr103 or Asp129 by the corresponding near-cognate codons (**Sup. Fig. S4DE**). For example, for Tyr-TAC, the tested near-cognate codon mutants were Asn-<u>A</u>AC, His-<u>C</u>AC and Asp-<u>G</u>AC at the first position; Phe-T<u>T</u>C, Cys-T<u>G</u>C and Ser-T<u>C</u>C for the middle position; and Tyr-TA<u>T</u>, stop-TA<u>G</u> and stop-TA<u>A</u> for the wobble. We similarly determined all the near-cognate codons at the first, middle and wobble base of the codon for Tyr-TAT, Asp-GAT and Asp-GAC, and we tested misincorporation of Asp and Tyr*,* at 12 different missense codons, as indicated in **Sup. Fig. S4DE**.

When the Asp129 codon was mutated to Tyr-TAT (**Fig. 3B**), we observe reduced tolerance in *Δtgt,* but not when it was mutated to Tyr-TAC, suggesting either less mistakes by tRNA-Tyr at Tyr TAT (tRNA^{Tyr} better incorporates tyrosine at TAT), or less misincorporation of aspartate by tRNA^{Asp} at the

4

Tyr TAT codon in the absence of Q. Conversely, we observed increased tolerance when Asp129 was mutated to both His codons (**Sup. Fig. S4E**), pointing to misdecoding of His codons by tRNA-Asp in the absence of Q. We did not observe major differences between WT and *Δtgt* when the Asp129 codon was replaced with both versions of valine, glycine, alanine codons. For unknown reasons, the results for glutamate codons were variable (**Sup. Fig. S4E**).

When the Tyr103 codon was replaced with both Asp codons, we observe increased β-lactamase tolerance (**Fig. 3B**), suggesting either decreased efficiency of decoding by tRNA^{Asp} at Asp codons, or increased misincorporation of tyrosine by tRNA^{Tyr} at Asp codons, (or both), in the absence of Q. These observations are consistent with previous studies in *E. coli* showing that absence of Q increases errors by tRNA^{Asp} and decreased errors by tRNA^{Tyr} (25).

Although tolerance tests were systematically performed by spotting carbenicillin treated cultures in parallel on plates without carbenicillin (to quantify survival of carbenicillin sensitive populations), and plates with carbenicillin (to differentiate between tolerance and resistance), we further quantified for each β-lactamase mutant, the frequency of appearance of colonies growing on plates containing carbenicillin (**Sup. Fig. S5 A to G and O to S**). For each mutant, we sequenced the *bla* gene on colonies growing on carbenicillin, in order to determine whether the carbenicillin resistance was due to reversion mutations (**Sup. Fig. S5H to N and T to X**). Note that *Δtgt* does not generally show any particular mutator phenotype compared to WT, as indicated by its low spontaneous rifampicin resistant mutant frequency (**Sup. Fig. S5Y**). Globally, reversion mutation frequencies were similar between WT and *Δtgt* and mostly at low levels for carbenicillin sensitive populations. Thus, we propose that our observations shown in Fig. 3 for increase or decrease of tolerance reflect differences in decoding during translation in *Δtgt.*

Finally, in addition to codon replacements with stop or sense codons, we also replaced the native Tyr103 TAC with the synonymous codon Tyr103 TAT (**Fig. 3CDEF**). While in the WT, both versions of β-lactamase conferred similar growth in carbenicillin with or without sub-MIC TOB, in the *Δtgt* strain the Tyr-TAT version grows better than the Tyr-TAC version upon exposure to TOB stress.

When we replaced the native Asp129 GAT with the synonymous codon Asp129 GAC, the GAC version did not appear to produce functional β-lactamase in *Δtgt* (**Sup. Fig. S4C**), suggesting increased mistranslation or inefficient decoding of the GAC codon by tRNA-Asp in the absence of Q. Decoding of GAT codon was affected in *Δtgt* in the presence of sub-MIC TOB.

Altogether, β-lactamase reporter results suggest that in the presence of sub-MIC TOB stress, the absence of Q namely leads to better translation of the TAT vs TAC codon, leading to differential translation of proteins with biases towards TAC or TAT codons.

Proteomics study identifies RsxA, among factors for which translation is most impacted in *Δtgt*

These observations show a link between Q modification of tRNA, differential decoding of Tyr codons (among others) and susceptibility to aminoglycosides. We hypothesized that proteins that are differentially translated according to their Tyr codon usage could be involved in the decreased efficiency of the response to aminoglycoside stress in *Δtgt.* We conducted a proteomics study comparing WT vs. *Δtgt,* in the absence and presence of sub-MIC TOB (proteomics T**able S1 and Fig. 4**). Loss of Q results in generally decreased detection of many proteins in TOB (shift towards the left in the volcano plot **Fig. 4A**), and in increases in the levels of 96 proteins. Among those, RsxA (encoded by VC1017) is 13x more abundant in the *Δtgt* strain compared to WT in TOB. RsxA is part of an anti-SoxR complex. SoxR is an oxidative stress response regulator(41) that controls, *sodA* (VC2694, superoxide dismutase) and *acrA* (VC0913, efflux) among other genes of regulon. The Rsx complex reduces and inactivates SoxR, preventing the induction of the regulon. Consistently, we find that the levels of SodA and AcrA proteins are decreased in *Δtgt* compared to WT in TOB (indicated in blue in **Fig. 4A**).

With 83% of Tyr-TAT codons, instead of the expected 53% average, RsxA (**indicated by a red arrow in Fig. 4B**) has a clear codon usage bias. To test if some of the differentially abundant protein groups in the Q deficient mutant show similar biases, the Tyr codon usage was calculated for the 96 more and 195 less abundant proteins expressed in TOB. A slight increase in Tyr TAT codons was observed in both sets of proteins (**Fig. 4B**), however this difference was not statistically significant (statistical analysis

not shown). More abundant proteins in *Δtgt* TOB with a codon usage bias towards TAT vs TAC are represented as light blue dots in **Fig. 4A**. As a slight increase in TAT-bias is seen in the proteins that are more abundant in WT compared to *Δtgt* in TOB, one cannot draw conclusions or infer predictions about codon decoding efficiencies in a tRNA modification mutant such as *Δtgt* from the proteomics data alone. In addition to mistranslation and codon decoding, other factors also influence detected protein levels, such as transcription, degradation, etc. Moreover, the localization and sequence context of the codons for which the efficiency of translation is impacted, may be important. Nevertheless, as translation of proteins with a codon usage bias towards TAC or TAT may be impacted in *Δtgt*, and as the most abundant protein in *Δtgt* in TOB, RsxA, shows a strong TAT bias, we decided to evaluate whether RsxA is post-transcriptionally regulated by the Q modification and whether it may affect fitness in the presence of TOB.

RsxA is post-transcriptionally upregulated in *Δtgt* due to more efficient decoding of tyrosine TAT codons in the absence of Q modification

Transcriptomic analysis comparing at least 2-fold differentially expressed genes between *V. cholerae Δtgt* and WT strain (**Table S2**) showed that, respectively, 53 and 26 genes were significantly downregulated in MH and sub-MIC TOB, and 34 were up in sub-MIC TOB. Gene ontology (GO) enrichment analysis showed that the most impacted GO categories were bacteriocin transport and iron import into the cell (45- and 40-fold enriched) in MH, and proteolysis and response to heat (38- and 15-fold enriched) in TOB. In both conditions, the levels of *rsxA* transcript remained unchanged.

RsxA carries 9 tyrosine codons among which the first 8 are TAT and the last one is TAC. RsxA is 13x more abundant in *Δtgt* than WT, but transcript levels measured by digital RT-PCR are comparable in both strains **(Fig. 4C)**. We constructed transcriptional and translational *gfp* fusions in order to evaluate the expression of *rsxA* in WT and *Δtgt* strains. As expected from digital RT-PCR results, no significant differences in fluorescence were observed for the transcriptional fusion of the *rsxA* promoter with *gfp* (**Fig. 4D**). For translational fusions, we used either the native *rsxA* sequence bearing 8 TAT + 1 TAC codons, or a mutant *rsxA* allele carrying all 9 TAC codons (hereafter called respectively RsxA^{TAT} and RsxA^{TAC}). Confirming the proteomics results, the RsxA^{TAT}-GFP fusion was more fluorescent in the *Δtgt* mutant, but not the RsxA^{TAC}-GFP one (**Fig. 4E** and detailed flow cytometry data in **Sup. Fig. S6ABD**). Since increased *rsxA* expression appeared to be somewhat toxic for growth, and in order to test translation on a reporter which confers no growth defect, we chose to test directly the translation of *gfp*, which originally carries 4 TAT (36%) and 7 TAC (64%) codons in its native sequence. We constructed two synonymous versions of the GFP protein, with all 11 tyrosine codons either changed to TAT or to TAC. Like what we observed with *rsxA*, the GFP^{TAT} version, but not the GFP^{TAC} one, generated more fluorescence in the *Δtgt* background, (**Fig. 4E** and detailed flow cytometry data in **Sup. Fig. S6CDE**).

Since not all TAT biased proteins are found to be enriched in *Δtgt* proteomics data, we asked whether the sequence context surrounding TAT codons could affect their decoding. Following the same principle as 6x-codon stretches in *gfp*, we inserted after its ATG codon, various sequences displayed by *rsxA*. We used either the native TAT or the TAC replacement while keeping the remaining sequence unchanged. As expected, the *gfp* carrying the TEY^{TAT}LLL sequence is more fluorescent in *Δtgt* compared to WT, while TEY^{TAC}LLL is not affected (**Sup. Fig. S6F)**. Surprisingly, the sequences LY^{TAT}RLL/ LY^{TAC}RLL and EY^{TAT}LR/ EY^{TAC}LR were unaffected (or even decreased for the latter) by the absence of *tgt*. Overall, these results demonstrate that RsxA is upregulated in the *Δtgt* strain at the translational level, and that proteins with a codon usage bias towards tyrosine TAT are prone to be more efficiently translated in the absence of Q modification, but this is also dependent on the sequence context.

Increased expression of RsxA hampers growth in sub-MIC TOB

We asked whether high levels of RsxA could be responsible of *Δtgt* strain's increased sensitivity to TOB. We cloned *rsxA* in an inducible plasmid in order to test the effect of its overexpression in WT (**Fig. 4F** and **Sup. Fig. S7ABCD**). Note that since *rsxA* is essential in *V. cholerae* (our TN-seq data (1,42)), we could not delete it. In the presence of sub-MIC TOB, overexpression of *rsxA* in the WT strain strongly

reduces growth (**Sup. Fig. S7B, black curve compared to blue**), while overexpression of *tgt* restores growth of the *Δtgt* strain (**Sup. Fig. S7D, green curve**). This shows that increased *rsxA* levels can be toxic during growth in sub-MIC TOB and is consistent with decreased growth of the *Δtgt* strain.

Unlike for *V. cholerae*, *rsxA* is not an essential gene in *E. coli*, and does not bear a TAT bias. It has however the same function. In order to confirm that the presence of RsxA can be toxic during growth in sub-MIC TOB, we additionally performed competition experiments in *E. coli* with simple and double mutants of *tgt* and *rsxA*. Since *Δtgt* strain's growth is more affected than WT at TOB 0.5 μg/ml (indicated with an arrow in **Sup. Fig. S7F**), we chose this concentration for competition and growth experiments. The results confirm that deletion of *rsxA* in *Δtgt* restores fitness in sub-MIC TOB (**Sup. Fig. S7G**).

tgt transcription is repressed by CRP and induced by tobramycin in *V. cholerae*

tgt was previously observed to be upregulated in *E. coli* isolates from urinary tract infection[43] and in *V. cholerae* after mitomycin C treatment (through indirect SOS induction[44]). We measured *tgt* transcript levels using digital RT-PCR in various transcriptional regulator deficient mutants (iron uptake repressor Fur, general stress response and stationary phase sigma factor RpoS and carbon catabolite control regulator CRP), as well as upon exposure to antibiotics, particularly because *tgt* is required for growth in sub-MIC TOB. We also tested the iron chelator dipyridyl (DP), the oxidant agent paraquat (PQ) and serine hydroxamate (SHX) which induces the stringent response.

Among all tested conditions, we found that sub-MIC TOB and the stringent response increase *tgt* transcript levels, while the carbon catabolite regulator CRP appears to repress it (**Fig. 5A**). We found a sequence between ATG -129 to -114: TTC**G**C^{AGGGAA}A**C**GCG which shows some similarity (in blue) to the *V. cholerae* CRP binding consensus $(^T/_A)_1(^G/_T)_2(^T/_C)_3$**$G_4$**$(^A/_C)_5^{NNNNNN}(^T/_G)_{12}$**$C_{13}$**$(^A/_G)_{14}(^C/_A)_{15}(^T/_A)_{16}$. However, CRP binding was not previously detected by ChIP-seq in the promoter region of *tgt* in *V. cholerae*[45]. CRP binding could be transitory or the repression of *tgt* expression by CRP could be an indirect effect.

Regarding induction by sub-MIC TOB, the mechanism remains to be determined. We previously showed that sub-MIC TOB induces the stringent response[1,46]. Since induction of *tgt* expression by SHX and by TOB seem to be in the same order of magnitude, we hypothesized that sub-MIC TOB could induce *tgt* through the activation of the stringent response. Using a *P1rrnB-gfp* fusion (1), which is down-regulated upon stringent response induction[47] (**Fig. 5B**). We found that the stringent response is significantly induced by sub-MIC TOB, both in WT and *Δtgt*, which is consistent with the possibility that sub-MIC TOB induces *tgt* expression through the stringent response activation.

Q modification levels can be dynamic and are directly influenced by *tgt* transcription levels

Although we have identified conditions regulating *tgt* expression, whether up/down-regulation of the modification factor affects the actual levels of tRNA Q modifications is unknown. We measured Q levels by mass spectrometry in WT and the *Δcrp* strain where the strongest impact on *tgt* expression was observed (**Fig. 5C**). We find a significant 1.6-fold increase in Q levels in *Δcrp*. We also tested the effect of sub-MIC TOB but smaller differences are probably not detected using our approach of MS in bulk cultures, hence we saw no significant increase (not shown). These results show that tRNA Q modification levels are dynamic and correlate with variations in *tgt* expression.

DNA repair genes are TAT-biased

We further analyzed *in silico* the codon usage of *V. cholerae* genome, and for each gene, we assigned a codon usage value to each codon (**Sup. Fig. S8F and doi:10.5281/zenodo.6875293**). This allowed the generation of lists of genes with divergent codon usage (**doi:10.5281/zenodo.6875293**).

Gene ontology enrichment analysis (**Sup. Fig. S8CDE**) indicates that DNA repair category appears to be enriched among the genes with a tyrosine codon usage bias towards TAT in *V. cholerae* with a *p-value* of 2.28×10^{-2} (**Sup. Fig. S8C, Fig. 6A**), among which *recO*, *recR* and *recA* (Fig. 6A, red arrows), involved in UV or CIP-associated DNA damage repair. Interestingly, LexA repressor of the SOS

response, which represses the promoters of many DNA recombination and repair genes, bears a strong bias towards TAC, suggesting that conditions leading to more efficient translation of TAT-biased DNA repair genes, would also lead to less efficient translation of their TAC-biased repressor. We hypothesized that translation of DNA repair transcripts could be more efficient in *Δtgt*, and that such basal pre-induction would be beneficial during genotoxic treatments such as CIP treatment (double strand break formation) or UV irradiation (single stranded DNA breaks).

We did not observe any difference for *Δtgt* tolerance to CIP even at early times of treatment (**Fig. 1E**). However, we did observe a slight increase in fitness in some competition experiments in sub-MIC CIP (**Fig. 1A**), but this effect was variable. On the other hand, the *V. cholerae Δtgt* strain appears to be 4 to 9 times more resistant to UV irradiation than the WT strain (**Fig. 6B**). This is consistent with the hypothesis of increased DNA repair efficiency in the *V. cholerae Δtgt* strain.

We also analyzed tyrosine codon usage for the DNA repair genes in *E. coli*, and did not observe the same bias (**Fig. 6C**), with 51% TAT-bias, i.e. the expected level for a random group of genes of the *E coli* genome, and with a TAC bias for *recOR* and *recA* (red arrows) and strong TAT-bias for *lexA* (blue arrow). (**Sup. Fig. 9D**, whole genome *E. coli*). These genes thus show the exact opposite bias in *E. coli* (**Fig. 6C**),
        Strikingly, unlike for *V. cholerae*, *E. coli Δtgt* mutant did not show increased UV resistance (**Fig. 6D**). This is consistent with the hypothesis that modification tuned translation of codon biased transcripts can be an additional means of regulation building upon already described and well characterized transcriptional regulation pathways.

Discussion

In the light of our results, and as summarized in **Fig. 7**, we propose that exposure to sub-MIC aminoglycosides increases *tgt* expression in *V. cholerae*, and impacts the decoding of tyrosine (among other) codons. tRNA modification tunable translation of codon biased transcripts contributes to phenotypic diversity. One of those transcripts encodes RsxA in *V. cholerae*, an anti-SoxR factor. SoxR controls a regulon involved in oxidative stress response and we have previously shown that sub-MIC aminoglycosides trigger oxidative stress in *V. cholerae*(48). TAT-biased RsxA levels are more abundant in the absence of *tgt*, and less abundant when Tgt levels increase. Increasing RsxA levels may thus reduce fitness in TOB by hampering efficient oxidative stress response. Better decoding at TAT codons in the absence of Q observed here in *V. cholerae* is also consistent with very recent findings in human tRNAs where the presence of Q increases translation of transcripts biased in C-ending codons (49).

As a corollary, decreased RsxA would lead to increased expression of the SoxR regulon, which would allow for more efficient response to oxidative stress, and increased fitness in the presence of sub-MIC TOB. While our results show that increased expression of *rsxA* decrease fitness in WT *V. cholerae*, we did not see any effect on fitness when we overexpressed *sodA* alone (not shown), suggesting that the decreased fitness due to *rsxA* overexpression is not solely due to low superoxide dismutase levels. The link between Q and oxidative stress has been previously found in eukaryotic organisms, where the presence of Q allows better response to oxidative stress(24). Note that, our results do not exclude additional factors to RsxA, which are post-transcriptionally regulated by Q and intervene in the response to sub-MIC aminoglycosides.

Our findings are in line with the concept of the so-called modification tunable transcripts (MoTTs)(20). Here we add to this list of bacterial MoTTs, TAT-biased transcripts for which translation is tuned by Tgt, such as RsxA, and DNA repair factors, in *V. cholerae*.

V. cholerae is the model organism for different species of *Vibrio*, including human and animal pathogens *V. parahaemolyticus* and *V. vulnificus*. We have previously shown that *V. cholerae's* response to sub-MIC antibiotic stress is transposable to other Gram-negative pathogens such as *K. pneumoniae, P. luminescens(48) and P. aeruginosa(50)*. Here, we have also addressed some of the effects of TOB in *E. coli Δtgt* mutant.

In *E. coli,* the deletion of *tgt* does not have such a dramatic effect on the susceptibility to TOB as it has in *V. cholerae* ((1) and **Sup. Fig S7F**). *V. cholerae* and *E. coli* globally show similar profiles of tyrosine codon usage (**Sup. Fig. S8AB**). Interestingly, unlike for *V. cholerae*, *E. coli rsxA* does not display a codon bias towards TAT. One can think that in regard to MoTTs, different organisms have evolved according

to the environments where they grow, selecting the integration of specific stress response pathways under specific post-transcriptional regulations. Moreover, results are also in line with the fact that synonymous mutations may influence the expression of genes(51). This is not the first instance where we show a difference between *E. coli* and *V. cholerae*, regarding sub-MIC antibiotic resistance and oxidative stress phenotypes. The two species display differential triggering of RpoS and SOS stress responses(48,52), while they both induce mutagenesis upon growth in sub-MIC antibiotics from different families(50,52). Moreover, *E. coli* and *V. cholerae* are very dissimilar in respect to the respiration complexes, iron-sulfur (Fe-S) cluster biogenesis and oxidative stress response pathways. For instance, *V. cholerae* lacks the Cyo/Nuo respiratory complex I, and also lacks the Suf Fe-S biogenesis system used under oxidative stress and low iron conditions. Interestingly, the list of TAT biased genes in *E. coli* comprise all three Fe-S cluster assembly factors *sufA*, *iscA*, *erpA*. Isc and Suf pathways differentially respond to iron levels. The Isc pathway is involved in the maturation of respiratory complex I Nuo in *E. coli*, and could originate in modulation of PMF and AG entry(53)**.** Fe-S clusters are found in DNA base excision repair proteins, SoxR(54) and oxidative stress response factors, among others. Perturbation of iron-homeostasis in the Q-deficient strain could also be seen with the higher expression of the Isc machinery genes and lower expression of the *suf* genes in *E. coli Δtgt* (28). However, *lacZ* fusions that allow to monitor levels of Fe-S clusters did not show any differences when Q was absent(28). Moreover, ErpA protein levels were reduced by 50% in E. coli *Δtgt*. The redundancy of Fe-S cluster loaders make interpretation of ErpA partial reduction difficult but it was shown that FNR required ErpA for correct insertion of its cluster, and that the loaded FNR is an activator of the *narGHIJ* and *moaABCDE* operons. Again, emphasizing the difficulty of interpreting such integrated metabolic loops, we found, in aerobic conditions, that the expression of the *narGHJI* genes was greatly reduced (by ~4 Log2Fold) in the absence of Q but the expression of the *moa* genes was induced (by ~2 log2-fold).

Other TAT-biased genes in *E. coli* are involved in energy and respiration (*sdhC, ygcR, grxC, hydN, sgcE*), transcription regulation (*cspH, cspB, mprA, cpxR, hdfR, zur, narL, nimR, rssB, nikR, ycjW, nanR, marR, stpA, lexA, hcaR, glaR, rcnR, hprR*). Note that *E. coli lexA* has a bias towards TAT, unlike *V. cholerae lexA* which has a bias towards TAC.

It was recently shown that *E. coli Δtgt* strain is more resistant than the WT to nickel toxicity most certainly because the nickel importer genes *nikABCDE* are less expressed but the underlying molecular mechanism had not been elucidated(28). As NikR, the repressor of the *nik* operon is enriched in TAT codons (100%), a more efficient translation of the *nikR* gene in the absence of Q would lead to the observed repression phenotype. In addition, the nickel exporter gene *rcnA* is also enriched is TAT (100%) while one of the genes for subunits of the nickel importer *nikD* is enriched in TAC codons (100%). In combination this could explain the clear resistance of the *tgt* strain to high levels of nickel.

However, protein levels are not always in line with the codon bias predictions, as exemplified above with ErpA. In summary, many additional experiments need to be performed to elucidate post-transcriptional regulation related phenotypes, but the differential expression of specific TAT/TAC biased proteins finally allows to propose a model for the pleiotropic phenotype caused by Q deficiency in *E. coli.*

Although tRNA modifications were initially thought to be static, studies reveal the existence of dynamic modifications, mostly shown in eukaryotes(55-57). Modification levels appear to depend on growth phase and rate(58,59), on external factors(60) and on environmental changes (reviewed in (35)) and stress. This leads to differential translation of stress response transcripts and translational reprogramming (2,61,62). In this process, tRNA modifications and modification levels have an impact on the translation of regulators, which in turn trigger optimized responses to stress.

Stress regulated tRNA modifications would facilitate homeostasis by reprogramming the translation of stress response genes. We show here that *tgt* expression levels are regulated by sub-MIC TOB, the stringent response and CRP, and that tRNAs Q modification levels increase with *tgt* expression.
How sub-MIC TOB increases *tgt* expression remains an open question. Since there is a correlation between sub-MIC TOB and stringent response dependent induction of *tgt*, one hypothesis could be that sub-MIC TOB induces *tgt* through stringent response activation. The stringent response is usually

triggered upon starvation, for example when amino acids are scarce. *tgt* expression was recently shown to be regulated by tyrosine levels and to affect tRNA-Tyr codon choice in *Trypanosoma brucei*(63). Tyrosine import into cells occurs through the TyrP transporter(64). Note that in *V. cholerae*, sub-MIC TOB strongly decreases *tyrP* (VCA0772) expression(46), and thus likely decreases tyrosine intake. We could not detect the TyrP protein in our proteomics data, we can thus not compare TyrP levels in *Δtgt* vs WT. We wondered whether supplementation with tyrosine or TyrP overexpression would reverse the *Δtgt* TOB sensitive fitness phenotype, but we observed no notable difference (not shown). Nevertheless, TyrP downregulation could be a signal mimicking tyrosine shortage and inducing *tgt,* leading to more efficient translation of TAC biased proteins, such as TyrP itself.

Essential/housekeeping genes are also generally TAC biased (**Sup. Fig. S9AB**), as well as ribosomal proteins which carry mostly tyrosine TAC codons both in *V. cholerae* and *E. coli*. It has been proposed that codon bias corresponding to abundant tRNAs at highly expressed genes, such as ribosomal protein genes, guarantees their proper expression and avoids titration of tRNAs, allowing for efficient expression of the rest of the proteome(65). Induction of *tgt* by stress could also possibly be a signal for the cell to favor the synthesis of essential factors.

Regarding *tgt* repression by CRP, the carbon catabolite regulator, it could be relevant here to note that CRP is involved in natural competence of *V. cholerae*, which is triggered by the presence of chitin. Chitin is used as a carbon source on crustacean shells where *V. cholerae* grows, and induces the CRP-cAMP response. Thus, modulation of *tgt* levels during natural transformation may modulate the expression of horizontally transferred genes which by definition may bear different GC content and codon usage. One can thus speculate that during chitin-induced exogenous DNA uptake, *tgt* repression by CRP could lead to better decoding of AT rich (i.e. TAT biased) mRNAs, increasing the chances of transiently expressing newly acquired DNA. Moreover, if *tgt* expression is repressed by CRP during competence state, this would favor the translation of TAT-biased DNA repair genes and possibly recombination of incoming DNA into the chromosome.

If this were the case, it would not be the first occurrence of a direct link between translation and DNA repair. A recent study reports that DNA double strand breaks can trigger the proteasomal degradation of a specific ribosomal protein in eukaryotes, with a direct impact on ribosome composition(66). Translational reprogramming in response to DNA damage can thus be an advantageous property selected during evolution.

Our results also demonstrate that we can identify other Q-dependent MoTT candidates using *in silico* codon usage analysis. In fact, since we now have extensively calculated the codon usage biases at all codons for *V. cholerae* and *E. coli* genes, this approach is readily adaptable to any tRNA modification for which we know which codons are differentially translated. However, the codon usage bias may not be sufficient to determine whether a given protein will be more or less efficiently translated in the presence or absence of a tRNA modification. The positions of the codons of interest and their sequence context may also be important for differential translation. For example, the presence of the codon of interest (e.g. TAT/TAC in the case of Q modification) in the N-terminal region vs the C-ter of a protein could have a bigger impact on the efficiency of translation. Similarly, the distance between two codons of interest, or the identity of the nearby codons may be important. There can also be a difference between highly transcribed genes and genes with low levels of mRNAs to be translated. Further studies are needed to characterize the determinants of tRNA modification dependent translational reprogramming. Note that codon usage may also directly impact gene expression at mRNA levels with an effect on transcription termination(67), especially for constitutive genes. Thus, the search for MoTTs could be facilitated by comparing transcriptomics to proteomics data.

The diversity of tRNA modifications, their specific effects on various proteins and cellular processes and the possibility that their expression may be regulated by various stresses make them now a promising field of study. Such regulation may allow a non-hereditary modulation of protein abundance, a possible way to tune the expression of essential or newly acquired genes, differing in

GC-content. It may also in some cases explain, antibiotic resistance profiles in bacterial collections with established genome sequences, and for which observed phenotypic resistance does not always correlate with known resistance factors(68).

Materials and methods

Media and Growth Conditions

Platings were done at 37°C, in Mueller-Hinton (MH) agar media. Liquid cultures were grown at 37°C in MH in aerobic conditions, with 180 rotations per minute.

Competition experiments were performed as described(1): overnight cultures from single colonies of mutant *lacZ*+ and WT *lacZ*- strains were washed in PBS (Phosphate Buffer Saline) and mixed 1:1 (500 µl + 500 µl). At this point 100 µl of the mix were serial diluted and plated on MH agar supplemented with X-gal (5-bromo-4-chloro-3-indolyl-β-D- galactopyranoside) at 40 µg/mL to assess T0 initial 1:1 ratio. At the same time, 10 µl from the mix were added to 2 mL of MH or MH supplemented with sub-MIC antibiotics (concentrations, unless indicated otherwise: TOB: tobramycin 0.6 µg/ml; GEN: 0.5 µg/ml; CIP: ciprofloxacin 0.01 µg/ml, CRB: carbenicillin 2.5 µg/ml), PQ: paraquat 10 µM, or H_2O_2: 2 mM. Cultures were incubated with agitation at 37°C for 20 hours, and then diluted and plated on MH agar plates supplemented with X-gal. Plates were incubated overnight at 37°C and the number of blue and white CFUs was assessed. Competitive index was calculated by dividing the number of blue CFUs (*lacZ*+ strain) by the number of white CFUs (*lacZ*- strain) and normalizing this ratio to the T0 initial ratio. When a plasmid was present, antibiotic was added to maintain selection: kanamycin 50 µg/ml for pSEVA.

Construction of complementation and overexpression plasmids in pSEVA238

Genes were amplified on *V. cholerae* genomic DNA using primers listed in Table S3 and cloned into pSEVA238 (69) under the dependence of the *Pm* promoter(70), by restriction digestion with XbaI+EcoRI and ligation using T4 DNA ligase. Sodium benzoate 1 mM was added in the medium as inducer.

Survival/tolerance tests were performed on early exponential phase cultures. The overnight stationary phase cultures were diluted 1000x and grown until OD 620 nm = 0.35 to 0.4, at 37°C with shaking, in Erlenmeyers containing 25 mL fresh MH medium. Appropriate dilutions were plated on MH plates to determine the total number of CFUs in time zero untreated cultures. 5 mL of cultures were collected into 50 mL Falcon tubes and treated with lethal doses of desired antibiotics (5 or 10 times the MIC: tobramycin 5 or 10 µg/mL, carbenicillin 50 µg/mL, ciprofloxacin 0.025 µg/mL) for 30 min, 1 hour, 2 hours and 4 hours if needed, at 37°C with shaking in order to guarantee oxygenation. Appropriate dilutions were then plated on MH agar without antibiotics and proportion of growing CFUs were calculated by doing a ratio with total CFUs at time zero. Experiments were performed 3 to 8 times.

MIC determination

Stationary phase cultures grown in MH were diluted 20 times in PBS, and 300 µL were plated on MH plates and dried for 10 minutes. Etest straps (Biomérieux) were placed on the plates and incubated overnight at 37°C.

Quantification of fluorescent neomycin uptake was performed as described(30). Neo-Cy5 is an aminoglycoside coupled to the fluorophore Cy5, and has been shown to be active against Gram-

bacteria(32,71). Briefly, overnight cultures were diluted 100-fold in rich MOPS (Teknova EZ rich defined medium). When the bacterial strains reached an OD 620 nm of ~0.25, they were incubated with 0.4 µM of Cy5 labeled Neomycin for 15 minutes at 37°C. 10 µl of the incubated culture were then used for flow cytometry, diluting them in 250 µl of PBS before reading fluorescence. WT *V. cholerae*, was incubated simultaneously without Neo-Cy5 as a negative control. Flow cytometry experiments were performed as described(72) and repeated at least 3 times. For each experiment, 100,000 events were counted on the Miltenyi MACSquant device.

PMF measurements

Quantification of PMF was performed using the Mitotracker Red CMXRos dye (Invitrogen) as described(73), in parallel with the neo-Cy5 uptake assay, using the same bacterial cultures. 50 µL of each culture were mixed with 60 µL of PBS. Tetrachlorosalicylanilide TCS (Thermofischer), a protonophore, was used as a negative control with a 500 µM treatment applied for 10 minutes at room temperature. Then, 25 nM of Mitotracker Red were added to each sample and let at room temperature for 15 minutes under aluminium foil. 20 µL of the treated culture were then used for flow cytometry, diluted in 200 µL of PBS before reading fluorescence.

tRNA overexpressions.

Synthetic fragments carrying the Ptrc promoter, the desired tRNA sequence and the natural transcriptional terminator sequence of VCt002 were ordered from IDT as double stranded DNA gBlocks, and cloned into pTOPO plasmid. Sequences are indicated in Table S3.

mRNA purification

For RNA extraction, overnight cultures were diluted 1:1000 in MH medium and grown with agitation at 37°C until an OD600 of 0.3-0.4 (exponential phase). 0.5 mL of these cultures were centrifuged and supernatant removed. Pellets were homogenized by resuspension with 1.5 mL of cold TRIzol Reagent. Next, 300 µL chloroform were added to the samples following mix by vortexing. Samples were then centrifuged at 4°C for 10 minutes. Upper (aqueous) phase was transferred to a new 2mL tube and mixed with 1 volume of 70% ethanol. From this point, the homogenate was loaded into a RNeasy Mini kit (Qiagen) column and RNA purification proceeded according to the manufacturer's instructions. Samples were then subjected to DNase treatment using TURBO DNA-free Kit (Ambion) according to the manufacturer's instructions.

mRNA quantifications by digital-RT-PCR

qRT-PCR reactions were prepared with 1 µL of diluted RNA samples using the qScript XLT 1-Step RT-qPCR ToughMix (Quanta Biosciences, Gaithersburg, MD, USA) within Sapphire chips. Digital PCR was conducted on a Naica Geode (programmed to perform the sample partitioning step into droplets, followed by the thermal cycling program suggested in the user's manual. Primer and probe sequences used in digital qRT-PCR reaction are listed in Table S3. Image acquisition was performed using the Naica Prism3 reader. Images were then analyzed using Crystal Reader software (total droplet enumeration and droplet quality control) and the Crystal Miner software (extracted fluorescence values for each droplet). Values were normalized against expression of the housekeeping gene *gyrA* as previously described(74).

tRNA levels quantification by qRT-PCR

First-strand cDNA synthesis and quantitative real-time PCR were performed with KAPA SYBR® FAST Universal (CliniSciences) on the QuantStudio Real-Time PCR (Thermo Fischer) using the primers indicated in Table S3. Transcript levels of each gene were normalized to *gyrA* as the reference gene

control(74). Gene expression levels were determined using the $2^{-\Delta\Delta Cq}$ method (Bustin et al., 2009; Livak and Schmittgen, 2001) in respect to the MIQE guidelines. Relative fold-difference was expressed either by reference to antibiotic free culture or the WT strain in the same conditions. All experiments were performed as three independent replicates with all samples tested in duplicate. Cq values of technical replicates were averaged for each biological replicate to obtain the ΔCq. After exponential transformation of the ΔCq for the studied and the normalized condition, medians and upper/lower values were determined.

Stop codon readthrough and ribosomal frameshifting quantification assay

V. cholerae electrocompetent cells were transformed with reporter dual reporter plasmids that were previously described(33). Overnight cultures of transformants were diluted 1:100 in MH medium supplemented with 5 µg/mL chloramphenicol to maintain plasmids, 200 µg/mL IPTG (Isopropyl β-D-1-thiogalactopyranoside) and in the presence or not of tobramycine 0,4 µg/mL and grown with shaking at 37°C until an OD600 of 0.3 (exponential phase).

Luciferase luminescence was quantified using the luciferase assay system (Promega, WI, USA, Cat.# E1500). Briefly, 90 µL of each culture were aliquoted in 1.5 mL tubes, treated with 10 µL K_2HPO_4 (1 M) and EDTA (20 mM) and quick-frozen in dry ice for 1 min. Tubes were then placed in room-temperature water for 5 min to allow the cultures to thaw. 300 µL of lysis buffer (Cell Culture Lysis Reagent 1X ; lysozyme 1.25mg/ml ; BSA 2.5mg/ml) were added in the tubes that were then placed back in water for 10 min. 100 µL of lysate were placed in 5 mL tubes with 100 µL of Luciferase Assay Reagent and luminescence was read for 10 sec using Lumat LB 9507 (EG&G Berthold).

For β-galactosidase activity quantification, 2 mL of the cultures were aliquoted and mixed with 50 µL chloroform and 50 µL SDS 0.1%. After vortexing for 45 sec, samples were placed 5 min at RT for cell lysis. 500 µL of the lysates were collected into 5 mL tubes and treated with 1.5 mL Z-Buffer (8.5 mg/mL Na_2HPO_4; 5.5 mg/mL $NaH_2PO_4H_2O$; 0.75 mg/mL KCl; 0.25 mg/mL $MgSO_4,7H_2O$) supplemented with 7 µL/ml 2-Mercaptoethanol. After 5 min incubation at 37°C, 500 µL ONPG (4 mg/mL) were added in the samples which were then placed at 37°C for 1h. Reaction has finally been stopped by addition on the tubes of 1mL Na_2CO_3 (1 M). 2 mL suspension were transferred to eppendorf tubes, centrifuged and OD 420 nm of the supernatant was read. β-galactosidase activity dosage was used for normalization of luminescence.

Construction of *gfp* reporters with codon stretches.

The positive control was *gfp*mut3 (stable *gfp*)(75) under the control of Ptrc promoter, the transcription start site, *rbs* and ATG start codon are indicated in bold and underlined.

TTGACAATTAATCATCCGGCTCGTATAATGTGTGG**A**ATTGTGAGCGGATAACAATTTCACAC**AGGAAAC**AGCG
CCGC**ATG**CGTAAAGGAGAAGAACTTTTCACTGGAGTTGTCCCAATTCTTGTTGAATTAGATGGTGATGTTAATG
GGCACAAATTTTCTGTCAGTGGAGAGGGTGAAGGTGATGCAACATACGGAAAACTTACCCTTAAATTTATTTG
CACTACTGGAAAACTACCTGTTCCATGGCCAACACTTGTCACTACTTTCGGTTATGGTGTTCAATGCTTTGCGAG
ATACCCAGATCATATGAAACAGCATGACTTTTTCAAGAGTGCCATGCCCGAAGGTTATGTACAGGAAAGAACT
ATATTTTTCAAAGATGACGGGAACTACAAGACACGTGCTGAAGTCAAGTTTGAAGGTGATACCCTTGTTAATA
GAATCGAGTTAAAAGGTATTGATTTTAAAGAAGATGGAAACATTCTTGGACACAAATTGGAATACAACTATAA
CTCACACAATGTATACATCATGGCAGACAAACAAAAGAATGGAATCAAAGTTAACTTCAAAATTAGACACAAC
ATTGAAGATGGAAGCGTTCAACTAGCAGACCATTATCAACAAAATACTCCAATTGGCGATGGCCCTGTCCTTTT
ACCAGACAACCATTACCTGTCCACACAATCTGCCCTTTCGAAAGATCCCAACGAAAAGAGAGACCACATGGTCC
TTCTTGAGTTTGTAACAGCTGCTGGGATTACACATGGCATGGATGAACTATACAAATAA

For the tested codon stretches, 6 repeats of the desired codon were added just after the ATG start codon of *gfp*. The DNA fragments were ordered as double stranded *eblocks* from Integrated DNA technologies (IDT), and cloned into pTOPO-Blunt using kanamycin resistance, following the manufacturer's instructions.

For tests of sequence context surrounding tyrosine codons of *rsxA*, DNA was ordered from IDT and cloned into pTOPO as described for codon stretches above, based on the following amino-acid sequences (tested sequences in bold):

VC1017RsxA *V. cholerae*

MLLLWQSRIMPGSEANIYITM**TEYLLL**LLIGTVLVNNFVLVKFLGLCPFMGVSKKLETAIGMGLATTFVLTLASVCAYL
VESYVLRPLGI**EYLR**TMSFILVIAVVVQFTEMVVHKTSPT**LYRLL**GIFLPLITTNCAVLGVALLNINENHNFIQSIIYGFG
AAVGFSLVLILFASMRERIHVADVPAPFKGASIAMITAGLMSLAFMGFTGLVKL

RsxA *E. coli*

M**TDYLLL**FVGTVLVNNFVLVKFLGLCPFMGVSKKLETAMGMGLATTFVMTLASICAWLIDTWILIPLNLIYLRTLAFIL
VIAVVVQFTEMVVRKTSPV**LYRLL**GIFLPLITTNCAVLGVALLNINLGHNFLQSALYGFSAAVGFSLVMVLFAAIRERL
AVADVPAPFRGNAIALITAGLMSLAFMGFSGLVKL

Quantification of *gfp* fusion expression by fluorescent flow cytometry

Flow cytometry experiments were performed as described(72) on overnight cultures and repeated at least 3 times. For each experiment, 50,000 to 100,000 events were counted on the Miltenyi MACSquant device.

Transcriptional fusion: *rsxA* promoter sequence was amplified using primers ZIP796/ZIP812. gfp was amplified from pZE1-*gfp*(76) using primers ZIP813/ZIP200. The two fragments were PCR assembled into *PrsxA-gfp* using ZIP796/ZIP200 and cloned into pTOPO-TA cloning vector. The *PrsxA-gfp* fragment was then extracted using *EcoRI* and cloned into the low copy plasmid pSC101 (1 to 5 copies per cell). The plasmid was introduced into desired strains, and fluorescence was measured on indicated conditions, by counting 100,000 cells on the Miltenyi MACSquant device. Likewise, the control plasmid *Pc-gfp* (constitutive) was constructed using primers ZIP513/ZIP200 and similarly cloned in pSC101.

For translational fusions, the constitutive Ptrc promoter, the *rsxA* gene (without stop codon) with desired codon usage fused to *gfp* (without ATG start codon) was ordered from IDT in the pUC-IDT vector (carbenicillin resistant).

Native sequence of *V. cholerae rsxA* gene, called *rsxA^{TAT}gfp* in this manuscript is shown below. For *rsxA^{TAC}gfp,* all tyrosine TAT codons were replaced with TAC.

ATGACCGAA**TAT**CTTTTGTTGTTAATCGGCACCGTGCTGGTCAATAACTTTGTACTGGTGAAGTTTTTGGGCTT
ATGTCCTTTTATGGGCGTATCAAAAAAACTAGAGACCGCCATTGGCATGGGGTTGGCGACGACATTCGTCCTC
ACCTTAGCTTCGGTGTGCGCT**TAT**CTGGTGGAAAGT**TAC**GTGTTACGTCCGCTCGGCATTGAG**TAT**CTGCGCA
CCATGAGCTTTATTTTGGTGATCGCTGTCGTAGTACAGTTCACCGAAATGGTGGTGCACAAAACCAGTCCGACA
CTC**TAT**CGCCTGCTGGGCATTTTCCTGCCACTCATCACCACCAACTGTGCGGTATTAGGGGGTTGCGCTGCTCAA
CATCAACGAAAATCACAACTTTATTCAATCGATCATT**TAT**GGTTTTGGCGCTGCTGTTGGCTTCTCGCTGGTGCT
CATCTTGTTCGCTTCAATGCGTGAGCGAATCCATGTAGCCGATGTCCCCGCTCCCTTTAAGGGCGCATCCATTG
CGATGATCACCGCAGGTTTAATGTCTTTGGCCTTTATGGGCTTTACCGGATTGGTGAAACTGGCTAGC

gfp^{TAC} and *gfp^{TAT}* (tyrosine 11 TAT instead of 11 TAC) were ordered from IDT as synthetic genes under the control pf Ptrc promoter in the pUC-IDT plasmid (carbenicillin resistant). The complete sequence of ordered fragments is indicated in Table S3, tyrosine codons are underlined.

Construction of *bla* reporters.

Point mutations for codon replacements were performed using primer pairs where the desired mutations were introduced and by whole plasmid PCR amplification on circular pTOPO-TA plasmid. Primers are listed Table S3

Tolerance tests with *bla* reporters.

A single colony from fresh transformation plates was inoculated in 24 well plates, each well containing 2 mL of MH. Cells were grown to early exponential phase without carbenicillin, and with or without tobramycin 20% of MIC (TOB 0.2 µg/mL). After 2 hours of incubation at 37°C with shaking (early

14

exponential phase), dilutions were spotted in parallel on plates with or without carbenicillin (time T0). Cultures were then treated with carbenicillin at 10xMIC (50 μg/mL) for 20 hours, at 37°C with shaking. Dilutions were spotted on plates with or without carbenicillin. Surviving cells shown here are sensitive to carbenicillin (no growth on carbenicillin containing plates), suggesting that increased or decreased survival was due to increased (erroneous translation) or decreased (faithful translation) β-lactamase activity at the time of treatment.

Growth on microtiter plate reader for *bla* reporter assays
Overnight cultures were diluted 1:500 in fresh MH medium, on 96 well plates. Each well contained 200 μL. Plates were incubated with shaking on TECAN plate reader device at 37°C, OD 620 nm was measured every 15 min. Tobramycin was used at sub-MIC: TOB 0.2 μg/mL. Kanamycin and carbenicillin were used at selective concentration: CRB 100 μg/mL, KAN 50 μg/mL.

Protein extraction
Overnight cultures of *V. cholerae* were diluted 1:100 in MH medium and grown with agitation at 37°C until an OD 600 nm of 0.3 (exponential phase). 50 mL of these cultures were centrifuged for 10 min at 4°C and supernatant removed. Lysis was achieved by incubating cells in the presence of lysis buffer (10 mM Tris-HCl pH 8, 150 mM Nacl, 1% triton 100X) supplemented with 0.1 mg/mL lysozyme and complete EDTA-free Protease Inhibitor Cocktail (Roche) for 1 hour on ice. Resuspension were sonicated 3x50 sec (power: 6, pulser: 90%), centrifuged for 1 h at 4°C at 5000 rpm and supernatants were quantified using Pierce™ BCA Protein Assay Kit (Cat. No 23225) following the manufacturer's instructions. Proteins were then stored at -80°C.

Proteomics MS and analysis
Sample preparation for MS
Tryptic digestion was performed using eFASP (enhanced Filter-Aided Sample Preparation) protocol(77). All steps were done in 30 kDa Amicon Ultra 0.5 mL filters (Millipore). Briefly, the sample was diluted with a 8M Urea, 100 mM ammonium bicarbonate buffer to obtain a final urea concentration of 6 M. Samples were reduced for 30 min at room temperature (RT) with 5 mM TCEP. Subsequently, proteins were alkylated in 5 mM iodoacetamide for 1 hour in the darkness at RT and digested overnight at 37°C with 1 μg trypsin (Trypsin Gold Mass Spectrometry Grade, Promega). Peptides were recovered by centrifugation, concentrated to dryness and resuspended in 2% acetonitrile (ACN)/0.1% FA just prior to LC-MS injection.
LC-MS/MS analysis
Samples were analyzed on a high-resolution mass spectrometer, Q Exactive™ Plus Hybrid Quadrupole-Orbitrap™ Mass Spectrometer (Thermo Scientific), coupled with an EASY 1200 nLC system (Thermo Fisher Scientific, Bremen). One μg of peptides was injected onto a home-made 50 cm C18 column (1.9 μm particles, 100 Å pore size, ReproSil-Pur Basic C18, Dr. Maisch GmbH, Ammerbuch-Entringen, Germany). Column equilibration and peptide loading were done at 900 bars in buffer A (0.1% FA). Peptides were separated with a multi-step gradient from 3 to 22 % buffer B (80% ACN, 0.1% FA) in 160 min, 22 to 50 % buffer B in 70 min, 50 to 90 % buffer B in 5 min at a flow rate of 250 nL/min. Column temperature was set to 60°C. The Q Exactive™ Plus Hybrid Quadrupole-Orbitrap™ Mass Spectrometer (Thermo Scientific) was operated in data-dependent mode using a Full MS/ddMS2 Top 10 experiment. MS scans were acquired at a resolution of 70,000 and MS/MS scans (fixed first mass 100 m/z) at a resolution of 17,500. The AGC target and maximum injection time for the survey scans and the MS/MS scans were set to 3E6, 20ms and 1E6, 60ms respectively. An automatic selection of the 10 most intense precursor ions was activated (Top 10) with a 35 s dynamic exclusion. The isolation window was set to

1.6 m/z and normalized collision energy fixed to 27 for HCD fragmentation. We used an underfill ratio of 1.0 % corresponding to an intensity threshold of 1.7E5. Unassigned precursor ion charge states as well as 1, 7, 8 and >8 charged states were rejected and peptide match was disable.

Data analysis

Acquired Raw data were analyzed using MaxQuant 1.5.3.8 version(78) using the Andromeda search engine(79) against *Vibrio cholerae* Uniprot reference proteome database (3,782 entries, download date 2020-02-21) concatenated with usual known mass spectrometry contaminants and reversed sequences of all entries. All searches were performed with oxidation of methionine and protein N-terminal acetylation as variable modifications and cysteine carbamidomethylation as fixed modification. Trypsin was selected as protease allowing for up to two missed cleavages. The minimum peptide length was set to 5 amino acids. The false discovery rate (FDR) for peptide and protein identification was set to 0.01. The main search peptide tolerance was set to 4.5 ppm and to 20 ppm for the MS/MS match tolerance. One unique peptide to the protein group was required for the protein identification. A false discovery rate cut-off of 1 % was applied at the peptide and protein levels. All mass spectrometry proteomics data have been deposited at ProteomeXchange Consortium via the PRIDE partner repository with the dataset identifier PXD035297.

The statistical analysis of the proteomics data was performed as follows: three biological replicates were acquired per condition. To highlight significantly differentially abundant proteins between two conditions, differential analyses were conducted through the following data analysis pipeline: (1) deleting the reverse and potential contaminant proteins; (2) keeping only proteins with at least two quantified values in one of the three compared conditions to limit misidentifications and ensure a minimum of replicability; (3) log2-transformation of the remaining intensities of proteins; (4) normalizing the intensities by median centering within conditions thanks to the normalizeD function of the R package DAPAR(80), (5) putting aside proteins without any value in one of both compared conditions: as they are quantitatively present in a condition and absent in another, they are considered as differentially abundant proteins and (6) performing statistical differential analysis on them by requiring a minimum fold-change of 2.5 between conditions and by using a LIMMA t test(81) combined with an adaptive Benjamini-Hochberg correction of the *p*-values thanks to the adjust.p function of the R package cp4p(82). The robust method of Pounds and Cheng was used to estimate the proportion of true null hypotheses among the set of statistical tests(83). The proteins associated with an adjusted *p*-value inferior to an FDR level of 1% have been considered as significantly differentially abundant proteins. Finally, the proteins of interest are therefore the proteins that emerge from this statistical analysis supplemented by those being quantitatively absent from one condition and present in another.

The mass spectrometry proteomics data have been deposited to the ProteomeXchange Consortium via the PRIDE partner repository with the dataset identifier PXD035297.

RNA purification for RNA-seq:

Cultures were diluted 1000X and grown in triplicate in MH supplemented or not with 0.6 µg/ml of tobramycin, corresponding to 50% of the MIC in liquid cultures to an OD 600nm of 0.4. RNA was purified with the RNAeasy mini kit (Qiagen) according to manufacturer instruction. Briefly, 4 ml of RNA-protect (Qiagen) reagent were added on 2 ml of bacterial cultures during 5 minutes. After centrifugation, the pellets were conserved at -80°C until extraction. Protocol 2 of the RNA protect Bacteria Reagent Handbook was performed, with the addition of a proteinase K digestion step, such as described in the protocol 4. Quality of RNA was controlled using the Bioanalyzer. Sample collection, total RNA extraction, library preparation, sequencing and analysis were performed as previously

described (44). The data for this RNA-seq study has been submitted in the GenBank repository under the project number (upload in progress).

Gene Ontology (GO) enrichment analysis.

GO enrichment analyses were performed on http://geneontology.org/ as follows: Binomial test was used to determine whether a group of gene in the tested list was more or less enriched than expected in a reference group. The annotation dataset used for the analysis was GO biological process complete. The analyzed lists were for each condition (MH/TOB), genes (**Table S2**) with at least 2-fold change in RNA-seq data of WT strain compared to *Δtgt*, and with an adjusted p-value <0,05. The total number of uploaded genes list to be analyzed were 53 genes for MH and 60 genes for TOB.
The reference gene list was *Vibrio cholerae* (all genes in database), 3782 genes. Annotation Version: PANTHER Overrepresentation Test (Released 20220712). GO Ontology database DOI: 10.5281/zenodo.6399963 Released 2022-03-22

Stringent response
P1rrnB-gfp fusion was constructed using *gfp* ASV(84), and cloned into plasmid pSC101. *P1rrnB-GFPasv* transcriptional fusion was amplified from strain R438 (E. coli MG1655 *attB::P1rrnB gfp-ASV::kan* provided by Ivan Matic) using primers AFC060 and AFC055 thus including 42 bp upstream of *rrnB* transcription initiation site. PCR product was then cloned in pTOPOblunt vector and subcloned to pSC101 by *EcoRI* digestion and ligation. The final construct was confirmed by sanger sequencing. The plasmid was then introduced by electroporation into the tested strains. Overnight cultures were performed in MH + carbenicillin 100 µg/mL and diluted 500x in 10 mL fresh MH or MH+ TOB 0.4 µg/mL, in an erlenmeyer. At time points 0 min, and every 30 during 3 hours, the OD 620 nm was measured and fluorescence was quantified in flow cytometry. For each experiment, 50,000 to 100,000 events were counted on the Miltenyi MACSquant device.

tRNA enriched RNA extraction
Overnight cultures of *V. cholerae* were diluted 1:1000 in MH medium and grown in aerobic conditions, with 180 rotations per minute at 37°C until an OD 600 nm of 0.5. tRNA enriched RNA extracts were prepared using cold TRIzol™ reagent as described(85) and contaminating DNA were eliminated using TURBO DNA-free Kit (Ambion). RNA concentration was controlled by UV absorbance using NanoDrop 2000c (Thermo Fisher Scientific). The profile of isolated tRNA fractions was assessed by capillary electrophoresis using an RNA 6000 Pico chip on Bioanalyzer 2100 (Agilent Technologies).

tRNA-enriched samples digestion for quantitative analysis of queuosine by mass spectrometry
Purified tRNA enriched RNA fractions were digested to single nucleosides using the New England BioLabs Nucleoside digestion mix (Cat No. M0649S). 10µl of the RNA samples diluted in ultrapure water to 100 ng/µL were mixed with 1µL of enzyme, 2µl of Nucleoside Digestion Mix Reaction Buffer (10X) in a final volume of 20 µL in nuclease-free 1.5 mL tubes. Tubes were wrapped with parafilm to prevent evaporation and incubated at 37°C overnight.

Queosine quantification by LC-MS/MS
Analysis of global levels of queuosine (Q) was performed on a Q exactive mass spectrometer (Thermo Fisher Scientific). It was equipped with an electrospray ionization source (H-ESI II Probe) coupled with an Ultimate 3000 RS HPLC (Thermo Fisher Scientific). The Q standard was purchased from Epitoire (Singapore).

17

Digested RNA was injected onto a ThermoFisher Hypersil Gold aQ chromatography column (100 mm * 2.1 mm, 1.9 µm particle size) heated at 30°C. The flow rate was set at 0.3 mL/min and run with an isocratic eluent of 1% acetonitrile in water with 0.1% formic acid for 10 minutes.

Parent ions were fragmented in positive ion mode with 10% normalized collision energy in parallel-reaction monitoring (PRM) mode. MS2 resolution was 17,500 with an AGC target of 2e5, a maximum injection time of 50 ms, and an isolation window of 1.0 m/z.

The inclusion list contained the following masses: G (284.1) and Q (410.2). Extracted ion chromatograms of base fragments (±5ppm) were used for detection and quantification (152.0565 Da for G; 295.1028 Da for Q). The secondary base fragment 163.0608 was also used to confirm Q detection but not for quantification.

Calibration curves were previously generated using synthetic standards in the ranges of 0.2 to 40 pmol injected for G and 0.01 to 1 pmol for Q. Results are expressed as a percentage of total G.

UV sensitivity measurements

Overnight cultures were diluted 1:100 in MH medium and grown with agitation at 37°C until an OD 600 nm of 0.5-0.7. Appropriate dilutions were then plated on MH agar. The proportion of growing CFUs after irradiation at 60 Joules over total population before irradiation was calculated, doing a ratio with total CFUs. Experiments were performed 3 to 8 times.

Rifampicin and carbenicillin spontaneous mutation tests

Stationary phase cultures were plated in parallel on MH and MH plate supplemented with RIF: rifampicin 1 µg/mL, or CRB: 50 µg/mL. The mutation frequency was calculated as CFU MH + RIF or CRB/total CFU on MH.

Quantification and statistical analysis

For comparisons between 2 groups, first an F-test was performed in order to determine whether variances are equal or different between comparisons. For comparisons with equal variance, Student's t-test was used. For comparisons with significantly different variances, we used Welch's t-test. For multiple comparisons, we used ANOVA. We used GraphPad Prism to determine the statistical differences (*p*-value) between groups. **** means p<0.0001, *** means p<0.001, ** means p<0.01, * means p<0.05. For survival tests, data were first log transformed in order to achieve normal distribution, and statistical tests were performed on these log-transformed data. The number of replicates for each experiment was 3<n<6. Means and geometric means for logarithmic values were also calculated using GraphPad Prism.

Bioinformatic analysis for whole genome codon bias determinations.

Data

Genomic data (fasta files containing CDS sequences and their translation, and GFF annotations) for *Vibrio cholerae* (assembly ASM674v1) were downloaded from the NCBI FTP site (ftp://ftp.ncbi.nlm.nih.gov).

The GFF annotation file was used to establish a correspondence between locus tags present in the fasta files and old locus tags.

Codon counting

For each gene, the codons were counted in the CDS sequence, assuming it to be in-frame. Along with their codon counts, genes were flagged with information extracted from the fasta headers and their translation into amino-acids: first amino-acid, position of first stop codon, number of stops, whether start and end coordinates were reported as well-bounded or not.

This step was performed using Python 3.8.3, with the help of the Mappy 2.20 (86) and Pandas 1.2.4 (87,88) libraries.

Gene filtering

Genes whose CDS did not start with a valid start codon were excluded from further computations.

A valid start codon is one among ATA, ATC, ATG, ATT, CTG, GTG, TTG, according to the genetic code for bacteria, archaea and plastids (translation table 11 provided by the NCBI at ftp://ftp.ncbi.nlm.nih.gov/entrez/misc/data/gc.prt).

Among the 3594 genes, four (VC_RS01260 (VC0258), VC_RS04215, VC_RS15175 and VC_RS15675 (VC_A0473)) did not have a valid start codon. All four genes had a possibly ill-defined start position (start position prefixed by "<" in the header of the fasta file).

The only other gene whose CDS had a potentially ill-defined start position (VC_RS07425) started with a valid start codon and contained no internal stop codon. We assumed this CDS was in frame and not detrimental for the outcome of further analyses.

Among the remaining genes (valid start codon and well-defined start position) 69 have a CDS containing internal stop codons. Given the fact that stop read-through can happen(89), we decided to keep those genes nonetheless. Given the above considerations, further computations were performed on the 3590 genes that had a valid start codon.

Codon usage bias computation

The global codon counts were computed for each codon by summing over the above selected genes.

For each gene as well as for the global total, the codons were grouped by encoded amino-acid (with also a group for the stop codons). Within each group, the proportion of each codon was computed by dividing its count by the sum of the counts of the codons in the group.

The codon usage bias for a given codon and a given gene was then computed by subtracting the corresponding proportion obtained from the global counts from the proportion obtained for this gene. Codon usage biases were then standardized by dividing each of the above difference by the standard deviation of these differences across all genes, resulting in standardized codon usage biases "by amino-acid" ("SCUB by aa" in short).

All these computations were performed using the already mentioned Pandas 1.2.4 Python library.

Associating genes to their preferred codon

For each codon group, genes were associated to the codon for which they had the highest "SCUB by aa" value. This defined a series of gene clusters denoted using the "aa_codon" pattern. For instance, "*_TGA" contains the genes for which TGA is the codon with the highest standardized usage bias among stop codons.

Extracting most positively biased genes from each cluster

Within each cluster, the distribution of "SCUB by aa" values for each codon was represented using violin plots. Visual inspections of these violin plots revealed that in most cases, the distribution was multi-modal.

An automated method was devised to further extract from a given cluster the genes corresponding to the sub-group with the highest "SCUB by aa" for the corresponding codon.

This was done by estimating a density distribution for "SCUB by aa" values using a Gaussian Kernel Density Estimate and finding a minimum in this distribution. The location of this minimum was used as a threshold above which genes were considered to belong to the most positively biased genes.

This was done using the SciPy 1.7.0 (90) Python library.

Violin plots were generated using the Matplotlib 3.4.2 (91) and Seaborn 0.11.1 (92) Python libraries.

Code availability

All code to perform these analyses was implemented in the form of Python scripts, Jupyter notebooks (93) and Snakemake(94) workflows, and are available in the following git repository: https://gitlab.pasteur.fr/bli/17009_only. Data are available at zenodo public repository with the doi indicated below:

Table: Whole genome codon usage of *V. cholerae*. Excel sheet. 10.5281/zenodo.6875293

Tables: *V. cholerae* codon usage biased genes. 10.5281/zenodo.6875293

Table S1: Proteomics identify differentially abundant proteins

Uniprot	Gene Name	Fasta headers
	I - More abundant in WT	
	I – 1. PresentF606WT_AbsentJ420tgt	
Q9KTY9	tgt	Queuine tRNA-ribosyltransferase
Q9KNM6	VC_2706	queuosine precursor transporter
Q9KNH8	VC_2761	Bcr/CflA family efflux transporter
Q9KMV7	VC_A0211	Sensory box sensor histidine kinase
Q9KN55	VC_A0110	Uncharacterized protein
Q9KP41	VC_2538	Thiamine ABC transporter, permease protein,
Q9KTU0	VC_0798	Citrate lyase, beta subunit
Q9KSB8	VC_1340	PrpE protein
Q9KRW0	VC_1524	ABC transporter, permease protein
Q9KMB6	VC_A0457	Uncharacterized protein
Q9KUU0	VC_0425	lacZ
Q9KND5	VC_A0030	Uncharacterized protein
Q9KNP5	zapB	Cell division protein ZapB
Q9KUS6	VC_0439	ThrE_2 domain-containing protein
Q9KLK9	VC_A0734	Uncharacterized protein
Q9KRP8	VC_1588	Transcriptional regulator, LysR family
Q9KRB9	VC_1723	TVP38/TMEM64 family membrane protein
Q9KNT7	argB	Acetylglutamate kinase
Q9KRX3	VC_1510	Uncharacterized protein
Q9KPM7	VC_2340	HD-GYP domain-containing protein
Q9KL36	VC_A0913	Hemin ABC transporter, periplasmic hemin-binding protein HutB
Q9KVY3	VC_0005	Putative membrane protein insertion efficiency factor
Q9KQV1	VC_1897	Hit family protein
Q9KMY2	VC_A0184	cspE Cold shock DNA-binding domain protein
Q9KL45	VC_A0903	Uncharacterized protein glycertae kinase
Q9KRM7	VC_1609	Uncharacterized protein ABC-2 type transport system permease
Q9KSC1	VC_1337	Citrate synthase
Q9KLD9	VC_A0807	ABC transporter, periplasmic substrate-binding protein
Q9KT63	VC_1042	Long-chain fatty acid transport protein
Q9KN12	VC_A0154	Uncharacterized protein Na+:H+ antiporter subunit E
Q9KN05	tnaA	Tryptophanase
Q9KS94	queE	7-carboxy-7-deazaguanine synthase
Q9KQI2	tmk	Thymidylate kinase
Q9KVP6	ubiC	Probable chorismate pyruvate-lyase
Q9KMP2	VC_A0281	Integrase
Q9KUW3	VC_0396	Transcriptional regulator, LuxR family
Q9KUK3	VC_0515	Uncharacterized protein
Q9KSC8	VC_1330	Uncharacterized protein
Q9KUQ7	VC_0458	UPF0235 protein yggU

	I – 2. MoreF606wt_ThanJ420tgt		log2FC WT/tgt	p value	Adjusted p value
Q9KTJ4	gmhB	D-glycero-beta-D-manno-heptose-1,7-bisphosphate 7-phosphatase	3,51	0,0001	0,0005
Q9KTU3	VC_0795	Citrate/sodium symporter	3,46	0,0085	0,0068
Q9KSB4	VC_1345	Putative dioxygenase	3,35	0,0024	0,0034
Q9KS61	cheR2	Chemotaxis protein methyltransferase	2,93	0,0053	0,0050
Q9KN74	VC_A0091	UPF0251 protein VC_A0091	2,86	0,0013	0,0025
Q9KR81	VC_1762	EH_Signature domain-containing protein	2,54	0,0023	0,0034
Q9KM90	VC_A0491	Uncharacterized protein	2,26	0,0013	0,0025
Q9KQ10	VC_2197	Flagellar hook protein FlgE	2,23	0,0036	0,0042
Q9KVI7	murI	Glutamate racemase	2,11	0,0015	0,0028
Q9KV46	VC_0312	NAD(P)H-flavin reductase	2,10	0,0004	0,0014
Q9KL60	VC_A0888	Transcriptional regulator malT , LuxR family	2,01	0,0038	0,0042
Q9KSV5	VC_1151	Uncharacterized protein lysO	1,85	0,0003	0,0012
Q9KUR5	VC_0450	Membrane-bound lytic murein transglycosylase C	1,81	0,0057	0,0052
Q9KVM8	VC_0113	ubiG? Methyltransferase-related protein	1,76	0,0047	0,0046
Q9KPC7	VC_2445	gspA General secretion pathway protein A	1,75	0,0039	0,0042
Q9KNL2	nfuA	Fe/S biogenesis protein NfuA	1,68	0,0010	0,0022
Q9KVI5	VC_0161	Transcriptional activator IlvY	1,63	0,0128	0,0090
Q9KL10	VC_A0940	Transcriptional regulator, DeoR family	1,62	0,0003	0,0012
Q9KR73	VC_1770	Uncharacterized protein	1,52	0,0112	0,0082
Q9KKR5	VC_A1037	Amino acid ABC transporter, ATP-binding protein	1,43	0,0080	0,0065
H9L4R1	VC_0412	MshO Uncharacterized protein	1,43	0,0094	0,0071
Q9KKN4	VC_A1068	LRP Transcriptional regulator, AsnC family	1,43	0,0061	0,0053
P45784	epsN	Type II secretion system protein N	1,38	0,0022	0,0034
Q9KU51	VC_0673	Probable membrane transporter protein	1,37	0,0076	0,0063
Q9KNR9	VC_2662	Uncharacterized protein	1,24	0,0008	0,0019
Q9KRY1	rsmF	Ribosomal RNA small subunit methyltransferase F	1,18	0,0060	0,0053
Q9KLX1	VC_A0620	Thiosulfate sulfurtransferase SseA, putative	1,10	0,0020	0,0034
Q9KV88	VC_0268	ygaJ Uncharacterized protein	1,09	0,0070	0,0060
Q9KPI7	VC_2380	Cobalamin biosynthesis protein CbiB, putative	1,00	0,0042	0,0042
	I – 3. PresentF606TOB_AbsentJ420TOB				
P0C6D1	irgB	Iron-regulated virulence regulatory protein IrgB			
P0C6D6	tcpN	TCP pilus virulence regulatory protein			
Q56632	vibA	Vibriobactin-specific 2,3-dihydro-2,3-dihydroxybenzoate dehydrogenase			
Q9KKP3	VC_A1059	Putative pseudouridine methyltransferase			
Q9KL40	hutX	Intracellular heme transport protein HutX			
Q9KLG0	fabV2	Enoyl-[acyl-carrier-protein] reductase [NADH] 2			
Q9KLJ6	glpB	Anaerobic glycerol-3-phosphate dehydrogenase subunit B			
Q9KLR1	VC_A0681	33-cGAMP-specific phosphodiesterase 1			
Q9KMY6	pepT	Peptidase T			
Q9KNL4	bioH	Pimeloyl-[acyl-carrier protein] methyl ester esterase			
Q9KPE3	coaE	Dephospho-CoA kinase			
Q9KRQ1	VC_1585	Catalase			

Q9KS61	cheR2	Chemotaxis protein methyltransferase 2
Q9KSB4	VC_1345	Putative dioxygenase
Q9KSW7	hisI	Histidine biosynthesis bifunctional protein HisIE
Q9KTY9	tgt	Queuine tRNA-ribosyltransferase
Q9KU27	VC_0702	Inosine/xanthosine triphosphatase
H9L4T3	VC_2212	Uncharacterized protein
Q9K2M8	VC_A0348	Uncharacterized protein
Q9KKK0	VC_A1105	DNA-binding response regulator
Q9KKX8	VC_A0972	MFS domain-containing protein
Q9KL71	VC_A0876	D-serine deaminase activator
Q9KLB3	VC_A0833	Transcriptional regulator, LysR family
Q9KLG6	VC_A0778	AHS2 domain-containing protein
Q9KLK5	VC_A0738	Uncharacterized protein
Q9KLK9	VC_A0734	Uncharacterized protein
Q9KLQ1	VC_A0691	Acetoacetyl-CoA reductase
Q9KM02	VC_A0587	PPC domain-containing protein
Q9KM77	VC_A0511	Anaerobic ribonucleoside-triphosphate reductase
Q9KM86	VC_A0496	Glutathione S-transferase, putative
Q9KM98	VC_A0483	Uncharacterized protein
Q9KMX3	VC_A0193	Na+/H+ antiporter, putative
Q9KN01	VC_A0165	GGDEF family protein
Q9KN09	VC_A0157	NADH dehydrogenase, putative
Q9KN25	VC_A0141	C4-dicarboxylate transport sensor protein, putative
Q9KN46	VC_A0119	ImpA_N domain-containing protein
Q9KN85	VC_A0080	GGDEF family protein
Q9KN89	VC_A0076	Gate domain-containing protein
Q9KN99	VC_A0066	Uncharacterized protein
Q9KNA1	VC_A0064	TonB system receptor, putative
Q9KNA2	VC_A0063	Protease II
Q9KNB4	VC_A0051	Uncharacterized protein
Q9KNE3	VC_A0022	Glutathione S-transfersae-related protein
Q9KNF6	VC_A0008	Methyl-accepting chemotaxis protein
Q9KNM6	VC_2706	Probable queuosine precursor transporter
Q9KNN0	VC_2702	Transcriptional regulator, LuxR family
Q9KPD7	cpdA	3,5-cyclic adenosine monophosphate phosphodiesterase CpdA
Q9KPJ7	VC_2370	Sensory box/GGDEF family protein
Q9KPR2	VC_2304	Uncharacterized protein
Q9KPY8	VC_2224	GGDEF family protein
Q9KQ04	VC_2203	Flagellar protein, putative
Q9KQ78	fliP	Flagellar biosynthetic protein FliP
Q9KQN1	VC_1967	Methyl-accepting chemotaxis protein
Q9KQQ9	VC_1939	Uncharacterized protein
Q9KQW7	VC_1880	DUF2062 domain-containing protein
Q9KR48	VC_1798	Eha protein
Q9KRH6	VC_1666	VIBCH ABC transporter, ATP-binding protein, putative

Q9KRJ6	VC_1644	Uncharacterized protein			
Q9KRL9	VC_1617	Transcriptional regulator, LysR family			
Q9KRN2	VC_1604	Transcriptional regulatory protein			
Q9KRW9	VC_1515	Chaperone, formate dehydrogenase-specific, putative			
Q9KSC1	VC_1337	Citrate synthase			
Q9KSC6	VC_1332	Uncharacterized protein			
Q9KSC9	VC_1329	Opacity protein-related protein			
Q9KSE2	VC_1315	Sensor histidine kinase			
Q9KSP0	VC_1216	GGDEF family protein			
Q9KSV5	VC_1151	Uncharacterized protein			
Q9KT20	VC_1085	Sensor histidine kinase			
Q9KT74	VC_1031	Inosine monophosphate dehydrogenase-related protein			
Q9KTC3	VC_0979	Oxidoreductase, short-chain dehydrogenase/reductase family			
Q9KTI4	VC_0918	UDP-N-acetyl-D-mannosaminuronic acid dehydrogenase			
Q9KTV0	VC_0787	Transcriptional regulator, LysR family			
Q9KU51	VC_0673	Probable membrane transporter protein			
Q9KUQ1	VC_0464	Transcriptional regulator, LuxR family			
Q9KUW6	VC_0393	Uncharacterized protein			
Q9KV54	VC_0303	Sensor histidine kinase			
Q9KVM2	VC_0119	Uroporphyrinogen-III synthase			
Q9KVM8	VC_0113	Methyltransferase-related protein			
Q9KVP4	VC_0097	Flagellar protein FliL			
Q9KVS6	VC_0063	ThiF protein			
I – 4. MoreF606TOB_ThanJ420TOB			**log2 FC WT/tgt**	**p value**	**Adjusted p value**
Q9KMV8	VC_A0210	33-cGAMP-specific phosphodiesterase 2	5,21	0,00000	0,00005
Q9KSR2	VC_1194	J domain-containing protein	3,68	0,00929	0,00488
Q9KKY6	VC_A0964	Glycine cleavage operon activator, putative	5,30	0,00002	0,00043
Q9KKL6	VC_A1087	Anti-sigma F factor antagonist, putative	3,72	0,00060	0,00202
Q9KSK7	VC_1249	ACT domain-containing protein	2,37	0,00973	0,00488
Q9KS89	VC_1370	GGDEF family protein	3,51	0,00007	0,00062
Q9KNA0	VC_A0065	P/Homo B domain-containing protein	3,48	0,00876	0,00488
Q9KT21	VC_1084	Sensory box sensor histidine kinase	1,77	0,00183	0,00235
Q9KRA1	VC_1741	Transcriptional regulator, TetR family	1,71	0,01423	0,00606
Q9KU00	cutC	Copper homeostasis protein CutC	1,85	0,01810	0,00696
Q9KTH7	VC_0925	Polysaccharide biosynthesis protein, putative	3,09	0,00236	0,00256
Q9KSD3	VC_1325	Galactoside ABC transporter, periplasmic D-galactose/D-glucose-binding protein SV=1"	1,77	0,02018	0,00745
Q9KUU2	arcA	ARCA_VIBCH Arginine deiminase	2,78	0,00191	0,00235
Q9KLB8	phhA	PH4H_VIBCH Phenylalanine-4-hydroxylase	2,16	0,03098	0,00967
Q9KPI7	VC_2380	Cobalamin biosynthesis protein CbiB, putative	1,83	0,00973	0,00488
Q9KSE3	VC_1314	Transporter, putative	2,64	0,02472	0,00834
Q9KQX3	VC_1874	Uncharacterized protein	2,66	0,00403	0,00309
Q9KMJ2	VC_A0356	Uncharacterized protein	2,60	0,00439	0,00321
Q9KRW3	VC_1521	Sensor histidine kinase	2,69	0,00011	0,00085

Q9KN34	rbsK	Ribokinase	2,49	0,00270	0,00269
Q9KQX5	VC_1872	AAA_PrkA domain-containing protein	2,94	0,00216	0,00245
Q9KS12	rtxA	Multifunctional-autoprocessing repeats-in-toxin	3,68	0,01920	0,00716
Q9KQ01	VC_2206	Uncharacterized protein	2,76	0,00003	0,00043
P45774	epsH	Type II secretion system protein H	2,58	0,02202	0,00772
Q9KU02	VC_0728	PPK2 domain-containing protein	3,08	0,01270	0,00574
Q9KKL7	VC_A1086	Response regulator	2,65	0,02350	0,00806
Q9KSG5	VC_1291	Uncharacterized protein	3,38	0,00096	0,00223
Q9KSV0	VC_1156	Sensor histidine kinase	2,48	0,00113	0,00224
Q9KN48	VC_A0117	Sigma-54 dependent transcriptional regulator	1,56	0,00974	0,00488
Q9KRG0	VC_1682	Peptide ABC transporter, permease protein	2,56	0,00020	0,00109
Q9KRG1	VC_1681	Peptide ABC transporter, permease protein	2,86	0,00015	0,00099
Q9KSD1	mglA	Galactose/methyl galactoside import ATP-binding protein MglA	2,08	0,02068	0,00754
Q9KLT8	VC_A0653	PTS system, sucrose-specific IIBC component	2,43	0,00003	0,00043
P0C6Q8	dam	DNA adenine methylase	2,26	0,00448	0,00324
P0C6D3	vibB	Vibriobactin-specific isochorismatase	2,32	0,00194	0,00235
Q9KLF1	VC_A0795	Resolvase, putative	2,33	0,00078	0,00215
Q9KNN7	VC_2694	Superoxide dismutase	1,34	0,00647	0,00419
Q9KNW3	VC_2617	Arginine N-succinyltransferase OS=Vibrio cholerae serotype	1,27	0,02884	0,00915
Q9KUA1	VC_0622	Histidine kinase	1,89	0,00950	0,00488
Q9KQX9	VC_1868	Methyl-accepting chemotaxis protein	2,27	0,01417	0,00606
Q9KS63	VC_1397	Chemotaxis protein CheA	2,42	0,02557	0,00852
Q9KR16	VC_1831	Sensor histidine kinase	2,54	0,00188	0,00235
Q9KKR5	VC_A1037	Amino acid ABC transporter, ATP-binding protein	1,56	0,02096	0,00754
Q9KPK6	grcA	GRCA_VIBCH Autonomous glycyl radical cofactor	2,66	0,00332	0,00269
Q9KQX4	VC_1873	UPF0229 protein VC_1873	2,70	0,02180	0,00770
Q9KTI9	VC_0913	HlyD_D23 domain-containing protein	1,71	0,02570	0,00852
Q9KTC7	VC_0975	NfeD domain-containing protein	2,07	0,00048	0,00177
Q9KU65	VC_0658	C-di-GMP phosphodiesterase A-related protein	2,14	0,00930	0,00488
Q9KNB6	VC_A0049	GGDEF family protein	2,45	0,00175	0,00235
Q9KNY0	VC_2600	Uncharacterized protein	1,81	0,00123	0,00224
Q9KTF2	mrdA	Peptidoglycan D,D-transpeptidase MrdA	1,65	0,01002	0,00488
Q9KQY2	VC_1865	Uncharacterized protein	1,78	0,00316	0,00269
Q9KL39	VC_A0909	Oxygen-independent coproporphyrinogen III oxidase, putative	2,04	0,01389	0,00602
Q9KVF6	VC_0190	DNA helicase uvrD	1,94	0,01686	0,00663
Q9KUM9	VC_0486	Transcriptional regulator, DeoR family	1,92	0,03066	0,00961
Q9KRI2	VC_1659	Uncharacterized protein	2,10	0,01469	0,00612
Q9KNJ0	VC_2748	Nitrogen regulation protein	1,87	0,00126	0,00224
Q9KP22	VC_2557	Uncharacterized protein OS	1,81	0,00291	0,00269
Q9KRV1	VC_1533	DTW domain-containing protein	1,83	0,00205	0,00235
Q9KQC8	VC_2072	Peptidase, insulinase family	1,58	0,00893	0,00488
Q9KUM3	VC_0492	Uncharacterized protein	2,34	0,00243	0,00259
Q9KQI3	VC_2015	DNA polymerase III, delta prime subunit	1,77	0,00063	0,00202
Q9KPT7	crl	Sigma factor-binding protein Crl	1,58	0,00088	0,00219

Q9KS69	VC_1390	Transcriptional regulator, LysR family	1,89	0,00007	0,00062
Q9KSC3	VC_1335	Transcriptional regulator, GntR family	1,55	0,00321	0,00269
Q9KRL1	VC_1629	Uncharacterized protein	1,89	0,00322	0,00269
Q9KLS5	VC_A0666	L-serine dehydratase	1,71	0,00079	0,00215
Q9KM52	VC_A0537	Uncharacterized protein	1,27	0,01088	0,00511
Q9KRI6	VC_1655	Magnesium transporter MgtE	1,72	0,00363	0,00282
Q9KTJ1	VC_0911	Trehalose-6-phosphate hydrolase	1,70	0,00042	0,00166
Q9KPZ9	VC_2208	Uncharacterized protein	1,79	0,01534	0,00629
Q9KM32	VC_A0557	GGDEF family protein	1,37	0,02135	0,00762
Q9KSA6	VC_1353	GGDEF family protein	1,52	0,00156	0,00231
Q9KUC2	VC_0600	AB hydrolase-1 domain-containing protein	1,72	0,00123	0,00224
Q9KM15	VC_A0574	N-acetyltransferase domain-containing protein	1,39	0,01767	0,00683
Q9KS83	VC_1376	GGDEF family protein	1,51	0,00363	0,00282
Q9KPT2	VC_2280	Uncharacterized protein	1,45	0,00471	0,00331
Q9KVN8	VC_0103	Uncharacterized protein	1,55	0,00249	0,00262
Q9KT24	VC_1081	Response regulator	1,65	0,02632	0,00861
Q9KRJ1	VC_1649	Trypsin, putative	1,54	0,00092	0,00220
Q9KLP6	VC_A0697	Sensory box/GGDEF family protein	1,63	0,00022	0,00109
Q9KQ23	ispE	ISPE_VIBCH 4-diphosphocytidyl-2-C-methyl-D-erythritol kinase ispE	1,57	0,00119	0,00224
H9L4T1	VC_A0450	Uncharacterized protein	1,76	0,00290	0,00269
Q9KU16	VC_0714	Uncharacterized protein	1,60	0,02409	0,00820
Q9KRS6	katG	KATG_VIBCH Catalase-peroxidase katG	1,39	0,01256	0,00571
P29485	tcpP	Toxin coregulated pilus biosynthesis protein P tcpP	1,56	0,00124	0,00224
Q9KU53	rppH	RPPH_VIBCH RNA pyrophosphohydrolase rppH	2,03	0,00467	0,00331
Q9KKX3	VC_A0977	ABC transporter, ATP-binding protein	1,84	0,02092	0,00754
Q9KQL5	VC_1983	Peptidase, putative	2,47	0,02205	0,00772
Q9KSG0	VC_1296	Phosphomethylpyrimidine kinase	3,54	0,00005	0,00054
Q9KPJ4	VC_2373	Glutamate synthase, large subunit	1,53	0,00120	0,00224
Q9KS96	VC_1363	Siroheme synthase component enzyme	1,31	0,00930	0,00488
Q9KP89	VC_2484	Long-chain-fatty-acid--CoA ligase, putative	1,53	0,00535	0,00367
Q9KSM2	VC_1234	Exodeoxyribonuclease I	1,59	0,02087	0,00754
Q9KSX5	VC_1131	Na_H_antiporter domain-containing protein	2,07	0,01089	0,00511
Q9KTJ2	VC_0910	PTS system, trehalose-specific IIBC component	1,33	0,00205	0,00235
Q9KKZ7	VC_A0953	Peptidyl-prolyl cis-trans isomerase C	1,30	0,00997	0,00488
Q9KUU7	VC_0418	dTTP/UTP pyrophosphatase	1,24	0,00258	0,00267
Q9KV39	birA	Bifunctional ligase/repressor BirA	1,47	0,00649	0,00419
Q9KS28	VC_1433	Uncharacterized protein	1,23	0,00965	0,00488
Q9KMM4	VC_A0307	HNHc domain-containing protein	1,46	0,00110	0,00224
Q9KUJ8	VC_0522	Beta-ketoadipate enol-lactone hydrolase, putative	1,37	0,00202	0,00235
Q9KVT7	purE	N5-carboxyaminoimidazole ribonucleotide mutase	1,45	0,00886	0,00488
Q9KRU5	VC_1539	Probable ketoamine kinase VC_1539	1,09	0,01619	0,00652
Q9KSU7	serC	Phosphoserine aminotransferase	1,41	0,00147	0,00231
Q9KQU2	VC_1906	Methyltranfer_dom domain-containing protein	2,00	0,00065	0,00202
Q9KRW4	VC_1520	ABC transporter, ATP-binding protein	1,17	0,00887	0,00488
Q9KU52	VC_0672	Phosphoenolpyruvate-protein phosphotransferase	1,41	0,00145	0,00231
Q9KLI6	VC_A0758	Arginine ABC transporter, permease protein	1,24	0,01152	0,00534

Q9KPQ9	panE	2-dehydropantoate 2-reductase	1,32	0,02013	0,00745
Q9KNW7	VC_2613	Phosphoribulokinase	1,22	0,00346	0,00278
Q9KT18	VC_1087	Response regulator	1,12	0,00908	0,00488
Q9KPP6	recB	RecBCD enzyme subunit RecB	1,24	0,00085	0,00218
Q9KQK1	VC_1997	Uncharacterized protein	1,16	0,00200	0,00235
Q9KUN3	argP	ARGP_VIBCH HTH-type transcriptional regulator ArgP	1,53	0,00885	0,00488
Q9KMW8	VC_A0198	Site-specific DNA-methyltransferase, putative	1,15	0,00300	0,00269
Q9KVB8	VC_0228	Uncharacterized protein	1,27	0,00223	0,00248
Q9KVE7	VC_0199	Hemolysin secretion ATP-binding protein, putative	1,29	0,00999	0,00488
Q9KQM5	menB	1,4-dihydroxy-2-naphthoyl-CoA synthase menB	1,40	0,00328	0,00269
Q9KR89	VC_1753	Paraquat-inducible protein A	1,11	0,00739	0,00467
Q9KQJ7	VC_2001	Putative glucose-6-phosphate 1-epimerase	1,57	0,01040	0,00501
P57070	lolB	Outer-membrane lipoprotein LolB	1,04	0,01285	0,00577
Q9KL63	VC_A0884	Uncharacterized protein	1,15	0,02695	0,00863
H9L4P1	VC_0259	Lipopolysaccharide biosynthesis protein RfbV	1,21	0,00560	0,00377
Q9KMU4	VC_A0225	Glutamine amidotransferase type-2 domain-containing protein	1,14	0,00164	0,00235
Q9KKU5	VC_A1005	Transcriptional regulator, MarR family	1,14	0,02484	0,00834
Q9KVK1	VC_0142	DUF4145 domain-containing protein	1,20	0,01451	0,00609
Q9KVB5	VC_0231	Uncharacterized protein	1,09	0,00932	0,00488
Q9KKS4	VC_A1026	Uncharacterized protein	1,31	0,00883	0,00488
Q9KUU0	VC_0425	Uncharacterized protein	1,54	0,01872	0,00702
Q9KTA5	VC_0998	Uncharacterized protein	1,15	0,00530	0,00367
Q9KNC4	gltS	Sodium/glutamate symporter	1,21	0,02667	0,00862
Q9KRS8	VC_1558	6-phospho-beta-glucosidase	1,37	0,00196	0,00235
Q9KMT9	VC_A0230	Iron(III) ABC transporter, ATP-binding protein	1,08	0,01196	0,00547
Q9KPZ0	VC_2222	Smr domain-containing protein	1,04	0,02562	0,00852
Q9KQE2	VC_2058	Uncharacterized protein	1,05	0,00651	0,00419
P57066	lolD	LOLD_VIBCH Lipoprotein-releasing system ATP-binding protein LolD	1,01	0,00981	0,00488
Q9KLE5	VC_A0801	Q9KLE5_VIBCH Inosine-guanosine kinase	1,00	0,02622	0,00861
Q9KS35	VC_1426	Spermidine/putrescine ABC transporter, permease protein	1,11	0,00158	0,00231
Q9KSV4	VC_1152	HDOD domain-containing protein	1,07	0,00926	0,00488
Q9KUM2	VC_0493	Q9KUM2_VIBCH Uncharacterized protein	1,76	0,01375	0,00600
Q9KNA9	VC_A0056	Q9KNA9_VIBCH Transcriptional regulator, MerR family	1,07	0,01454	0,00609
Q9KQ71	VC_2130	Flagellum-specific ATP synthase FliI	1,15	0,00357	0,00282
Q9KLD8	VC_A0808	NodN-related protein	1,27	0,00802	0,00488
Q9KP78	VC_2497	HD-GYP domain-containing protein	1,09	0,00149	0,00231
Q60153	tcpA	TCPA_VIBCH Toxin coregulated pilin	1,01	0,02653	0,00862
Q9KRU1	VC_1543	Uncharacterized protein	1,09	0,00268	0,00269
Q9KQ38	VC_2166	Trp repressor-binding protein	1,46	0,01086	0,00511
Q9KQN3	VC_1965	TetR_C_33 domain-containing protein	1,28	0,00698	0,00445
Q9KN86	VC_A0079	Uncharacterized protein	1,23	0,00556	0,00377
Q9KRD3	VC_1709	Zinc protease, insulinase family	1,25	0,00993	0,00488
Q9KKS7	VC_A1023	Uncharacterized protein	1,16	0,00537	0,00367

Q9KVB7	VC_0229	Uncharacterized protein	1,66	0,01838	0,00696
Q9KNR2	VC_2669	5-carboxymethyl-2-hydroxymuconate delta isomerase, putative	1,22	0,01524	0,00628
Q9KUI6	mutS	MUTS_VIBCH DNA mismatch repair protein MutS	1,07	0,00298	0,00269
Q9KVF0	VC_0196	ATP-dependent DNA helicase RecQ	1,04	0,00303	0,00269
Q9KTJ3	VC_0909	Trehalose operon repressor	1,03	0,00981	0,00488
Q9KVH1	VC_0175	Deoxycytidylate deaminase-related protein	1,28	0,01307	0,00584
Q9KR77	VC_1766	Uncharacterized protein	1,01	0,01408	0,00606
Q9KTL4	truC	tRNA pseudouridine synthase C truC	1,09	0,00416	0,00310
Q9KUM4	VC_0491	Uncharacterized protein	1,10	0,00571	0,00379
P52022	dnaE	DNA polymerase III subunit alpha	1,07	0,00324	0,00269
Q9KP97	VC_2476	UPF0149 protein VC_2476	1,70	0,02715	0,00865
Q9KS92	VC_1367	GGDEF family protein	1,19	0,00957	0,00488
Q9KU08	ppx	Exopolyphosphatase ppx	1,04	0,01694	0,00663
Q9KSI6	VC_1270	Glyoxylase II family protein	1,32	0,01645	0,00653
Q9KRA6	bpt	Aspartate/glutamate leucyltransferase bpt	1,04	0,01838	0,00696
Q9KQF5	topB	DNA topoisomerase 3 topB	1,05	0,02938	0,00928
Q9KNF3	malT	HTH-type transcriptional regulator MalT	1,10	0,00227	0,00249
Q9KPE8	VC_2420	Flavodoxin	1,39	0,00897	0,00488
Q9KNT4	ppc	Phosphoenolpyruvate carboxylase ppc	1,05	0,00302	0,00269
Q9KU29	VC_0700	Soluble lytic murein transglycosylase	1,07	0,00291	0,00269
Q9KQV0	VC_1898	Methyl-accepting chemotaxis protein	1,01	0,00574	0,00379
Q9KPE7	VC_2421	ampD protein	1,04	0,02430	0,00824
Q9KU20	rluD	Ribosomal large subunit pseudouridine synthase D rluD	1,03	0,00290	0,00269
Q9KNQ5	VC_2676	Cell division protein FtsN, putative	1,20	0,01452	0,00609
H9L4T5	VC_0847	Integrase, phage family	1,28	0,02687	0,00863
Q9KQ28	VC_2176	UPF0162 protein VC_2176	1,04	0,00311	0,00269
Q9KUC0	mrcB	PBPB_VIBCH Penicillin-binding protein 1B	1,15	0,01050	0,00502
Q9KPV6	uppS	UPPS_VIBCH Ditrans,polycis-undecaprenyl-diphosphate synthase	1,03	0,00800	0,00488
Q9KVU5	rsmB	RSMB_VIBCH Ribosomal RNA small subunit methyltransferase B	1,02	0,01178	0,00542
Q9KMC3	VC_A0441	Uncharacterized protein	1,17	0,00930	0,00488
Q9KVL9	VC_0122	Adenylate cyclase	1,23	0,02356	0,00806
Q9KUW9	metH	Methionine synthase	1,28	0,02670	0,00862
Q9KL09	VC_A0941	Acyl-CoA thioester hydrolase-related protein	1,03	0,02584	0,00853
Q9KMY4	VC_A0182	Sigma-54 dependent transcriptional regulator	1,00	0,00859	0,00488
Q9KQ13	flgH	Flagellar L-ring protein	1,06	0,01335	0,00593
Q9KT38	VC_1067	GGDEF domain-containing protein	1,04	0,02971	0,00935
Q9KM78	VC_A0510	Uncharacterized protein	1,01	0,01640	0,00653
P0C6R0	irgA	IRGA_VIBCH Iron-regulated outer membrane virulence protein	1,03	0,02028	0,00745
Q9KPD8	VC_2432	Uncharacterized protein	1,23	0,03115	0,00968
Q9KVS4	thiG	THIG_VIBCH Thiazole synthase	1,50	0,03191	0,00983
Q9KMG4	higA-1	Antitoxin HigA-1	1,30	0,01712	0,00665
Q9KUY5	VC_0373	Uncharacterized protein	1,25	0,02357	0,00806
Q9KMG8	VC_A0388	Uncharacterized protein	1,58	0,00081	0,00215

Uniprot	Gene Name	Fasta headers			
		II - More abundant in _Δtgt_			
		II – 1. PresentJ420tgt_AbsentF606wt			
O34419	rstR1	Cryptic phage CTXphi transcriptional repressor RstR			
Q9KN37	rbsA	Ribose import ATP-binding protein RbsA			
Q9KT77	moaE	Molybdopterin synthase catalytic subunit			
Q9KVG9	vspR	Transcriptional regulator VspR			
H9L4R3	VC_A0444	RelE protein			
Q9KKW7	VC_A0983	L-lactate permease			
Q9KL14	VC_A0935	Uncharacterized protein			
Q9KLD8	VC_A0808	NodN-related protein			
Q9KLF6	VC_A0788	DnaJ-related protein			
Q9KLJ2	VC_A0752	Thioredoxin 2			
Q9KLV6	VC_A0635	Transcriptional regulator, LysR family			
Q9KM02	VC_A0587	PPC domain-containing protein			
Q9KM27	VC_A0562	Uncharacterized protein			
Q9KMP9	VC_A0271	Uncharacterized protein			
Q9KNC6	VC_A0039	Uncharacterized protein			
Q9KNE3	VC_A0022	Glutathione S-transfersae-related protein			
Q9KNI2	VC_2757	Uncharacterized protein			
Q9KNM7	VC_2705	Sodium/solute symporter, putative			
Q9KPF0	VC_2418	Thiol:disulfide interchange protein			
Q9KQ76	VC_2125	Flagellar motor switch protein FliN			
Q9KQG6	VC_2032	Uncharacterized protein			
Q9KQS3	VC_1925	C4-dicarboxylate transport sensor protein			
Q9KR71	VC_1772	WYL domain-containing protein			
Q9KRG4	VC_1678	Phage shock protein A			
Q9KRH0	VC_1672	DNA-3-methyladenine glycosidase I			
Q9KRM1	VC_1615	Uncharacterized protein			
Q9KRR5	VC_1571	Quinol oxidase, subunit I			
Q9KSM4	VC_1232	Uncharacterized protein			
Q9KSN9	VC_1217	N-acetyltransferase domain-containing protein			
Q9KTS9	VC_0809	SWIM-type domain-containing protein			
Q9KTV0	VC_0787	Transcriptional regulator, LysR family			
Q9KUN2	VC_0483	Uncharacterized protein			
Q9KUW6	VC_0393	Uncharacterized protein			
Q9KVR9	VC_0070	Uncharacterized protein			
		II – 2. MoreJ420tgt_ThanF606wt	**log2 wt/tgt**	**p value**	**Adjusted p value**
Q9KNX3	kefG	Glutathione-regulated potassium-efflux system ancillary protein KefG	-7,30	0,00001	0,00036
Q9KLB8	phhA	Phenylalanine-4-hydroxylase	-4,14	0,00010	0,00068
P09545	hlyA	Hemolysin	-3,90	0,00039	0,00140

Q9KQN1	VC_1967	Methyl-accepting chemotaxis protein	-3,84	0,00567	0,00521
Q9KV16	queG	Epoxyqueuosine reductase	-3,39	0,00416	0,00420
H9L4T3	VC_2212	Uncharacterized protein - putative Fe3+-citrate ABC transporter	-3,32	0,00017	0,00094
Q9KTJ9	syd	Syd	-3,29	0,00057	0,00177
Q9KNW3	VC_2617	Arginine N-succinyltransferase	-2,93	0,00002	0,00050
Q9KU56	mutH	DNA mismatch repair protein MutH	-2,90	0,00004	0,00050
Q9KTZ6	VC_0734	Malate synthase	-2,81	0,00306	0,00389
Q9KKQ7	mtlA	PTS system mannitol-specific EIICBA component	-2,80	0,00214	0,00343
Q9KLB3	VC_A0833	Transcriptional regulator, LysR family	-2,66	0,00379	0,00420
Q9KTM2	VC_0880	Uncharacterized protein	-2,50	0,00364	0,00420
Q9KSQ4	hutH	Histidine ammonia-lyase	-2,42	0,00105	0,00227
Q9KPR5	VC_2301	Transcriptional activator, putative	-2,39	0,00075	0,00195
Q9KNF6	VC_A0008	Methyl-accepting chemotaxis protein	-2,27	0,00264	0,00357
Q9KRF2	VC_1690	Alpha-1,6-galactosidase, putative	-2,25	0,00022	0,00110
Q9KS52	VC_1408	Transcriptional regulator, TetR family	-2,20	0,00047	0,00154
Q9KUN3	argP	HTH-type transcriptional regulator ArgP	-2,20	0,00006	0,00050
Q9KU74	VC_0649	Transcriptional regulator, MarR family	-2,08	0,00232	0,00343
Q9KRA1	VC_1741	Transcriptional regulator, TetR family	-2,03	0,00074	0,00195
Q9KQ71	VC_2130	Flagellum-specific ATP synthase FliI	-1,89	0,00016	0,00094
Q9KUU2	arcA	Arginine deiminase	-1,88	0,00990	0,00732
Q9KM69	VC_A0519	Fructose repressor	-1,80	0,00183	0,00331
Q9KS51	VC_1409	Multidrug resistance protein, putative	-1,77	0,00895	0,00699
Q9KS17	VC_1444	Uncharacterized protein	-1,73	0,01228	0,00882
P0C6Q5	tcpF	Toxin coregulated pilus biosynthesis protein F	-1,72	0,00006	0,00050
Q9KVH8	VC_0168	Cytochrome c5	-1,65	0,00187	0,00331
Q9KP69	VC_2507	PINc domain-containing protein	-1,62	0,00903	0,00699
Q9KM51	VC_A0538	Cytochrome b561, putative	-1,62	0,00417	0,00420
Q9KTY1	VC_0749	Iron-sulfur cluster assembly scaffold protein IscU	-1,59	0,00072	0,00195
Q9KMJ5	VC_A0351	Uncharacterized protein	-1,56	0,00615	0,00534
Q9KS13	VC_1449	Uncharacterized protein	-1,54	0,01266	0,00895
Q9KLM0	VC_A0723	3-hydroxy-3-methylglutaryl CoA reductase	-1,53	0,00266	0,00357
Q9KV51	VC_0306	Thioredoxin	-1,50	0,00255	0,00357
Q9KRR1	VC_1575	Uncharacterized protein	-1,32	0,00274	0,00358
Q9F854	hisD	Histidinol dehydrogenase	-1,28	0,00385	0,00420
Q9KUS1	pdxA	4-hydroxythreonine-4-phosphate dehydrogenase	-1,25	0,00082	0,00195
Q9KSI8	VC_1268	Uncharacterized protein	-1,13	0,00714	0,00600
Q9KPA8	VC_2465	Sigma-E factor regulatory protein RseB	-1,08	0,00400	0,00420
Q9KLG6	VC_A0778	AHS2 domain-containing protein	-1,08	0,00343	0,00420
Q9KVJ1	VC_0153	Uncharacterized protein	-1,05	0,00936	0,00708
	II – 3. PresentJ420tgtTOB_AbsentF606wtTOB				
Q9KNM4	gmk	Guanylate kinase			
Q9KNC1	VC_A0044	Uncharacterized protein put mb protease https://www.researchgate.net/figure/Fig-S22-Effect-			

		of-Transposon-Insertion-in-Candidate-Protease-Genes-on-TcpP-Stability_fig7_295417927			
Q9KRS9	VC_1557	Transcriptional regulator, LacI family lipid A biosynthesis acyltransferase			
Q9KQH2	VC_2026	Uncharacterized protein rRNA accumulation protein YceD			
Q9KRR2	VC_1574	Uncharacterized protein put Transmembrane signal peptide protein			
Q9KT04	VC_1101	Uncharacterized protein putative tryptophan/tyrosine transport system substrate-binding protein or T6SS			
Q9KVH8	VC_0168	Cytochrome c5			
Q9KR31	VC_1816	Uncharacterized protein 1 HYP TRANSPORTER			
Q9KQN0	VC_1968	Transcriptional regulator, HTH_3 family sutR regulator utilization of sulfur			
Q9KNT7	argB	Acetylglutamate kinase ornithine and arginine biosynthesis			
Q9KU61	VC_0662	Branched-chain amino acid transport system carrier protein brnQ transport leucine, valine, and isoleucine			
Q9KPR5	VC_2301	Transcriptional activator, putative putative anti-ECFsigma factor, ChrR			
Q9KQ26	prmC	Release factor glutamine methyltransferase			
Q9KM00	VC_A0589	Peptide ABC transporter, permease protein, putative oligopeptide ABC transporter membrane subunit YejE			
Q9KVR7	VC_0072	Sensory box/GGDEF family protein			
II – 4. MoreJ420tgtTOB_ThanF606wtTOB			**log2 wt/tgt**	**p value**	**Adjusted p value**
Q9KSP4	VC_1212	DNA polymerase	-2,38	0,01099	0,00512
Q9KR61	nanK	N-acetylmannosamine kinase	-4,31	0,00003	0,00043
Q9KT86	rnfA/rsxA	Ion-translocating oxidoreductase complex subunit A	-3,56	0,00002	0,00043
Q9KRT1	VC_1555	Uncharacterized protein	-1,48	0,00902	0,00488
Q9KV51	VC_0306	Thioredoxin trxA	-1,69	0,02226	0,00776
Q9KM51	VC_A0538	Cytochrome b561, putative	-2,87	0,00756	0,00474
Q9KNR9	VC_2662	Uncharacterized protein	-1,31	0,03255	0,00995
Q9KR73	VC_1770	Uncharacterized protein	-1,31	0,01849	0,00696
P0C6C8	fur	Ferric uptake regulation protein	-2,39	0,00030	0,00141
Q9KMN5	VC_A0293	Uncharacterized protein	-2,14	0,00017	0,00099
Q9KV88	VC_0268	Uncharacterized protein	-2,11	0,00406	0,00309
Q9KNQ9	rraA	Regulator of ribonuclease activity A	-2,42	0,00310	0,00269
Q9KPZ5	VC_2217	Beta-N-acetylhexosaminidase	-2,91	0,00054	0,00191
Q9KTN7	tadA	tRNA-specific adenosine deaminase	-2,04	0,00110	0,00224
Q9KRP5	VC_1591	Oxidoreductase, short-chain dehydrogenase/reductase family	-2,14	0,00804	0,00488
P0C6C4	flaB	Flagellin B	-1,88	0,00131	0,00228
Q9KTZ8	VC_0732	Transcriptional regulator, LysR family oxyR like	-1,96	0,00070	0,00210
Q9KSV6	VC_1150	Uncharacterized protein	-1,29	0,01007	0,00488
Q9KVM9	VC_0112	Cytochrome c4	-2,60	0,01486	0,00616
Q9KVK6	cdgJ	Cyclic di-GMP phosphodiesterase CdgJ	-3,89	0,00017	0,00099
Q9KR96	VC_1746	Transcriptional regulator, TetR family	-1,85	0,00299	0,00269

P0C6C5	flaC	Flagellin C OS=Vibrio cholerae serotype	-1,82	0,00042	0,00166
Q9KPX7	VC_2235	Methyltransf_11 domain-containing protein	-1,53	0,00144	0,00231
Q9KL76	VC_A0871	Transcriptional regulator, GntR family	-1,20	0,00284	0,00269
Q9KQ58	VC_2146	Uncharacterized protein	-1,38	0,00181	0,00235
Q9KKP2	ribB	3,4-dihydroxy-2-butanone 4-phosphate synthase	-2,73	0,00036	0,00157
Q9KNL7	greB	Transcription elongation factor GreB	-2,29	0,02154	0,00765
Q9KV61	VC_0296	Biotin carboxyl carrier protein of acetyl-CoA carboxylase	-1,70	0,00429	0,00317
Q9KUN2	VC_0483	Uncharacterized protein	-1,46	0,00180	0,00235
P0C6P9	tpx	Thiol peroxidase	-1,42	0,01847	0,00696
Q9KN91	VC_A0074	GGDEF family protein	-1,35	0,00934	0,00488
Q9KV27	nudC	NADH pyrophosphatase	-1,38	0,00104	0,00224
Q9KTF3	mrdB	Peptidoglycan glycosyltransferase	-1,35	0,00766	0,00476
Q9F854	hisD	Histidinol dehydrogenase	-1,60	0,00994	0,00488
Q9KV12	miaA	tRNA dimethylallyltransferase	-1,44	0,00177	0,00235
Q9KT82	VC_1023	Putative gluconeogenesis factor	-1,72	0,02103	0,00754
Q9KKQ1	VC_A1051	Uncharacterized protein	-1,32	0,00452	0,00324
Q9KKZ9	VC_A0951	UPF0145 protein VC_A0951	-1,30	0,01376	0,00600
Q9KLK6	luxP	Autoinducer 2-binding periplasmic protein LuxP	-1,19	0,00413	0,00310
Q9KTX4	ndk	Nucleoside diphosphate kinase	-1,10	0,01640	0,00653
Q9KMJ8	VC_A0345	Uncharacterized protein	-1,18	0,01699	0,00663
Q9KU82	rimP	Ribosome maturation factor RimP	-1,24	0,01367	0,00600
Q9KSF3	VC_1303	Para-aminobenzoate synthase, component I	-1,14	0,02352	0,00806
Q9KS93	queC	7-cyano-7-deazaguanine synthase	-1,01	0,01568	0,00635
Q9KQM0	VC_1978	5-deoxynucleotidase	-1,18	0,00153	0,00231
Q9KST2	trpE	Anthranilate synthase component 1	-1,86	0,03127	0,00968
Q9KN74	VC_A0091	UPF0251 protein	-1,10	0,01555	0,00634
Q9KL95	VC_A0851	HATPase_c domain-containing protein	-1,55	0,00154	0,00231
Q9KNJ9	VC_2739	AsmA domain-containing protein	-1,16	0,03228	0,00991

Tables S2. RNA-seq V. cholerae WT/Δtgt, in MH and TOB. Only significant differences higher than 2-fold are shown.

MH					
locus_tag	old_locus_tag	gene	baseMean	log2FC WT/Δtgt	padj
VC_RS03715	VC0741,VC_0741	tgt	3412	6,91	3,3E-168
VC_RS13030	VC2706,VC_2706	yhhQ	5207	5,12	4,6E-148
VC_RS17680	VC_A0913,VCA0913	hutB	298	3,23	1,1E-06
VC_RS17670	VC_A0911,VCA0911	exbB	234	3,18	5,8E-07
VC_RS17690	VC_A0915,VCA0915	hutD	131	2,91	3,5E-05
VC_RS17675	VC_A0912,VCA0912	exbD	329	2,88	1,6E-09
VC_RS17685	VC_A0914,VCA0914	btuC/fecCD	362	2,80	2,7E-05
VC_RS03875	VC0773,VC_0773	entC	64	2,53	2,4E-04
VC_RS16165	VC_A0576,VCA0576	hutA	4750	2,51	5,1E-06
VC_RS17665	VC_A0910,VCA0910	tonB1	400	2,46	9,5E-07
VC_RS14430	VC_A0229,VCA0229	febD	356	2,44	1,4E-07
VC_RS17655	VC_A0908,VCA0908	hutX	1037	2,37	9,5E-07
VC_RS14435	VC_A0230,VCA0230	fhuC	617	2,34	1,7E-04
VC_RS17660	VC_A0909,VCA0909	hutW	1132	2,23	7,3E-07
VC_RS02435	VC0475,VC_0475	cirA	826	2,02	1,7E-03
VC_RS14425	VC_A0228,VCA0228	fepD	454	2,02	1,9E-07
VC_RS17650	VC_A0907,VCA0907	hutZ	3146	1,87	8,8E-06
VC_RS17955	VC_A0977,VCA0977	yejF	454	1,81	3,9E-08
VC_RS14420	VC_A0227,VCA0227	gcvH	2378	1,78	1,4E-05
VC_RS17950	VC_A0976,VCA0976		103	1,70	2,7E-02
VC_RS08170	VC1688,VC_1688	mglC	137	1,65	1,2E-02
VC_RS07460	VC1542,VC_1542	ligA	54	1,64	1,3E-04
VC_RS03070	VC0606,VC_0606	glnK	174	1,59	7,0E-03
VC_RS07475	VC1545,VC_1545	exbB	306	1,54	1,3E-04
VC_RS07470	VC1544,VC_1544	exbD	354	1,46	4,2E-04
VC_RS16600	VC_A0676,VCA0676	napF	1952	1,45	4,1E-02
VC_RS13690	VC_A0064,VCA0064	thiS	198	1,44	1,8E-03
VC_RS13695	VC_A0065,VCA0065	thiG	180	1,42	6,3E-04
VC_RS01835	VC0365,VC_0365	bfr	2422	1,39	1,1E-06
VC_RS07465	VC1543,VC_1543		1162	1,39	3,2E-04
VC_RS10685	VC2210,VC_2210	viuB	550	1,34	8,9E-04
VC_RS02430	VC0474,VC_0474	irgB	157	1,33	1,8E-02
VC_RS07595	VC1572,VC_1572		27	1,28	2,9E-02
VC_RS00985	VC0201,VC_0201	fhuC	92	1,27	3,2E-02
VC_RS00980	VC0200,VC_0200	fhuA	2454	1,25	3,7E-03
VC_RS07600	VC1573,VC_1573	fumC	197	1,25	9,7E-05
VC_RS10690	VC2211,VC_2211	viuA	527	1,24	4,5E-05
VC_RS07480	VC1546,VC_1546	exbB	303	1,23	2,0E-03
VC_RS03900	VC0778,VC_0778	fepG	53	1,19	4,6E-02
VC_RS03080	VC0608,VC_0608	fbpA	4516	1,18	1,3E-04

VC_RS13685	VC_A0063,VCA0063	ptrB	280	1,16	5,1E-03
VC_RS04975	VC1009,VC_1009		505	1,16	1,1E-05
VC_RS02570	VC0504,VC_0504	susC (tonB-like)	42	1,11	3,2E-02
VC_RS06170	VC1265,VC_1265	cytochrome C	511	1,10	1,3E-02
VC_RS07485	VC1547,VC_1547	exbB	692	1,09	6,0E-04
VC_RS05755	VC1174,VC_1174	trpE	263	1,07	9,7E-05
VC_RS03865	VC0771,VC_0771	vibB	412	1,06	1,1E-03
VC_RS16595	VC_A0675,VCA0675	narQ	770	1,03	4,9E-02
VC_RS16075	VC_A0558,VCA0558	yfjD	516	1,03	2,5E-02
VC_RS01830	VC0364,VC_0364	bfd	321	1,02	8,2E-03
VC_RS14440	VC_A0231,VCA0231	yqhC	272	1,00	2,7E-02
VC_RS02480	VC0486,VC_0486	srlR	748	1	3,2E-03
VC_RS12970	VC2694,VC_2694	sodA	503	0,80	5,1E-03

TOB					
locus_tag	old_locus_tag	gene	baseMean	log2FoldChange WT/Δtgt	padj
VC_RS03715	VC0741,VC_0741	tgt	3412	5,991	5,0E-181
VC_RS13030	VC2706,VC_2706	yhhQ	5207	4,392	6,2E-114
VC_RS02575	VC0505,VC_0505		8	3,806	2,8E-02
VC_RS00075	VC0018,VC_0018	ibpA	4235	1,919	1,5E-03
VC_RS04265	VC0855,VC_0855	dnaK	17310	1,863	3,5E-03
VC_RS02570	VC0504,VC_0504	susC (tonB)	42	1,823	2,1E-04
VC_RS04385	VC0885,VC_0885		97	1,812	1,7E-03
VC_RS03575	VC0711,VC_0711	clpB	2525	1,688	1,2E-02
VC_RS04835	VC0977,VC_0977	cnoX	522	1,595	2,3E-03
VC_RS02995	VC0589,VC_0589	yadG	518	1,586	2,3E-02
VC_RS12835	VC2665,VC_2665	groES1	2421	1,555	4,6E-02
VC_RS18020	VC_A0989,VCA0989	dinF	136	1,511	2,5E-02
VC_RS04870	VC0985,VC_0985	htpG	9334	1,507	4,5E-02
VC_RS05980	VC1217,VC_1217	yjgM	88	1,406	7,7E-03
VC_RS04390	VC0886,VC_0886		208	1,381	5,8E-03
VC_RS16915	VC_A0744,VCA0744	glpK	1194	1,317	1,8E-09
VC_RS12880	VC2674,VC_2674	hslU	1673	1,268	1,6E-02
VC_RS12885	VC2675,VC_2675	hslV	365	1,261	5,9E-03
VC_RS00930	VC0188,VC_0188	prlC	2248	1,194	8,4E-03
VC_RS01320	VC0271,VC_0271	corC	728	1,155	1,2E-03
VC_RS02400	VC0468,VC_0468	gshB	1377	1,124	1,8E-04
VC_RS06455	VC1325,VC_1325	mglB	1478	1,089	8,0E-05
VC_RS09260	VC1920,VC_1920	lon	3601	1,066	2,3E-02
VC_RS02395	VC0467,VC_0467	ygqE	541	1,055	6,7E-04
VC_RS17520	VC_A0881,VCA0881		196	1,033	1,4E-02
VC_RS17525	VC_A0882,VCA0882		289	1,021	3,2E-03
VC_RS12360	VC2564,VC_2564	dbpA	618	-1,017	3,0E-02
VC_RS15790	VC_A0494,VCA0494	acetyltransferase	70	-1,028	3,7E-02

VC_RS03960	VC0792,VC_0792	yjfF oad	28	-1,029	2,6E-02
VC_RS14205	VC_A0179,VCA0179	psuT	156	-1,038	3,3E-02
VC_RS18615	VC_1646		27	-1,057	4,6E-02
VC_RS05270	VC1071,VC_1071	arsJ	117	-1,093	4,0E-03
VC_RS07060	VC1458,VC_1458	zot	640	-1,102	1,8E-02
VC_RS09405	VC1953,VC_1953	nupX	95	-1,131	2,3E-02
VC_RS18070	VC_A1000,VCA1000	leuE	62	-1,139	3,8E-02
VC_RS12345	VC2561,VC_2561	cobA	78	-1,143	3,3E-02
VC_RS15320			90	-1,171	1,4E-02
VC_RS06240	VC1279,VC_1279	betT	572	-1,246	9,9E-04
VC_RS15780	VC_A0492,VCA0492	RfbP-related protein	323	-1,262	8,5E-07
VC_RS07075	VC1461,VC_1461	cep ctx	2195	-1,282	1,9E-04
VC_RS12540	VC2600,VC_2600	yejM	397	-1,31	3,0E-03
VC_RS01360	VC0280,VC_0280	cadB	47	-1,346	5,1E-03
VC_RS16860	VC_A0732,VCA0732	ygiW	881	-1,417	1,5E-03
VC_RS18060	VC_A0998,VCA0998	nemA	385	-1,446	3,0E-02
VC_RS08700	VC1801,VC_1801		74	-1,462	2,6E-02
VC_RS01365	VC0281,VC_0281	cadA ldcI	60	-1,489	1,7E-03
VC_RS07640	VC1581,VC_1581	nuoL	56	-1,502	5,4E-03
VC_RS18100	VC_A1006,VCA1006	osmC	77	-1,521	2,0E-03
VC_RS07080	VC1462,VC_1462	rstB2	4846	-1,523	1,2E-04
VC_RS17365	VC_A0847,VCA0847	yjeH	141	-1,535	3,6E-04
VC_RS05275	VC1073,VC_1073		235	-1,617	1,0E-05
VC_RS08705	VC1802,VC_1802		35	-1,77	8,5E-03
VC_RS08695			66	-1,778	1,3E-03
VC_RS08680	VC1798,VC_1798	eha	131	-1,804	2,2E-05
VC_RS08690	VC1800,VC_1800		183	-1,851	8,0E-05
VC_RS07065	VC1459,VC_1459	ace	152	-1,939	4,0E-02
VC_RS08685	VC1799,VC_1799	phage transposase	302	-2,376	1,4E-08
VC_RS07040	VC1454,VC_1454	rstA1	29530	-2,705	1,9E-04
VC_RS07070	VC1460,VC_1460	orfU ctx	1156	-2,774	3,9E-08
VC_RS07085	VC1463,VC_1463	rstA2	29040	-2,893	5,1E-05

Table S3: Primers, plasmids and strains

gene expressions from pSEVA

plasmid in strain TOP10	name	primers used for gene amplification
M027	pSEVA238	MCSSEVA238-5 GCAAGAAGCGGATACAGGAG MCSSEVA238-3 GGTTTTCCCAGTCACGACGC
R591	pSEVA-tgt	5tgtEcoRI CGCGGAATTCGTGAAATTAAAATTTGAACTG and 3tgtXbaI CGCGTCTAGATCAGGCTTTGTCTTTTTGTAGTGG
Q298	pSEVA-rsxA	ZIP753 GCCCGAATTCCATTTGCCACTTATTGCG and ZIP754 GCCGCCGAATTCTTACAGTTTCACCAATCCGGTAAAGCC
Q294	pSEVA-soxR	ZIP757 GGGGCCCCCCCCGAATTCGTAAAGCGTTTTTTTAATAAAACGGG and ZIP758 CCGAATTCTTAACGGCTCCACTCTTCTGGATGCGATAAGCG
Q291	pSEVA-katG	ZIP755 GCGCGCCCCGAATTCATTTCCCATTTAGTGAAAAGGG and ZIP756 GAATTCTTACATCGCGGCCAGTTTTGCCACC

tRNA overexpression fragments cloned in pTOPO-blunt-kanamycin R (Ptrc promoter and VCt002 terminator are underlined, anticodon in red)

plasmid in TOP10	name	sequence
L961	Ptrc-eco-tRNA-Tyr wtGUA	GAGCTGTTGACAATTAATCATCCGGCTCGTATAATGTGTGGGGTGGGGTTCCCGAGCGGCCAAAGGGAGCAGACTGTAAATCTGCCGTCACAGACTTCGAAGGTTCGAATCCTTCCCCCACCACCACTTATTCGAGCTTAAGCTCAAAAAACTACA
M660	Ptrc-eco-tRNA-Tyr mutAUA	GAGCTGTTGACAATTAATCATCCGGCTCGTATAATGTGTGGGGTGGGGTTCCCGAGCGGCCAAAGGGAGCAGACTATAAATCTGCCGTCACAGACTTCGAAGGTTCGAATCCTTCCCCCACCACCACTTATTCGAGCTTAAGCTCAAAAAACTACA
L957	Ptrc-eco-tRNA-Asp wt GUC	GAGCTGTTGACAATTAATCATCCGGCTCGTATAATGTGTGGGGAGCGGTAGTTCAGTCGGTTAGAATACCTGCCTGTCACGCAGGGGGTCGCGGGTTCGAGTCCCGTCCGTTCCGCCACTTATTCGAGCTTAAGCTCAAAAAACTACA
L960	Ptrc-vch-tRNA-Tyr wtGUA	GAGCTGTTGACAATTAATCATCCGGCTCGTATAATGTGTGGGGAGGGGTTCCCGAGTGGCCAAAGGGAGCAGACTGTAAATCTGCCGGCTCCGCCTTCGATGGTTCGAATCCGTCCCCCTCCACCACTTATTCGAGCTTAAGCTCAAAAAACTACA
L959	Ptrc-vch-tRNA-Tyr mutAUA	GAGCTGTTGACAATTAATCATCCGGCTCGTATAATGTGTGGGGAGGGGTTCCCGAGTGGCCAAAGGGAGCAGACTATAAATCTGCCGGCTCCGCCTTCGATGGTTCGAATCCGTCCCCCTCCACCACTTATTCGAGCTTAAGCTCAAAAAACTACA
L956	Ptrc-vch-tRNA-Asp wtGUC	GAGCTGTTGACAATTAATCATCCGGCTCGTATAATGTGTGGGGAGCGGTAGTTCAGTCGGTTAGAATACCGGCCTGTCACGCCGGGGGTCGCGGGTTCGAGTCCCGTCCGCTCCGCCACTTATTCGAGCTTAAGCTCAAAAAACTACA
L955	Ptrc-vch-tRNA-mutAspAUC	GAGCTGTTGACAATTAATCATCCGGCTCGTATAATGTGTGGGGAGCGGTAGTTCAGTCGGTTAGAATACCGGCCTATCACGCCGGGGGTCGCGGGTTCGAGTCCCGTCCGCTCCGCCACTTATTCGAGCTTAAGCTCAAAAAACTACA
M651	Ptrc-vch-tRNA-Asn wtGUU	GAGCTGTTGACAATTAATCATCCGGCTCGTATAATGTGTGGTCCTCCTTAGCTCAGTCGGTAGAGCGACGGACTGTTAATCCGCAGGTCGCTGGTTCAAGTCCAGCAGGAGGAGCCACTTATTCGAGCTTAAGCTCAAAAAACTACA
L962	Ptrc-vch-tRNA-Asn mutAUU	GAGCTGTTGACAATTAATCATCCGGCTCGTATAATGTGTGGTCCTCCTTAGCTCAGTCGGTAGAGCGACGGACTATTAATCCGCAGGTCGCTGGTTCAAGTCCAGCAGGAGGAGCCACTTATTCGAGCTTAAGCTCAAAAAACTACA
M646	Ptrc-vch-tRNA-HIS wtGUG	GAGCTGTTGACAATTAATCATCCGGCTCGTATAATGTGTGGGTGGCTATAGCTCAGTTGGTAGAGCCCCGGATTGTGATTCCGGTTGTCGTGGGTTCGAGCCCCATTAGCCACCCCACTTATTCGAGCTTAAGCTCAAAAAACTACA
L997	Ptrc-vch-tRNA-HIS mutAUG	GAGCTGTTGACAATTAATCATCCGGCTCGTATAATGTGTGGGTGGCTATAGCTCAGTTGGTAGAGCCCCGGATTATGATTCCGGTTGTCGTGGGTTCGAGCCCCATTAGCCACCCCACTTATTCGAGCTTAAGCTCAAAAAACTACA
M653	Ptrc-vch-tRNA-Phe wtGAA	GAGCTGTTGACAATTAATCATCCGGCTCGTATAATGTGTGGGCCCGGATAGCTCAGTCGGTAGAGCAGAGGATTGAAAATCCTCGTGTCGGTGGTTCGATTCCGCCTCCGGGCACCACTTATTCGAGCTTAAGCTCAAAAAACTACA

translational fusions ordered in pUC_IDT (carbenicillin R)

plasmid in strain DH5α	name	sequence

R973	Ptrc-rsxATAC-gfp	TTGACAATTAATCATCCGGCTCGTATAATGTGTGGAATTGTGAGCGGATAACAATTTCACACAGGA AACAGCGCCGCATGACCGAATACCTTTTGTTGTTAATCGGCACCGTGCTGGTCAATAACTTTGTAC TGGTGAAGTTTTTGGGCTTATGTCCTTTTATGGGCGTATCAAAAAAACTAGAGACCGCCATTGGCA TGGGGTTGGCGACGACATTCGTCCTCACCTTAGCTTCGGTGTGCGCTTACCTGGTGGAAAGTTAC GTGTTACGTCCGCTCGGCATTGAGTACCTGCGCACCATGAGCTTTATTTTGGTGATCGCTGTCGTA GTACAGTTCACCGAAATGGTGGTGCACAAAACCAGTCCGACACTCTACCGCCTGCTGGGCATTTTC CTGCCACTCATCACCACCAACTGTGCGGTATTAGGGGTTGCGCTGCTCAACATCAACGAAAATCAC AACTTTATTCAATCGATCATTTACGGTTTTGGCGCTGCTGTTGGCTTCTCGCTGGTGCTCATCTTGT TCGCTTCAATGCGTGAGCGAATCCATGTAGCCGATGTCCCCGCTCCCTTTAAGGGCGCATCCATTG CGATGATCACCGCAGGTTTAATGTCTTTGGCCTTTATGGGCTTTACCGGATTGGTGAAACTGGCTA GCAAAGGAGAAGAACTTTTCACTGGAGTTGTCCCAATTCTTGTTGAATTAGATGGTGATGTTAATG GGCACAAATTTTCTGTCAGTGGAGAGGGTGAAGGTGATGCTACATACGGAAAGCTTACCCTTAAA TTTATTTGCACTACTGGAAAACTACCTGTTCCATGGCCAACACTTGTCACTACTTTGACCTATGGTG TTCAATGCTTTTCCCGTTATCCGGATCATATGAAACGGCATGACTTTTTCAAGAGTGCCATGCCCGA AGGTTATGTACAGGAACGCACTATATCTTTCAAAGATGACGGGAACTACAAGACGCGTGCTGAAG TCAAGTTTGAAGGTGATACCCTTGTTAATCGTATCGAGTTAAAAGGTATTGATTTTAAAGAAGATG GAAACATTCTCGGACACAAACTCGAGTACAACTATAACTCACACAATGTATACATCACGGCAGACA AACAAAAGAATGGAATCAAAGCTAACTTCAAAATTCGCCACAACATTGAAGATGGGAGGCGTTCAA CTAGCAGACCATTATCAACAAAATACTCCAATTGGCGATGGCCCTGTCCTTTTACCAGACAACCATT ACCTGTCGACACAATCTGCCCTTTCGAAAGATCCCAACGAAAAGCGTGACCACATGGTCCTTCTTG AGTTTGTAACTGCTGCTGGGATTACACATGGCATGGATGAGCTCTACAAATAA
R972	Ptrc-rsxATATWT-gfp	TTGACAATTAATCATCCGGCTCGTATAATGTGTGGAATTGTGAGCGGATAACAATTTCACACAGGA AACAGCGCCGCATGACCGAATATCTTTTGTTGTTAATCGGCACCGTGCTGGTCAATAACTTTGTAC TGGTGAAGTTTTTGGGCTTATGTCCTTTTATGGGCGTATCAAAAAAACTAGAGACCGCCATTGGCA TGGGGTTGGCGACGACATTCGTCCTCACCTTAGCTTCGGTGTGCGCTTATCTGGTGGAAAGTTACG TGTTACGTCCGCTCGGCATTGAGTATCTGCGCACCATGAGCTTTATTTTGGTGATCGCTGTCGTAG TACAGTTCACCGAAATGGTGGTGCACAAAACCAGTCCGACACTCTATCGCCTGCTGGGCATTTTCC TGCCACTCATCACCACCAACTGTGCGGTATTAGGGGTTGCGCTGCTCAACATCAACGAAAATCACA ACTTTATTCAATCGATCATTTATGGTTTTGGCGCTGCTGTTGGCTTCTCGCTGGTGCTCATCTTGTTC GCTTCAATGCGTGAGCGAATCCATGTAGCCGATGTCCCCGCTCCCTTTAAGGGCGCATCCATTGCG ATGATCACCGCAGGTTTAATGTCTTTGGCCTTTATGGGCTTTACCGGATTGGTGAAACTGGCTAGC AAAGGAGAAGAACTTTTCACTGGAGTTGTCCCAATTCTTGTTGAATTAGATGGTGATGTTAATGG GCACAAATTTTCTGTCAGTGGAGAGGGTGAAGGTGATGCTACATACGGAAAGCTTACCCTTAAAT TTATTTGCACTACTGGAAAACTACCTGTTCCATGGCCAACACTTGTCACTACTTTGACCTATGGTGT TCAATGCTTTTCCCGTTATCCGGATCATATGAAACGGCATGACTTTTTCAAGAGTGCCATGCCCGA AGGTTATGTACAGGAACGCACTATATCTTTCAAAGATGACGGGAACTACAAGACGCGTGCTGAAG TCAAGTTTGAAGGTGATACCCTTGTTAATCGTATCGAGTTAAAAGGTATTGATTTTAAAGAAGATG GAAACATTCTCGGACACAAACTCGAGTACAACTATAACTCACACAATGTATACATCACGGCAGACA AACAAAAGAATGGAATCAAAGCTAACTTCAAAATTCGCCACAACATTGAAGATGGAGGCGTTCAA CTAGCAGACCATTATCAACAAAATACTCCAATTGGCGATGGCCCTGTCCTTTTACCAGACAACCATT ACCTGTCGACACAATCTGCCCTTTCGAAAGATCCCAACGAAAAGCGTGACCACATGGTCCTTCTTG AGTTTGTAACTGCTGCTGGGATTACACATGGCATGGATGAGCTCTACAAATAA
R975	Ptrc-gfpTAC	GAGCTGTTGACAATTAATCATCCGGCTCGTATAATGTGTGGAATTGTGAGCGGATAACAATTTCAC ACAGGAAACACATATGCGTAAAGGAGAAGAACTTTTCACTGGAGTTGTCCCAATTCTTGTTGAATT AGATGGTGATGTTAATGGGCACAAATTTTCTGTCAGTGGAGAGGGTGAAGGTGATGCAACA<u>TAC</u> GGAAAACTTACCCTTAAATTTATTTGCACTACTGGAAAACTACCTGTTCCATGGCCAACACTTGTCA CTACTTTCGGT<u>TAC</u>GGTGTTCAATGCTTTGCGAGA<u>TAC</u>CAGATCATATGAAACAGCATGACTTTTT CAAGAGTGCCATGCCCGAAGGT<u>TAC</u>GTACAGGAAAGAACTATATTTTTCAAAGATGACGGGAAC<u>T AC</u>AAGACACGTGCTGAAGTCAAGTTTGAAGGTGATACCCTTGTTAATAGAATCGAGTTAAAAGGT ATTGATTTTAAAGAAGATGGAAACATTCTTGGACACAAATTGGAA<u>TAC</u>AAC<u>TAC</u>AACTCACACAAT GTA<u>TAC</u>ATCATGGCAGACAAACAAAAGAATGGAATCAAAGTTAACTTCAAAATTAGACACAACAT TGAAGATGGAAGCGTTCAACTAGCAGACCAT<u>TAC</u>CAACAAAATACTCCAATTGGCGATGGCCCTG TCCTTTTACCAGACAACCAT<u>TAC</u>CTGTCCACACAATCTGCCCTTTCGAAAGATCCCAACGAAAAGA GAGACCACATGGTCCTTCTTGAGTTTGTAACAGCTGCTGGGATTACACATGGCATGGATGAACTA<u>T AC</u>AAATAA
R974	Ptrc-gfpTAT	GAGCTGTTGACAATTAATCATCCGGCTCGTATAATGTGTGGAATTGTGAGCGGATAACAATTTCAC ACAGGAAACACATATGCGTAAAGGAGAAGAACTTTTCACTGGAGTTGTCCCAATTCTTGTTGAATT AGATGGTGATGTTAATGGGCACAAATTTTCTGTCAGTGGAGAGGGTGAAGGTGATGCAACA<u>TAT</u> GGAAAACTTACCCTTAAATTTATTTGCACTACTGGAAAACTACCTGTTCCATGGCCAACACTTGTCA CTACTTTCGGT<u>TAT</u>GGTGTTCAATGCTTTGCGAGA<u>TAT</u>CCAGATCATATGAAACAGCATGACTTTTT CAAGAGTGCCATGCCCGAAGGT<u>TAT</u>GTACAGGAAAGAACTATATTTTTCAAAGATGACGGGAAC<u>T AT</u>AAGACACGTGCTGAAGTCAAGTTTGAAGGTGATACCCTTGTTAATAGAATCGAGTTAAAAGGT ATTGATTTTAAAGAAGATGGAAACATTCTTGGACACAAATTGGAA<u>TAT</u>AAC<u>TAT</u>AACTCACACAAT GTA<u>TAT</u>ATCATGGCAGACAAACAAAAGAATGGAATCAAAGTTAACTTCAAAATTAGACACAACAT TGAAGATGGAAGCGTTCAACTAGCAGACCAT<u>TAT</u>CAACAAAATACTCCAATTGGCGATGGCCCTG TCCTTTTACCAGACAACCAT<u>TAT</u>CTGTCCACACAATCTGCCCTTTCGAAAGATCCCAACGAAAAGAG AGACCACATGGTCCTTCTTGAGTTTGTAACAGCTGCTGGGATTACACATGGCATGGATGAACTA<u>TA TA</u>AAATAA

plasmid in strain (WT/Δtgt)	codon replacement	introduction of point mutation in circular pTOPO-TA (kanamycin R) by PCR using primers :
N509/N511	bla wt	Tyr103TAC Asp129GAT
N512/N514	bla Tyr103TAC > Tyr TAT synonymous	ZIP555 GACTTGGTTGAGTATTCACCAGTCACAGAAAAGC ZIP556 TCTGTGACTGGTGAATACTCAACCAAGTCATTCTGAGAATAG
N471/N477	bla Tyr103TAC >stopTAG	ZIP557 GACTTGGTTGAGTAGTCACCAGTCACAGAAAAGC ZIP558 TCTGTGACTGGTGACTACTCAACCAAGTCATTCTGAGAATAG
N296/N298	bla Tyr103TAC >stopTGA	ZIP559 GACTTGGTTGAGTGATCACCAGTCACAGAAAAGC ZIP560 TCTGTGACTGGTGATCACTCAACCAAGTCATTCTGAGAATAG
N293/N295	bla Tyr103TAC >stopTAA	ZIP561 GACTTGGTTGAGTAATCACCAGTCACAGAAAAGC ZIP562 TCTGTGACTGGTGATTACTCAACCAAGTCATTCTGAGAATAG
N466/N472	bla Tyr103TAC >His CAC	ZIP566 GACTTGGTTGAGCACTCACCAGTCACAGAAAAGC ZIP567 TCTGTGACTGGTGAGAGCTCAACCAAGTCATTCTGAGAATAG
N467/N473	bla Tyr103TAC >His CAT	ZIP568 GACTTGGTTGAGCATTCACCAGTCACAGAAAAGC ZIP569 TCTGTGACTGGTGAATGCTCAACCAAGTCATTCTGAGAATAG
N484/N490	bla Tyr103 >Asp GAC	ZIP570 GACTTGGTTGAGGACTCACCAGTCACAGAAAAGC ZIP571 TCTGTGACTGGTGAGTCCTCAACCAAGTCATTCTGAGAATAG
N485/N491	bla Tyr103 >Asp GAT	ZIP572 GACTTGGTTGAGGATTCACCAGTCACAGAAAAGC ZIP573 TCTGTGACTGGTGAATCCTCAACCAAGTCATTCTGAGAATAG
N486/N492	bla Tyr103 >Asn AAT	ZIP574 GACTTGGTTGAGAATTCACCAGTCACAGAAAAGC ZIP575 TCTGTGACTGGTGAATTCTCAACCAAGTCATTCTGAGAATAG
N468/N494	bla Tyr103 >Asn AAC	ZIP576 GACTTGGTTGAGAACTCACCAGTCACAGAAAAGC ZIP577 TCTGTGACTGGTGAGTTCTCAACCAAGTCATTCTGAGAATAG
N487/N493	bla Tyr103 >Phe TTC	ZIP578 GACTTGGTTGAGTTCTCACCAGTCACAGAAAAGC ZIP579 TCTGTGACTGGTGAGAACTCAACCAAGTCATTCTGAGAATAG
O508/O517	bla Tyr103 >Ser TCT	ZIP671 GACTTGGTTGAGTCTTCACCAGTCACAGAAAAGC ZIP672 TCTGTGACTGGTGAAGACTCAACCAAGTCATTCTGAGAATAG
O509/O518	bla Tyr103 >Ser TCC	ZIP673 GACTTGGTTGAGTCCTCACCAGTCACAGAAAAGC ZIP674 TCTGTGACTGGTGAGGACTCAACCAAGTCATTCTGAGAATAG
O510/O519	bla Tyr103 >Cys TGT	ZIP675 GACTTGGTTGAGTGTTCACCAGTCACAGAAAAGC ZIP676 TCTGTGACTGGTGAACACTCAACCAAGTCATTCTGAGAATAG
O511/O520	bla Tyr103>Cys TGC	ZIP677 GACTTGGTTGAGTGCTCACCAGTCACAGAAAAGC ZIP678 TCTGTGACTGGTGAGCACTCAACCAAGTCATTCTGAGAATAG
N515/N517	bla Ap129 >TyrTAC	ZIP582 CTGCCATAACCATGAGTTACAACACTGCGGC ZIP583 AGTTGGCCGCAGTGTTGTAACTCATGGTTATGGCAGCACTGC
N470/N476	bla Ap129 >TyrTAT	ZIP584 CTGCCATAACCATGAGTTATAACACTGCGGC ZIP585 AGTTGGCCGCAGTGTTATAACTCATGGTTATGGCAGCACTGC
O512/O521	bla Ap129 >Val GTT	ZIP679 CTGCCATAACCATGAGTGTTAACACTGCGGC ZIP680 AGTTGGCCGCAGTGTTAACACTCATGGTTATGGCAGCACTGC
O513/O522	bla Ap129 >Val GTC	ZIP681 CTGCCATAACCATGAGTGTCAACACTGCGGC ZIP682 AGTTGGCCGCAGTGTTGACACTCATGGTTATGGCAGCACTGC
O514/O523	bla Ap129 >Ala GCT	ZIP683 CTGCCATAACCATGAGTGCTAACACTGCGGC ZIP684 AGTTGGCCGCAGTGTTAGCACTCATGGTTATGGCAGCACTGC
P242/O524	bla Ap129 >Ala GCC	ZIP685 CTGCCATAACCATGAGTGCCAACACTGCGGC ZIP686 AGTTGGCCGCAGTGTTGGCACTCATGGTTATGGCAGCACTGC
O515/O525	bla Ap129 >Gly GGT	ZIP687 CTGCCATAACCATGAGTGGTAACACTGCGGC ZIP688 AGTTGGCCGCAGTGTTACCACTCATGGTTATGGCAGCACTGC
O516/O526	bla Ap129 >Gly GGC	ZIP689 CTGCCATAACCATGAGTGGCAACACTGCGGC ZIP690 AGTTGGCCGCAGTGTTGCCACTCATGGTTATGGCAGCACTGC
P230/P234	bla Ap129 >Glu GAG	ZIP731 CTGCCATAACCATGAGTGAGAACACTGCGGC ZIP732 AGTTGGCCGCAGTGTTCTCACTCATGGTTATGGCAGCACTGC
P231/P239	bla Ap129 >Glu GAA	ZIP733 CTGCCATAACCATGAGTGAAAACACTGCGGC ZIP734 AGTTGGCCGCAGTGTTTTCACTCATGGTTATGGCAGCACTGC
P232/P236	bla Ap129 >His CAT	ZIP735 CTGCCATAACCATGAGTCATAACACTGCGGC ZIP736 AGTTGGCCGCAGTGTTATGACTCATGGTTATGGCAGCACTGC
asp10	bla Ap129 >His CAC	ZIP737 CTGCCATAACCATGAGTCACAACACTGCGGC ZIP738 AGTTGGCCGCAGTGTTGTGACTCATGGTTATGGCAGCACTGC
P233/P237	bla Ap129GAT >Asp GAC synonymous	ZIP739 CTGCCATAACCATGAGTGACAACACTGCGGC ZIP740 AGTTGGCCGCAGTGTTGTCACTCATGGTTATGGCAGCACTGC

plasmid in strain TOP10	primers for transcriptional fusion PrsxA-gfp	
Q282	ZIP796	GGATACAAAAAAGTAAACCC
	ZIP812	CTCCTTTACGCATAGTTATATAAATGTTTGCTTCCGATCCCGGCATTATCCTG
	ZIP813	CAGGATAATGCCGGGATCGGAAGCAAACATTTATATAACTATGCGTAAAGGAG
	ZIP200	TATCAAGCTTATTTGTATAGTTCATCCATGCC
target for amplification	primers for q-RT-PCR tRNAs	
tRNATyr	ZIP719	GGAGGGGTTCCCGAGTGG
	ZIP720	GGTGGAGGGGGACGGATT
tRNAAsp	ZIP721	GGAGCGGTAGTTCAGTCG
	ZIP722	TGGCGGAGCGGACGGGAC
tRNAHis	ZIP723	GTGGCTATAGCTCAGTTG
	ZIP724	TGGGGTGGCTAATGG
tRNAAsn	ZIP725	TCCTCCTTAGCTCAGTCGG
	ZIP726	TGGCTCCTCCTGCTGG
gyrA	gyrA_F	AAT GTG CTG GGC AAC GAC TG
	gyrA_R	GAG CCA AAG TTA CCT GG CC
target for amplification	primers for digital-RT-PCR fluorescent probes	
tgt		fwd CAA CAC CAC TGG ATC CTC ATT rev GGT AGT AAC GCA GGT TAT GG 5' - [FAM] A CCT GCA TCA TCT GGA TCG CTG TAA - 3' [BHQ2]
rsxA		fwd TCA CGC ATT GAA GCG AAC rev CAC CAA CTG TGC GGT ATT AG 5' - [FAM] A GCG CCA AAA CCA TAA ATG ATC GAT - 3' [BHQ2]
gyrA		fwd AAT GTG CTG GGC AAC GAC TG rev GAG CCA AAG TTA CCT GG CC 5' - [CY5] - CAC CCT CAT GGT GAC AGT GCG GTT T - 3' [BHQ2]
Strains		
V. cholerae	strain #	reference
N16961 hapR+	F606	laboratory collection
N16961 hapR+ ΔlacZ	K329	Babosan et al, 2022
Δtgt::spec	J420	Babosan et al, 2022
ΔtolA::kan	J983	Negro et al, 2019
Δcrp::kan	Q081	Deletion of *crp* in F606 as described in Lang et al, 2021
ΔrluF::kan	M567	Babosan et al, 2022
ΔrluF::kan Δtgt::spec	M569	Deletion of *rluF* in J420, as described for deletion of *rluF* in WT in Babosan et al, 2022
E. coli	strain #	construction
MG1655	C349	laboratory collection
Δtgt::kan	J233	P1 transduction of tgt::kan from Keio collection into MG1655
Δtgt	R181	Kanamycin resistance cassette was removed using the FLP/FRT system (Zhu et al, 1995)
ΔrsxA::kan	R207	P1 transduction of tgt::kan from Keio collection into MG1655
Δtgt ΔrsxA::kan	R223	P1 transduction of rsxA::kan from Keio collection into R181 *Δtgt*

(42) (95)

Acknowledgements

Author contributions

Conceived and designed the analysis: ZB, DM; Collected the data: ZB, LF, AB, AC, ML, MD, BL, QG-G, FB, CF; Contributed data or analysis tools: BL, ON, CF, MM, MD, QG-G, FB, VdC-L; Performed the analysis: ZB, LF, AB, AC, ML, BL; Wrote the paper: ZB, VdC-L.

Figure legends

Figure 1. *V. cholerae Δtgt* shows decreased aminoglycoside tolerance. A. Competition experiments between WT and *Δtgt* with the indicated antibiotic or oxidant at sub-MIC concentration*. NT: non-treated.* **B.** Competition experiments between WT and *Δtgt* carrying the indicated plasmids. MH: *non-treated*. **CDEF**. Survival of exponential phase cultures after various times of incubation with the indicated antibiotic at lethal concentration. **G.** PMF measurement of exponential phase cultures using Mitotracker. **H**. Neomycin uptake measurement by flow cytometry using fluorescent Cy5 coupled neomycin. For multiple comparisons, we used one-way ANOVA on GraphPad Prism. **** means p<0.0001, *** means p<0.001, ** means p<0.01, * means p<0.05. ns: non-significant. Number of replicates for each experiment: 3<n<8.

Figure 2. Codon decoding differences for *V. cholerae* WT and *Δtgt*. A. Stop codon readthrough levels show increased mistranslation at TAA and TAG for *Δtgt*. Blue: WT. Red: *Δtgt.* NT: no treatment. *TOB:* growth in the presence of tobramycin at 20% of the MIC. Reporters described in (33). Y axis represents stop codon readthrough*1000. **B to H**. **Codon specific translation efficiency in WT and *Δtgt* using 6xcodon stretches in GFP.** Y axis represents the percentage of fluorescence compared to WT GFP in non-treated WT strain (WT NT). Each specified codon is repeated 6x within the coding sequence of the GFP (e.g. TACTACTACTACTACTAC). For multiple comparisons, we used one-way ANOVA on GraphPad Prism. **** means p<0.0001, *** means p<0.001, ** means p<0.01, * means p<0.05. ns: non-significant. Number of replicates for each experiment: 3<n<8.

Figure 3. Differential translation at sense codons evaluated by carbenicillin tolerance of mutated β-lactamase reporters. **A:** rationale. **B.** Cells were grown to early exponential phase without carbenicillin, and with (down) or without (top) tobramycin 20% of MIC, and treated with carbenicillin at 10xMIC for 20h. Dilutions were spotted on plate without carbenicillin. Surviving cells shown here are sensitive to carbenicillin (no growth on carbenicillin containing plates), suggesting that increased or decreased survival was due to increased (erroneous translation) or decreased (faithful translation) β-lactamase activity at the time of treatment. Number of replicates for each experiment: 3. One representative experiment is shown. **CDEF.** Growth on Tecan microtiter plates. Growth was followed by measuring the OD 620 nm every 15 minutes during 800 minutes.

Figure 4. Post-transcriptional upregulation of RsxA in *Δtgt* due to a Tyr codon bias towards TAT and toxicity in sub-MIC TOB. A. Volcano plot showing less and more abundant proteins in *Δtgt* compared to WT during growth in sub-MIC TOB. **B.** Tyr codon usage of more and less abundant proteins in *Δtgt* TOB and whole *V. cholerae* genome. **C.** *rsxA* mRNA levels measured by digital RT-PCR. **D.** Transcriptional expression levels from the *rsxA* promoter measured by flow cytometry. **E.** Translational fusion of *rsxA* to *gfp* and *gfp* alone, with differences in codon usage. *** means p<0.001, ** means p<0.01. ns: non-significant. **F.** Relative OD 620 nm of WT strain carrying either empty plasmid or plasmid overexpressing RsxA comparing growth in sub-MIC TOB divided by growth in the absence of treatment.

Figure 5. Regulation of *tgt* expression and tRNA Q levels. A: *tgt* transcript levels measured by digital-RT-PCR. Y-axis represents relative abundance compared to the non-treated (NT) condition in WT. For

multiple comparisons, we used one-way ANOVA on GraphPad Prism. **** means *p*<0.0001, *** means *p*<0.001, ** means *p*<0.01. Only significant differences are shown. **B.** stringent response induction measured with *P1rrn-gfp* reporter. The first panel show growth (OD 600 nm) as a function of time. The second panel shows GFP fluorescence as a function of time. The third panel shows fluorescence (Y-axis) as a function of growth (X-axis: OD 600 nm). **C.** Q levels in tRNA enriched RNA extracts, measured by mass spectrometry**.** **** means p<0.0001, *** means p<0.001. Number of replicates for each experiment: 3

Figure 6. DNA repair after UV irradiation is more efficient in *V. cholerae Δtgt*. A and C. Tyrosine codon usage of DNA repair genes A: in *V. cholerae. C: in E. coli.* **B and D.** Survival of *Δtgt* relative to WT after UV irradiation (linear scale) B: in *V. cholerae. D: in E. coli.* For multiple comparisons, we used one-way ANOVA on GraphPad Prism. **** means p<0.0001, ns: non-significant.

Figure 7. Model. Expression of *tgt* is up-regulated in *V. cholerae* upon exposure to sub-MIC aminoglycosides and influences the decoding of tyrosine TAC vs TAT codons, which can trigger phenotypic diversity depending on codon biases of different transcripts. The *rsxA* transcript bears a tyrosine codon bias and its translation can be tuned by tRNA Q modification. RsxA is an anti-SoxR factor. SoxR controls a regulon involved in oxidative stress response and sub-MIC aminoglycosides trigger oxidative stress in *V. cholerae.* When Tgt/Q levels in tRNA increase, RsxA synthesis is low and active SoxR levels are high, facilitating the bacterial response to aminoglycoside dependent oxidative stress.

Supplementary figure legends

Sup. figure S1. Codon decoding differences between WT and *Δtgt*. A. Frameshifting levels for *V. cholerae* WT and for *Δtgt.* FSX -1: frameshifts at *dnaX* natural -1 frameshifting sequence. **FSB +1:** frameshifts at *prfB* natural +1 frameshifting sequence. MH: no antibiotic. TOB: sub-MIC tobramycin treatment (0.2 µg/ml). Reporters described in(33). Y axis represents frameshifting percentage. For multiple comparisons, we used one-way ANOVA on GraphPad Prism. ns means non-significant differences. Number of replicates for each experiment: 3. **B. Stop codon readthrough in *E. coli* MG1655 WT and *Δtgt*.** Growth in the presence of tobramycin at 50% of the MIC (0.2 µg/ml in MH); NT: non-treated. Reporters described in(33). Y axis represents stop codon readthrough percentage*10. ** means $p < 0.01$. Number of replicates for each experiment: 8<n<14.

Sup. figure S2. Impact of tRNA overexpression on fitness during growth in sub-MIC TOB. In vitro competition experiments of *V. cholerae* WT and mutant strains in the absence or presence of sub-MIC tobramycin (50% of the MIC, TOB 0.6 µg/ml). MH: no antibiotic treatment. The Y-axis represents $\log_{10}$ of competitive index calculated as described in the methods. A competitive index of 1 indicates equal growth of both strains. The X-axis indicates which tRNA is overexpressed, from the high copy pTOPO plasmid. The anticodon sequence is indicated (e.g. tRNA-TyrAUA decodes the TAT codon). The following tRNAs-GUN are the canonical tRNAs which are present in the genome, and modified by Tgt: TyrGUA, HisGUG, AsnGUU, AspGUC. The following tRNAs-AUN are synthetic tRNAs which are not present in the genome: TyrAUA, HisAUG, AsnAUU, AspAUC. tRNA-PheGAA is used as non Tgt-modified control. **A.** Competition between WT and *Δtgt* strains carrying a plasmid overexpressing the same tRNA. **B** and **C.** Competition between WT strain carrying the indicated tRNA overexpression against the same strain carrying the empty plasmid (p0). B: WT strain. C: *Δtgt.* For multiple comparisons, we used one-way ANOVA on GraphPad Prism. **** means $p < 0.0001$, * means $p < 0.05$. Number of replicates for each experiment: 3<n<8. In A, only significant differences are indicated. In B and C: ns means non-significant. **D. E. F. Absence of *tgt* does not visibly affect tRNA-GUN levels.** qRTPCR. A: relative tRNA abundance in *Δtgt* compared to WT strain in the absence of treatment (NT) and in the presence of sub-MIC tobramycin (TOB). B and C: effect of TOB on tRNA levels in the WT (B) and *Δtgt* (C) strain.

Sup. figure S3. No effect of *rluF* deletion on fitness in *V. cholerae* WT and *Δtgt* strains. In vitro competition experiments of *V. cholerae* WT and mutant strains in the absence or presence of sub-MIC aminoglycosides tobramycin TOB and gentamicin (GEN) (50% of the MIC, TOB 0.6 µg/ml, GEN 0.5 µg/ml). MH: no antibiotic treatment. The Y-axis represents $\log_{10}$ of competitive index calculated as described in the methods. A competitive index of 1 indicates equal growth of both strains. The X-axis indicates growth conditions. For multiple comparisons, we used one-way ANOVA on GraphPad Prism. **** means $p < 0.0001$, * means $p < 0.05$. Number of replicates for each experiment: 3<n<8. In A, only significant differences are indicated. In B and C: ns means non-significant.

Sup. figure S4. Mistranslation at stop codons evaluated by carbenicillin tolerance of mutated β-lactamase reporters. **A:** rationale. Increased amino-acid misincorporation at the tested codon will lead to production of active β-lactamase only in a proportion of the translated proteins, which are not heritable as opposed to DNA mutations. Such a process is thus expected to yield transiently tolerant, and not necessarily resistant, bacterial cells. The strength of this approach lays in the fact that it does not evaluate general translation error levels, but misincorporation of specific amino-acids by specific tRNAs at specific codons of interest. **B**. Experimental setup. Cells were grown to early exponential

phase without carbenicillin, and treated with carbenicillin at 10xMIC (50 µg/ml) for 20h. Dilutions were spotted on plates without and with carbenicillin. Surviving cells are more tolerant to CRB, but not resistant. If resistance is observed (CFU on CRB containing plates), this points to apparition of resistance mutations. **C.** Asp129GAT was mutated to the synonymous Asp129GAC. Growth curves measured using microtiter plate reader are shown. **D and E.** Tables show the MIC of tobramycin for each β-lactamase allele. D. for codon replacements at Tyr103, E: for codon replacements at Asp129. Cells were grown to early exponential phase without carbenicillin, and with (down) or without (top) tobramycin 20% of MIC, and treated with carbenicillin at 10xMIC for 20h. Dilutions were spotted on plate without carbenicillin. Surviving cells shown here are sensitive to carbenicillin (no growth on carbenicillin containing plates), suggesting that increased or decreased survival was due to increased (erroneous translation) or decreased (faithful translation) β-lactamase activity at the time of treatment. The experiment was repeated 3x.

Sup. figure S5. Quantification of carbenicillin resistance appearance on Tyr103 (A to N) and Asp129 (O to X) mutants. **A to G and O to S:** Frequency of carbenicillin resistant CFU formation (CRB resistant CFUs divided by total number of CFUs). **H to N and T to X:** Frequency of carbenicillin resistant genetic mutants determined by sequencing *bla* gene on the colonies growing on CRB. For *bla* versions mutated at Asp129 (O t o X), the frequencies of appearance of CRB resistant mutants were in line with the absence of mutator phenotype, even considering the fact that the mutated *bla* gene is carried by the plasmid pTOPO, which is present at up to a hundred copies inside the cells, increasing the chances to get a spontaneous mutation. For unknown reasons, high levels of reversion mutants were obtained for Asp to GluGAA but this was variable (W). This can also explain the variability observed for Glu in Sup. Fig. S4E. For *bla* versions mutated at Tyr103 (A to N), the frequencies of colonies growing on CRB were also low. Two interesting observations can be however made. First, the frequency of colonies growing on carb were high (up to 10^{-3}) for *bla* mutants at Tyr103 replaced with both His/both Asn/Ser TCC/Cys TGT codons, but those were not genetic revertants, as no mutation was detected in these codons. This is also consistent with high MIC values for these *bla* mutants (Sup. fig. S4D), meaning that either the β-lactamase protein with the mutated amino-acid (e.g. with His103 instead of Tyr103) is still functional, or that mistranslation by tRNA-Tyr is high at those codons, even in the WT strain, and produces enough functional Tyr103 β-lactamase to grow in presence of carb. The latter can for instance be true for Tyr103 to cysteine, since the Cys TGC version is carb sensitive while the cys TGT version is carb resistant. The second intriguing and unexplained observation is the high frequency of revertants (~10^{-4}) at Ser TCT, yielding functional Tyr TAT codons. This was the case for both WT and *Δtgt*. **Y.** mutation frequency of WT and *Δtgt* determined by spontaneous rifampicin resistant colony formation.

Sup. figure S6. Post-transcriptional upregulation of RsxA in *Δtgt* due to a Tyr codon bias towards TAT and toxicity in sub-MIC TOB. A to E. Translational fusion of *rsxA* to *gfp* (A. 4 hours exponential phase cultures, B. overnight stationary phase cultures) and *gfp* alone (C. 4 hours exponential phase cultures without antibiotics, D. in the presence of sub-MIC TOB), with differences in codon usage, measured by flow cytometry. Y axis represents mean fluorescence. **F.** Relative fluorescence of *Δtgt* compared to WT, various sequences displayed by *rsxA* inserted in *gfp* after its ATG codon, following the same principle as 6x-codon stretches, measured by flow cytometry. We used either the native TAT or the TAC replacement while keeping the remaining sequence unchanged.

Sup. figure S7. *rsxA* **levels impact growth in the presence of sub-MIC TOB. ABCD.** Growth curves in microtiter plate reader, in *V. cholerae* in indicated conditions**.** P-tgt+: pSEVA expressing *tgt*. P-rsx+: pSEVA expressing *rsxA*. P-control: empty pSEVA. **E**. Growth curves in microtiter plate reader, in *E. coli* WT and *Δtgt* in MH or in the presence of tobramycin at the indicated concentrations (in µg/mL). **F.** Left: Competition experiments in *E. coli*, with indicated strains. Right: Relative OD 620 nm of indicated strain comparing growth in TOB (0.4 µg/ml) divided by growth in the absence of treatment.

Sup. figure S8. Codon usage. A and B: Tyrosine codon usage in A: V. cholerae and B: E. coli in the whole genome and selected groups of genes. C. Gene ontology analysis of overrepresented gene categories with TAT usage bias in *V. cholerae*. D. Gene ontology analysis of underrepresented gene categories with TAT usage bias in *V. cholerae*. E. Gene ontology analysis of overrepresented gene categories with TAC usage bias in *V. cholerae*. F. Codon usage bias calculation example with VC1017 *rsxA* tyrosine TAC and TAT codons.

References

1. Babosan, A., Fruchard, L., Krin, E., Carvalho, A., Mazel, D. and Baharoglu, Z. (2022) Non-essential tRNA and rRNA modifications impact the bacterial response to sub-MIC antibiotic stress. *microLife*.

2. Pollo-Oliveira, L. and de Crecy-Lagard, V. (2019) Can Protein Expression Be Regulated by Modulation of tRNA Modification Profiles? *Biochemistry*, **58**, 355-362.

3. Suzuki, T. (2021) The expanding world of tRNA modifications and their disease relevance. *Nat Rev Mol Cell Biol*.

4. Chujo, T. and Tomizawa, K. (2021) Human transfer RNA modopathies: diseases caused by aberrations in transfer RNA modifications. *FEBS J*, **288**, 7096-7122.

5. Zhong, W., Koay, A., Ngo, A., Li, Y., Nah, Q., Wong, Y.H., Chionh, Y.H., Ng, H.Q., Koh-Stenta, X., Poulsen, A. *et al.* (2019) Targeting the Bacterial Epitranscriptome for Antibiotic Development: Discovery of Novel tRNA-(N(1)G37) Methyltransferase (TrmD) Inhibitors. *ACS Infect Dis*, **5**, 326-335.

6. de Crecy-Lagard, V. and Jaroch, M. (2021) Functions of Bacterial tRNA Modifications: From Ubiquity to Diversity. *Trends Microbiol*, **29**, 41-53.

7. Urbonavicius, J., Qian, Q., Durand, J.M., Hagervall, T.G. and Bjork, G.R. (2001) Improvement of reading frame maintenance is a common function for several tRNA modifications. *EMBO J*, **20**, 4863-4873.

8. Taylor, D.E., Trieber, C.A., Trescher, G. and Bekkering, M. (1998) Host mutations (miaA and rpsL) reduce tetracycline resistance mediated by Tet(O) and Tet(M). *Antimicrob Agents Chemother*, **42**, 59-64.

9. Parker, J. (1982) Specific mistranslation in hisT mutants of Escherichia coli. *Mol Gen Genet*, **187**, 405-409.

10. Bruni, C.B., Colantuoni, V., Sbordone, L., Cortese, R. and Blasi, F. (1977) Biochemical and regulatory properties of Escherichia coli K-12 hisT mutants. *J Bacteriol*, **130**, 4-10.

11. Thongdee, N., Jaroensuk, J., Atichartpongkul, S., Chittrakanwong, J., Chooyoung, K., Srimahaeak, T., Chaiyen, P., Vattanaviboon, P., Mongkolsuk, S. and Fuangthong, M. (2019) TrmB, a tRNA m7G46 methyltransferase, plays a role in hydrogen peroxide resistance and positively modulates the translation of katA and katB mRNAs in Pseudomonas aeruginosa. *Nucleic Acids Res*, **47**, 9271-9281.

12. Aubee, J.I., Olu, M. and Thompson, K.M. (2016) The i6A37 tRNA modification is essential for proper decoding of UUX-Leucine codons during rpoS and iraP translation. *RNA*, **22**, 729-742.

13. Vecerek, B., Moll, I. and Blasi, U. (2007) Control of Fur synthesis by the non-coding RNA RyhB and iron-responsive decoding. *EMBO J*, **26**, 965-975.

14. Hou, Y.M., Matsubara, R., Takase, R., Masuda, I. and Sulkowska, J.I. (2017) TrmD: A Methyl Transferase for tRNA Methylation With m(1)G37. *Enzymes*, **41**, 89-115.

15. Chionh, Y.H., McBee, M., Babu, I.R., Hia, F., Lin, W., Zhao, W., Cao, J., Dziergowska, A., Malkiewicz, A., Begley, T.J. *et al.* (2016) tRNA-mediated codon-biased translation in mycobacterial hypoxic persistence. *Nature communications*, **7**, 13302.

16. Fleming, B.A., Blango, M.G., Rousek, A.A., Kincannon, W.M., Tran, A., Lewis, A.J., Russell, C.W., Zhou, Q., Baird, L.M., Barber, A.E. *et al.* (2022) A tRNA modifying enzyme as a tunable regulatory nexus for bacterial stress responses and virulence. *Nucleic Acids Res*.

17. Thompson, K.M. and Gottesman, S. (2014) The MiaA tRNA modification enzyme is necessary for robust RpoS expression in Escherichia coli. *J Bacteriol*, **196**, 754-761.
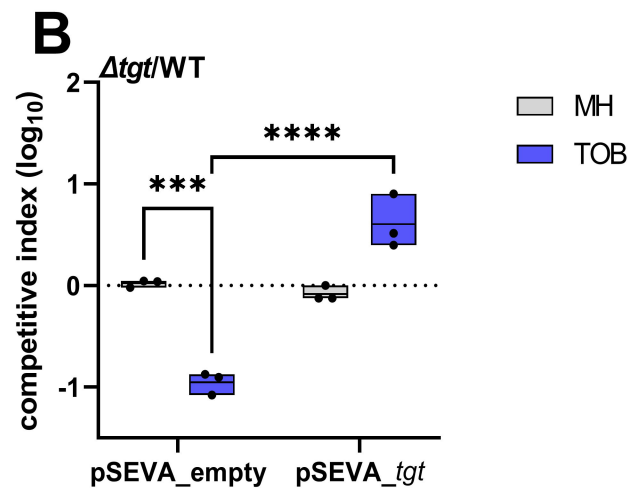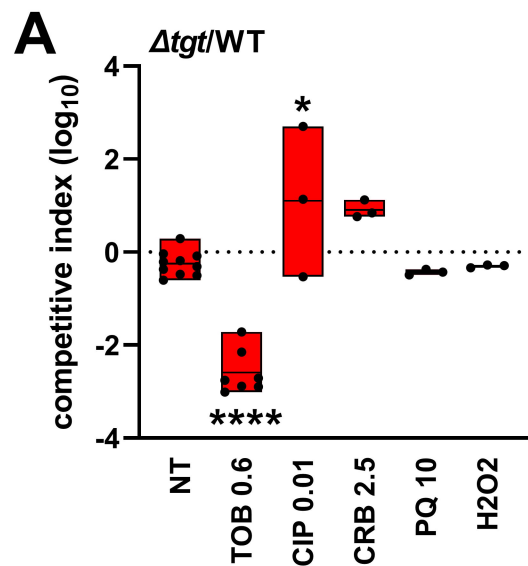
18.   Kimura, S., Dedon, P.C. and Waldor, M.K. (2020) Comparative tRNA sequencing and RNA mass spectrometry for surveying tRNA modifications. *Nat Chem Biol*, **16**, 964-972.

19.   Masuda, I., Matsubara, R., Christian, T., Rojas, E.R., Yadavalli, S.S., Zhang, L., Goulian, M., Foster, L.J., Huang, K.C. and Hou, Y.M. (2019) tRNA Methylation Is a Global Determinant of Bacterial Multi-drug Resistance. *Cell Syst*, **8**, 302-314 e308.

20.   Endres, L., Dedon, P.C. and Begley, T.J. (2015) Codon-biased translation can be regulated by wobble-base tRNA modification systems during cellular stress responses. *RNA Biol*, **12**, 603-614.

21.   Advani, V.M. and Ivanov, P. (2019) Translational Control under Stress: Reshaping the Translatome. *Bioessays*, **41**, e1900009.

22.   Ehrenhofer-Murray, A.E. (2017) Cross-Talk between Dnmt2-Dependent tRNA Methylation and Queuosine Modification. *Biomolecules*, **7**.

23.   Meier, F., Suter, B., Grosjean, H., Keith, G. and Kubli, E. (1985) Queuosine modification of the wobble base in tRNAHis influences 'in vivo' decoding properties. *EMBO J*, **4**, 823-827.

24.   Nagaraja, S., Cai, M.W., Sun, J., Varet, H., Sarid, L., Trebicz-Geffen, M., Shaulov, Y., Mazumdar, M., Legendre, R., Coppee, J.Y. *et al.* (2021) Queuine Is a Nutritional Regulator of Entamoeba histolytica Response to Oxidative Stress and a Virulence Attenuator. *mBio*, **12**.

25.   Manickam, N., Joshi, K., Bhatt, M.J. and Farabaugh, P.J. (2016) Effects of tRNA modification on translational accuracy depend on intrinsic codon-anticodon strength. *Nucleic Acids Res*, **44**, 1871-1881.

26.   Manickam, N., Nag, N., Abbasi, A., Patel, K. and Farabaugh, P.J. (2014) Studies of translational misreading in vivo show that the ribosome very efficiently discriminates against most potential errors. *RNA*, **20**, 9-15.

27.   Noguchi, S., Nishimura, Y., Hirota, Y. and Nishimura, S. (1982) Isolation and characterization of an Escherichia coli mutant lacking tRNA-guanine transglycosylase. Function and biosynthesis of queuosine in tRNA. *J Biol Chem*, **257**, 6544-6550.

28.   Pollo-Oliveira, L., Davis, N., Hossain, I., Ho, P., Yuan, Y., Garcia, P.S., Pereira, C., Byrne, S.R., Leng, J., Sze, M. *et al.* (2022) The absence of the Queuosine tRNA modification leads to pleiotropic phenotypes revealing perturbations of metal and oxidative stress homeostasis in Escherichia coli K12. *Metallomics*.

29.   Carvalho, A., Mazel, D. and Baharoglu, Z. (2021) Deficiency in cytosine DNA methylation leads to high chaperonin expression and tolerance to aminoglycosides in Vibrio cholerae. *Plos Genetics*, **17**.

30.   Lang, M.N., Krin, E., Korlowski, C., Sismeiro, O., Varet, H., Coppee, J.Y., Mazel, D. and Baharoglu, Z. (2021) Sleeping ribosomes: Bacterial signaling triggers RaiA mediated persistence to aminoglycosides. *Iscience*, **24**.

31.   Rivera, M., Hancock, R.E., Sawyer, J.G., Haug, A. and McGroarty, E.J. (1988) Enhanced binding of polycationic antibiotics to lipopolysaccharide from an aminoglycoside-supersusceptible, tolA mutant strain of Pseudomonas aeruginosa. *Antimicrob Agents Chemother*, **32**, 649-655.

32.   Sabeti Azad, M., Okuda, M., Cyrenne, M., Bourge, M., Heck, M.P., Yoshizawa, S. and Fourmy, D. (2020) Fluorescent aminoglycoside antibiotics and methods for accurately monitoring uptake by bacteria. *ACS Infect Dis*.

33.   Fabret, C. and Namy, O. (2021) Translational accuracy of a tethered ribosome. *Nucleic Acids Res*, **49**, 5308-5318.

34.   Kimura, S. and Waldor, M.K. (2019) The RNA degradosome promotes tRNA quality control through clearance of hypomodified tRNA. *Proc Natl Acad Sci U S A*, **116**, 1394-1403.

35.   Barraud, P. and Tisne, C. (2019) To be or not to be modified: Miscellaneous aspects influencing nucleotide modifications in tRNAs. *IUBMB Life*, **71**, 1126-1140.
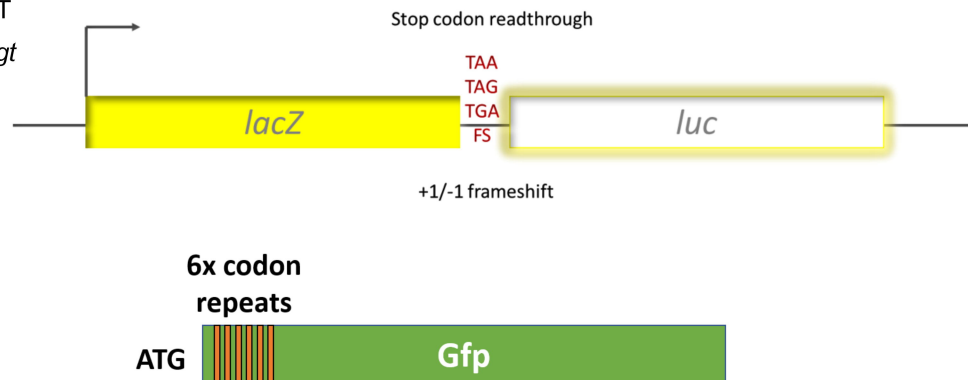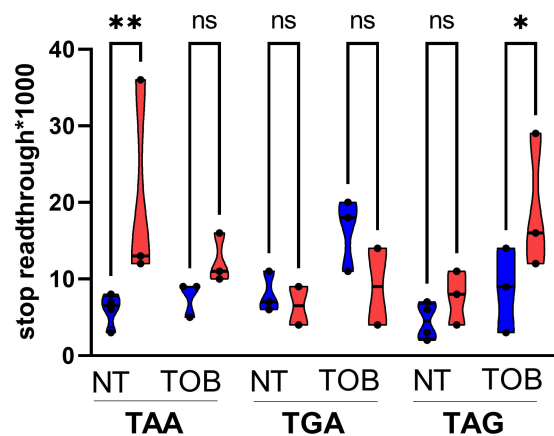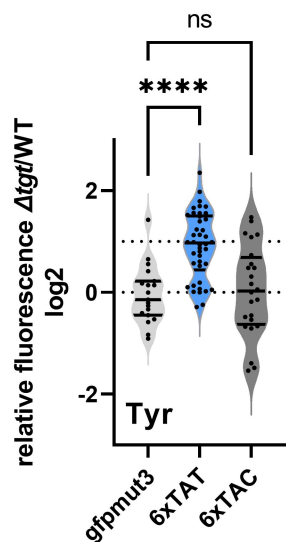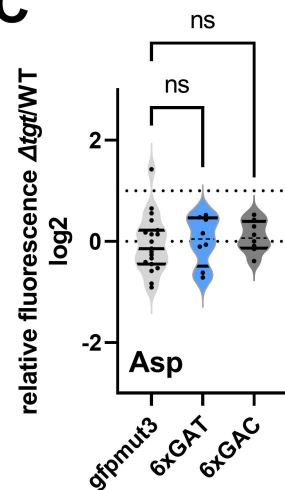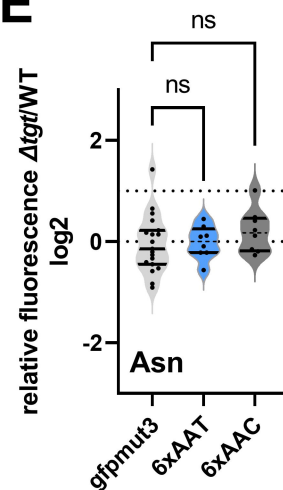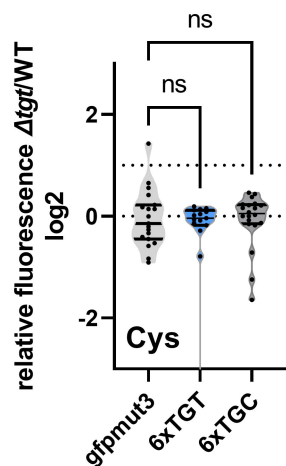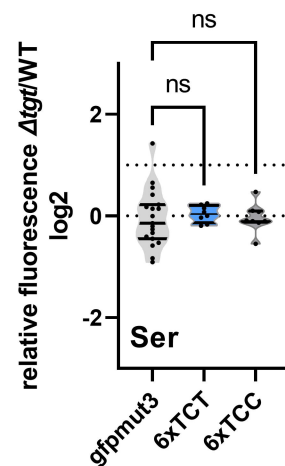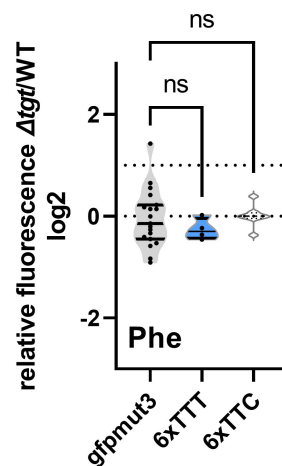
36.   Tuorto, F., Legrand, C., Cirzi, C., Federico, G., Liebers, R., Muller, M., Ehrenhofer-Murray, A.E., Dittmar, G., Grone, H.J. and Lyko, F. (2018) Queuosine-modified tRNAs confer nutritional control of protein translation. *EMBO J*, **37**.

37.   Addepalli, B. and Limbach, P.A. (2016) Pseudouridine in the Anticodon of Escherichia coli tRNATyr(QPsiA) Is Catalyzed by the Dual Specificity Enzyme RluF. *J Biol Chem*, **291**, 22327-22337.

38.   Doucet, N., De Wals, P.Y. and Pelletier, J.N. (2004) Site-saturation mutagenesis of Tyr-105 reveals its importance in substrate stabilization and discrimination in TEM-1 beta-lactamase. *J Biol Chem*, **279**, 46295-46303.

39.   Escobar, W.A., Miller, J. and Fink, A.L. (1994) Effects of site-specific mutagenesis of tyrosine 105 in a class A beta-lactamase. *Biochem J*, **303 (Pt 2)**, 555-558.

40.   Jacob, F., Joris, B., Lepage, S., Dusart, J. and Frere, J.M. (1990) Role of the conserved amino acids of the 'SDN' loop (Ser130, Asp131 and Asn132) in a class A beta-lactamase studied by site-directed mutagenesis. *Biochem J*, **271**, 399-406.

41.   Koo, M.S., Lee, J.H., Rah, S.Y., Yeo, W.S., Lee, J.W., Lee, K.L., Koh, Y.S., Kang, S.O. and Roe, J.H. (2003) A reducing system of the superoxide sensor SoxR in Escherichia coli. *EMBO J*, **22**, 2614-2622.

42.   Negro, V., Krin, E., Aguilar Pierle, S., Chaze, T., Giai Gianetto, Q., Kennedy, S.P., Matondo, M., Mazel, D. and Baharoglu, Z. (2019) RadD Contributes to R-Loop Avoidance in Sub-MIC Tobramycin. *MBio*, **10**.

43.   Bielecki, P., Muthukumarasamy, U., Eckweiler, D., Bielecka, A., Pohl, S., Schanz, A., Niemeyer, U., Oumeraci, T., von Neuhoff, N., Ghigo, J.M. *et al.* (2014) In vivo mRNA profiling of uropathogenic Escherichia coli from diverse phylogroups reveals common and group-specific gene expression profiles. *mBio*, **5**, e01075-01014.

44.   Krin, E., Pierle, S.A., Sismeiro, O., Jagla, B., Dillies, M.A., Varet, H., Irazoki, O., Campoy, S., Rouy, Z., Cruveiller, S. *et al.* (2018) Expansion of the SOS regulon of Vibrio cholerae through extensive transcriptome analysis and experimental validation. *BMC Genomics*, **19**, 373.

45.   Manneh-Roussel, J., Haycocks, J.R.J., Magan, A., Perez-Soto, N., Voelz, K., Camilli, A., Krachler, A.M. and Grainger, D.C. (2018) cAMP Receptor Protein Controls Vibrio cholerae Gene Expression in Response to Host Colonization. *MBio*, **9**.

46.   Carvalho, A., Krin, E., Korlowski, C., Mazel, D. and Baharoglu, Z. (2021) Interplay between Sublethal Aminoglycosides and Quorum Sensing: Consequences on Survival in V. cholerae. *Cells*, **10**.

47.   Kolmsee, T., Delic, D., Agyenim, T., Calles, C. and Wagner, R. (2011) Differential stringent control of Escherichia coli rRNA promoters: effects of ppGpp, DksA and the initiating nucleotides. *Microbiology (Reading)*, **157**, 2871-2879.

48.   Baharoglu, Z., Krin, E. and Mazel, D. (2013) RpoS Plays a Central Role in the SOS Induction by Sub-Lethal Aminoglycoside Concentrations in Vibrio cholerae. *Plos Genetics*, **9**.

49.   Huber, S.M., Begley, U., Sarkar, A., Gasperi, W., Davis, E.T., Surampudi, V., Lee, M., Melendez, J.A., Dedon, P.C. and Begley, T.J. (2022) Arsenite toxicity is regulated by queuine availability and oxidation-induced reprogramming of the human tRNA epitranscriptome. *Proc Natl Acad Sci U S A*, **119**, e2123529119.

50.   Gutierrez, A., Laureti, L., Crussard, S., Abida, H., Rodriguez-Rojas, A., Blazquez, J., Baharoglu, Z., Mazel, D., Darfeuille, F., Vogel, J. *et al.* (2013) beta-lactam antibiotics promote bacterial mutagenesis via an RpoS-mediated reduction in replication fidelity. *Nature communications*, **4**, 1610.

51.   Kudla, G., Murray, A.W., Tollervey, D. and Plotkin, J.B. (2009) Coding-sequence determinants of gene expression in Escherichia coli. *Science*, **324**, 255-258.
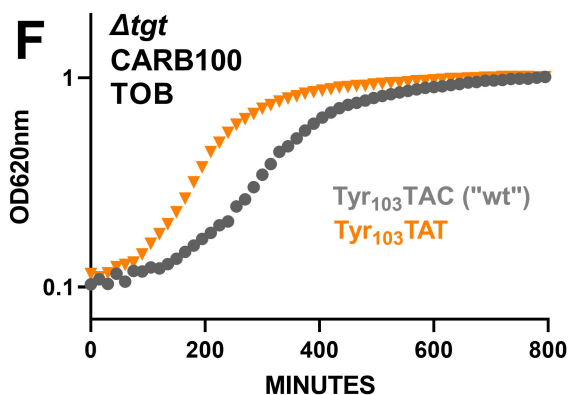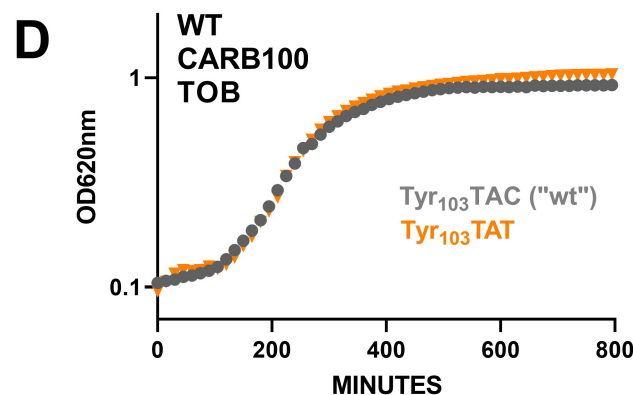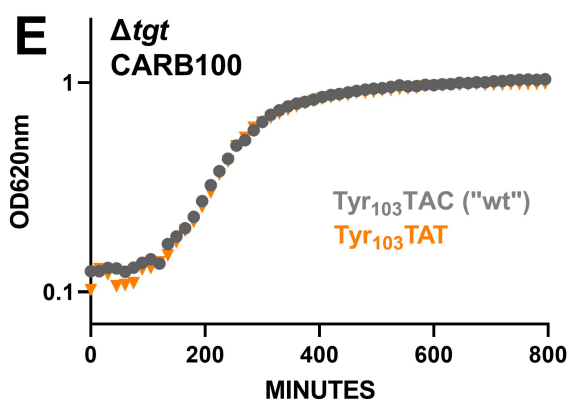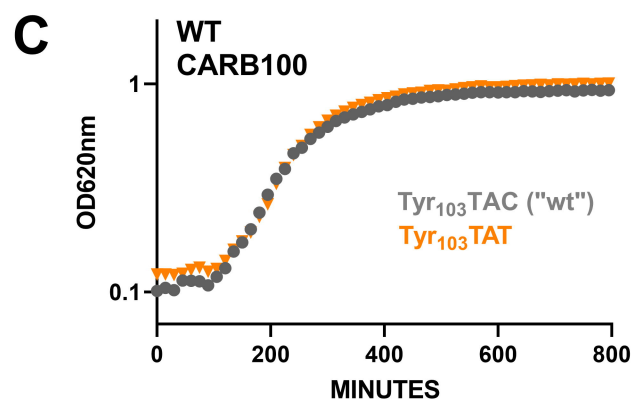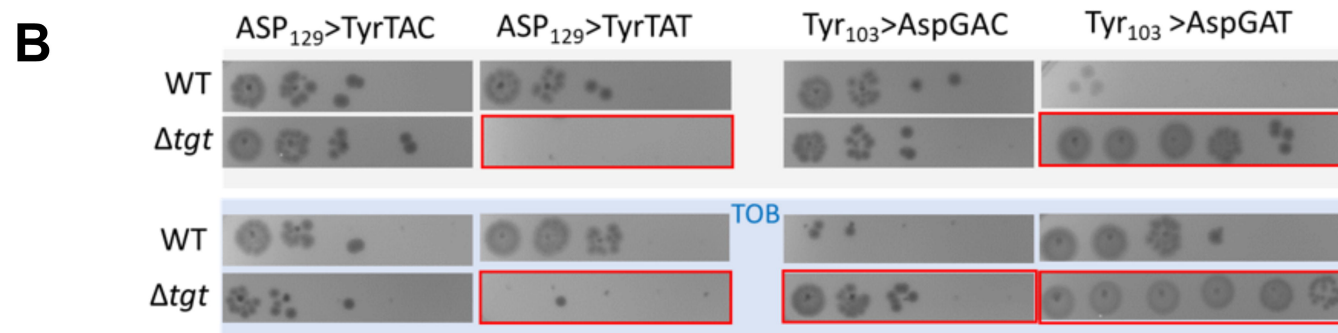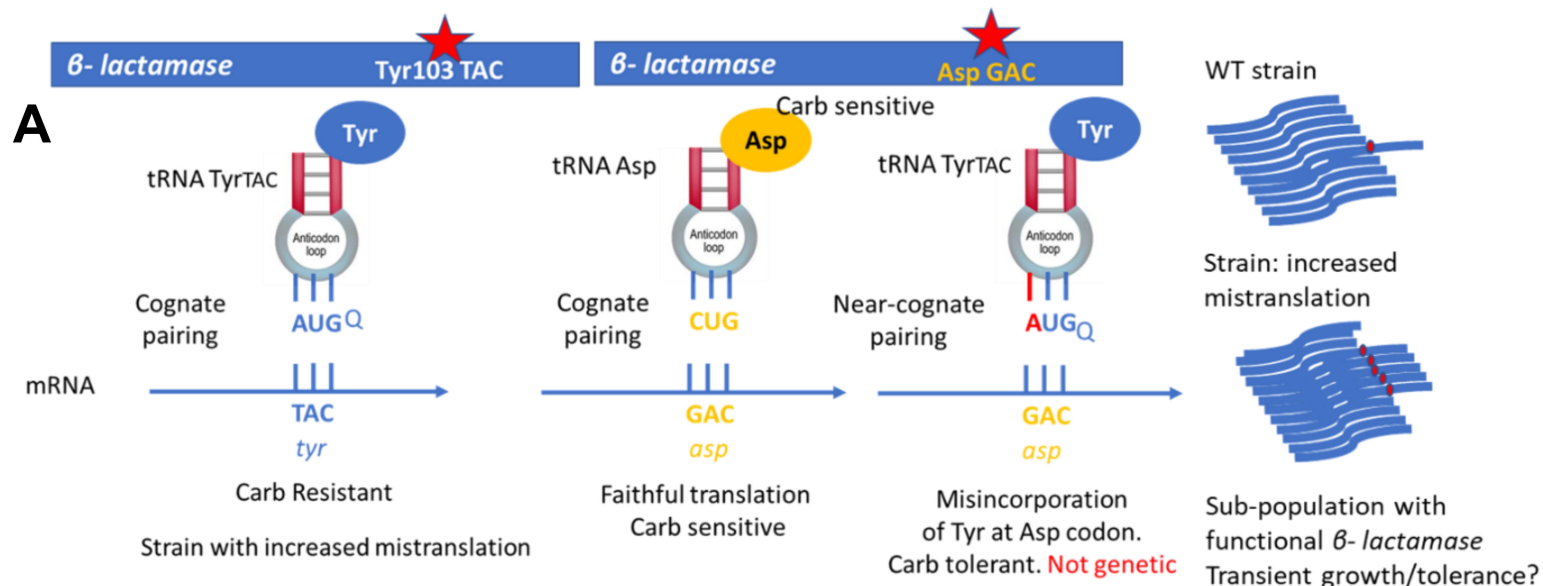
52.   Baharoglu, Z. and Mazel, D. (2011) Vibrio cholerae Triggers SOS and Mutagenesis in Response to a Wide Range of Antibiotics: a Route towards Multiresistance. *Antimicrobial Agents and Chemotherapy*, **55**, 2438-2441.

53.   Ezraty, B. and Barras, F. (2016) The 'liaisons dangereuses' between iron and antibiotics. *FEMS Microbiol Rev*, **40**, 418-435.

54.   Roche, B., Aussel, L., Ezraty, B., Mandin, P., Py, B. and Barras, F. (2013) Iron/sulfur proteins biogenesis in prokaryotes: formation, regulation and diversity. *Biochim Biophys Acta*, **1827**, 455-469.

55.   Chan, C.T., Dyavaiah, M., DeMott, M.S., Taghizadeh, K., Dedon, P.C. and Begley, T.J. (2010) A quantitative systems approach reveals dynamic control of tRNA modifications during cellular stress. *PLoS Genet*, **6**, e1001247.

56.   Torrent, M., Chalancon, G., de Groot, N.S., Wuster, A. and Madan Babu, M. (2018) Cells alter their tRNA abundance to selectively regulate protein synthesis during stress conditions. *Sci Signal*, **11**.

57.   Chan, C.T., Pang, Y.L., Deng, W., Babu, I.R., Dyavaiah, M., Begley, T.J. and Dedon, P.C. (2012) Reprogramming of tRNA modifications controls the oxidative stress response by codon-biased translation of proteins. *Nature communications*, **3**, 937.

58.   Keith, G., Rogg, H., Dirheimer, G., Menichi, B. and Heyham, T. (1976) Post-transcriptional modification of tyrosine tRNA as a function of growth in Bacillus subtilis. *FEBS Lett*, **61**, 120-123.

59.   Moukadiri, I., Garzon, M.J., Bjork, G.R. and Armengod, M.E. (2014) The output of the tRNA modification pathways controlled by the Escherichia coli MnmEG and MnmC enzymes depends on the growth conditions and the tRNA species. *Nucleic Acids Res*, **42**, 2602-2623.

60.   Frey, B., McCloskey, J., Kersten, W. and Kersten, H. (1988) New function of vitamin B12: cobamide-dependent reduction of epoxyqueuosine to queuosine in tRNAs of Escherichia coli and Salmonella typhimurium. *J Bacteriol*, **170**, 2078-2082.

61.   Persson, B.C. (1993) Modification of tRNA as a regulatory device. *Mol Microbiol*, **8**, 1011-1016.

62.   Galvanin, A., Vogt, L.M., Grober, A., Freund, I., Ayadi, L., Bourguignon-Igel, V., Bessler, L., Jacob, D., Eigenbrod, T., Marchand, V. *et al.* (2020) Bacterial tRNA 2'-O-methylation is dynamically regulated under stress conditions and modulates innate immune response. *Nucleic Acids Res*, **48**, 12833-12844.

63.   Dixit, S., Kessler, A.C., Henderson, J., Pan, X., Zhao, R., D'Almeida, G.S., Kulkarni, S., Rubio, M.A.T., Hegedusova, E., Ross, R.L. *et al.* (2021) Dynamic queuosine changes in tRNA couple nutrient levels to codon choice in Trypanosoma brucei. *Nucleic Acids Res*, **49**, 12986-12999.

64.   Whipp, M.J. and Pittard, A.J. (1977) Regulation of aromatic amino acid transport systems in Escherichia coli K-12. *J Bacteriol*, **132**, 453-461.

65.   Frumkin, I., Lajoie, M.J., Gregg, C.J., Hornung, G., Church, G.M. and Pilpel, Y. (2018) Codon usage of highly expressed genes affects proteome-wide translation efficiency. *Proc Natl Acad Sci U S A*, **115**, E4940-E4949.

66.   Riepe, C., Zelin, E., Frankino, P.A., Meacham, Z.A., Fernandez, S.G., Ingolia, N.T. and Corn, J.E. (2021) Double stranded DNA breaks and genome editing trigger loss of ribosomal protein RPS27A. *FEBS J*.

67.   Zhao, F., Zhou, Z., Dang, Y., Na, H., Adam, C., Lipzen, A., Ng, V., Grigoriev, I.V. and Liu, Y. (2021) Genome-wide role of codon usage on transcription and identification of potential regulators. *Proc Natl Acad Sci U S A*, **118**.

68.   Oprea, M., Njamkepo, E., Cristea, D., Zhukova, A., Clark, C.G., Kravetz, A.N., Monakhova, E., Ciontea, A.S., Cojocaru, R., Rauzier, J. *et al.* (2020) The seventh pandemic of cholera in Europe revisited by microbial genomics. *Nature communications*, **11**, 5347.

69.   Silva-Rocha, R., Martinez-Garcia, E., Calles, B., Chavarria, M., Arce-Rodriguez, A., de Las Heras, A., Paez-Espino, A.D., Durante-Rodriguez, G., Kim, J., Nikel, P.I. *et al.* (2013) The Standard
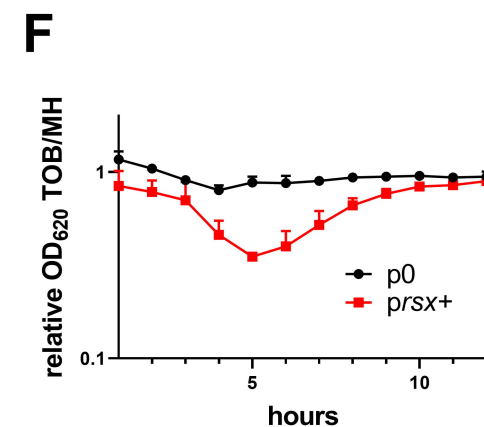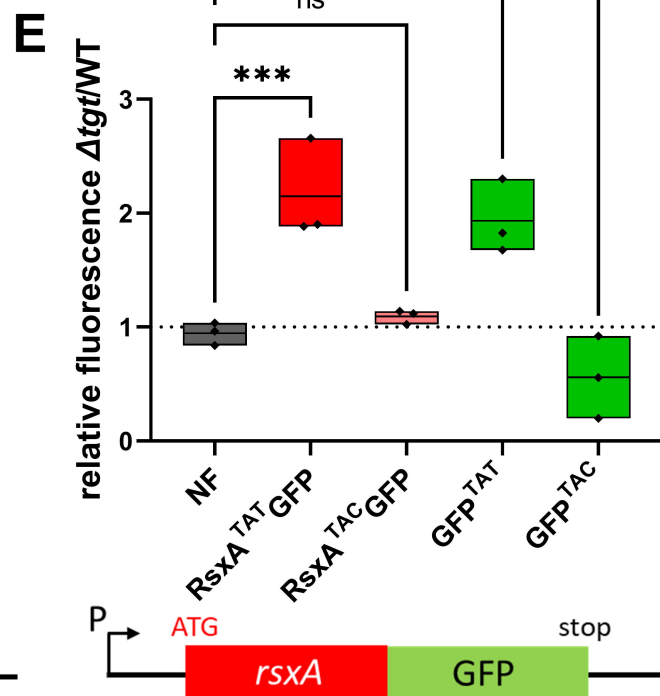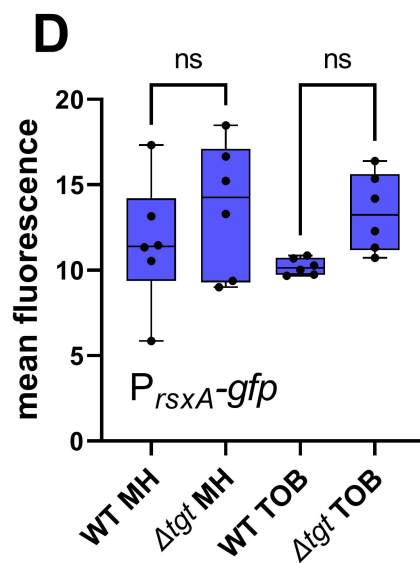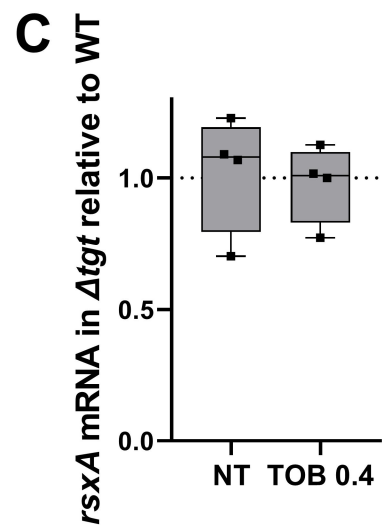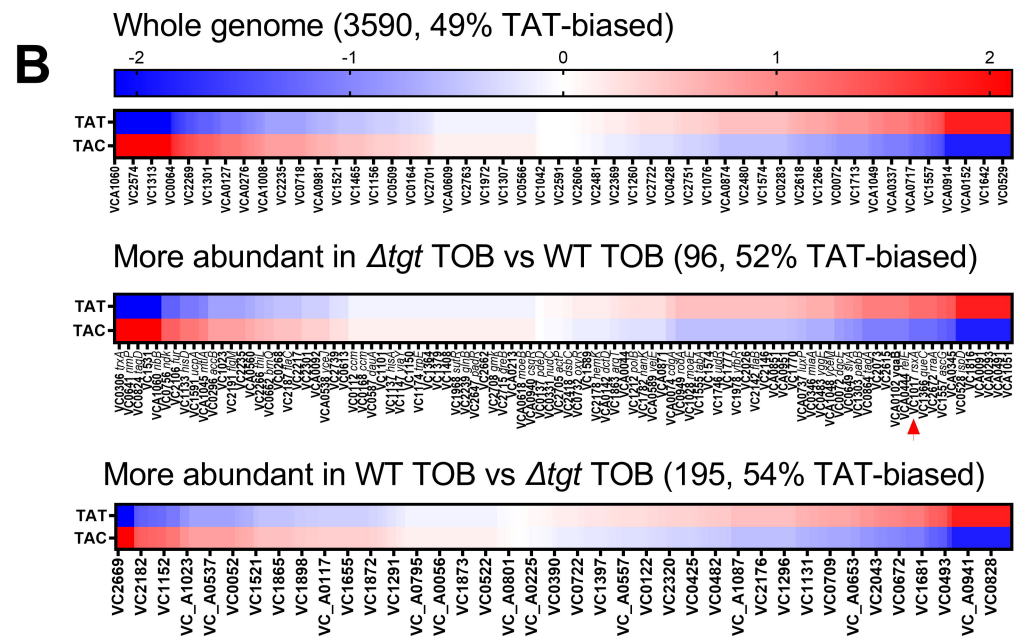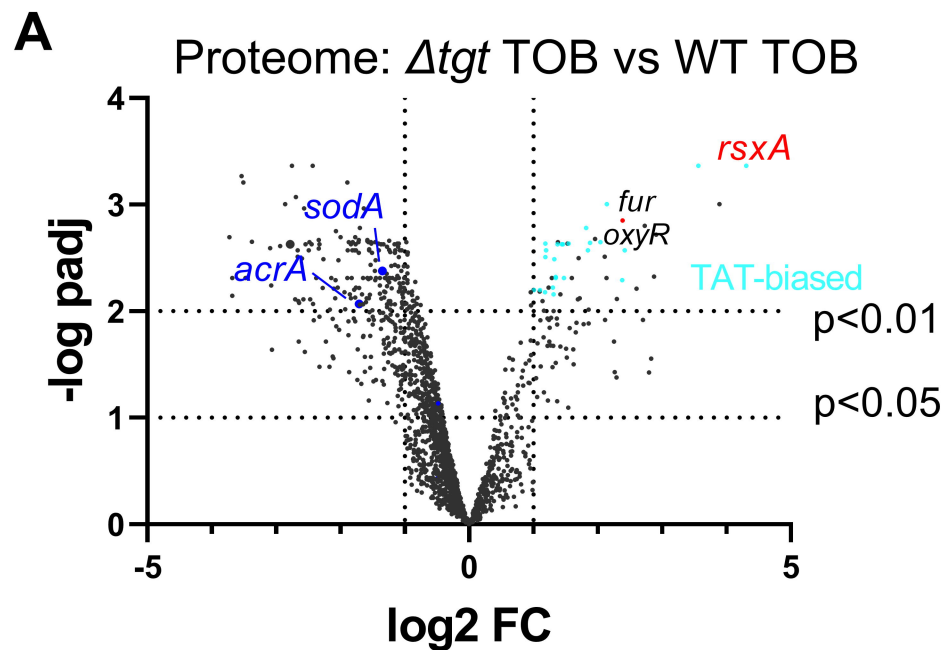
European Vector Architecture (SEVA): a coherent platform for the analysis and deployment of complex prokaryotic phenotypes. *Nucleic Acids Res*, **41**, D666-675.

70. Kessler, B., Timmis, K.N. and de Lorenzo, V. (1994) The organization of the Pm promoter of the TOL plasmid reflects the structure of its cognate activator protein XylS. *Mol Gen Genet*, **244**, 596-605.

71. Okuda, M. (2015), Université Paris Sud - Paris XI.

72. Baharoglu, Z., Bikard, D. and Mazel, D. (2010) Conjugative DNA transfer induces the bacterial SOS response and promotes antibiotic resistance development through integron activation. *PLoS Genet*, **6**, e1001165.

73. El Mortaji, L., Tejada-Arranz, A., Rifflet, A., Boneca, I.G., Pehau-Arnaudet, G., Radicella, J.P., Marsin, S. and De Reuse, H. (2020) A peptide of a type I toxin-antitoxin system induces Helicobacter pylori morphological transformation from spiral shape to coccoids. *Proc Natl Acad Sci U S A*, **117**, 31398-31409.

74. Lo Scrudato, M. and Blokesch, M. (2012) The regulatory network of natural competence and transformation of Vibrio cholerae. *PLoS Genet*, **8**, e1002778.

75. Cormack, B.P., Valdivia, R.H. and Falkow, S. (1996) FACS-optimized mutants of the green fluorescent protein (GFP). *Gene*, **173**, 33-38.

76. Elowitz, M.B. and Leibler, S. (2000) A synthetic oscillatory network of transcriptional regulators. *Nature*, **403**, 335-338.

77. Erde, J., Loo, R.R. and Loo, J.A. (2014) Enhanced FASP (eFASP) to increase proteome coverage and sample recovery for quantitative proteomic experiments. *J Proteome Res*, **13**, 1885-1895.

78. Cox, J., Neuhauser, N., Michalski, A., Scheltema, R.A., Olsen, J.V. and Mann, M. (2011) Andromeda: a peptide search engine integrated into the MaxQuant environment. *J Proteome Res*, **10**, 1794-1805.

79. Tyanova, S., Temu, T. and Cox, J. (2016) The MaxQuant computational platform for mass spectrometry-based shotgun proteomics. *Nat Protoc*, **11**, 2301-2319.

80. Wieczorek, S., Combes, F., Lazar, C., Giai Gianetto, Q., Gatto, L., Dorffer, A., Hesse, A.M., Coute, Y., Ferro, M., Bruley, C. *et al.* (2017) DAPAR & ProStaR: software to perform statistical analyses in quantitative discovery proteomics. *Bioinformatics*, **33**, 135-136.

81. Ritchie, M.E., Phipson, B., Wu, D., Hu, Y., Law, C.W., Shi, W. and Smyth, G.K. (2015) limma powers differential expression analyses for RNA-sequencing and microarray studies. *Nucleic Acids Res*, **43**, e47.

82. Giai Gianetto, Q., Combes, F., Ramus, C., Bruley, C., Coute, Y. and Burger, T. (2016) Calibration plot for proteomics: A graphical tool to visually check the assumptions underlying FDR control in quantitative experiments. *Proteomics*, **16**, 29-32.

83. Pounds, S. and Cheng, C. (2006) Robust estimation of the false discovery rate. *Bioinformatics*, **22**, 1979-1987.

84. Andersen, J.B., Sternberg, C., Poulsen, L.K., Bjorn, S.P., Givskov, M. and Molin, S. (1998) New unstable variants of green fluorescent protein for studies of transient gene expression in bacteria. *Appl Environ Microbiol*, **64**, 2240-2246.

85. Galvanin, A., Ayadi, L., Helm, M., Motorin, Y. and Marchand, V. (2019) Mapping and Quantification of tRNA 2'-O-Methylation by RiboMethSeq. *Methods Mol Biol*, **1870**, 273-295.

86. Li, H. (2018) Minimap2: pairwise alignment for nucleotide sequences. *Bioinformatics*, **34**, 3094-3100.

87. McKinney, W. (2010) Data Structures for Statistical Computing in Python. *Stéfan van der Walt, Jarrod Millman, editors.* , **Proceedings of the 9th Python in Science Conference**, 56--61.
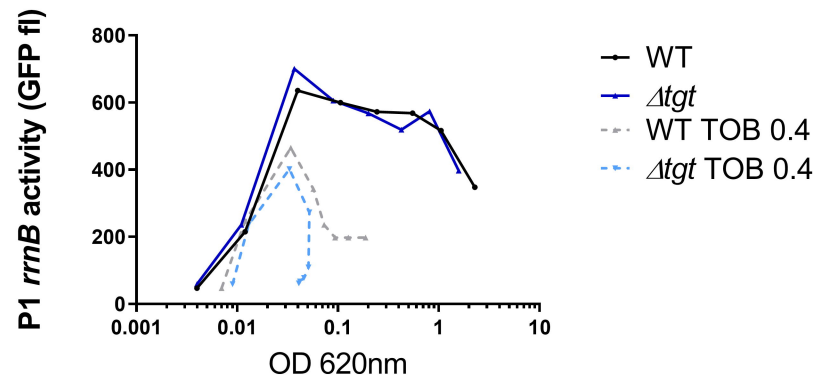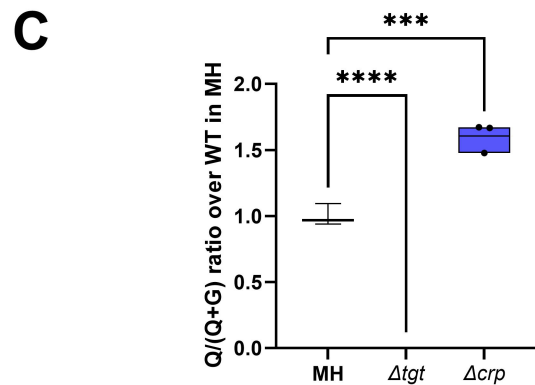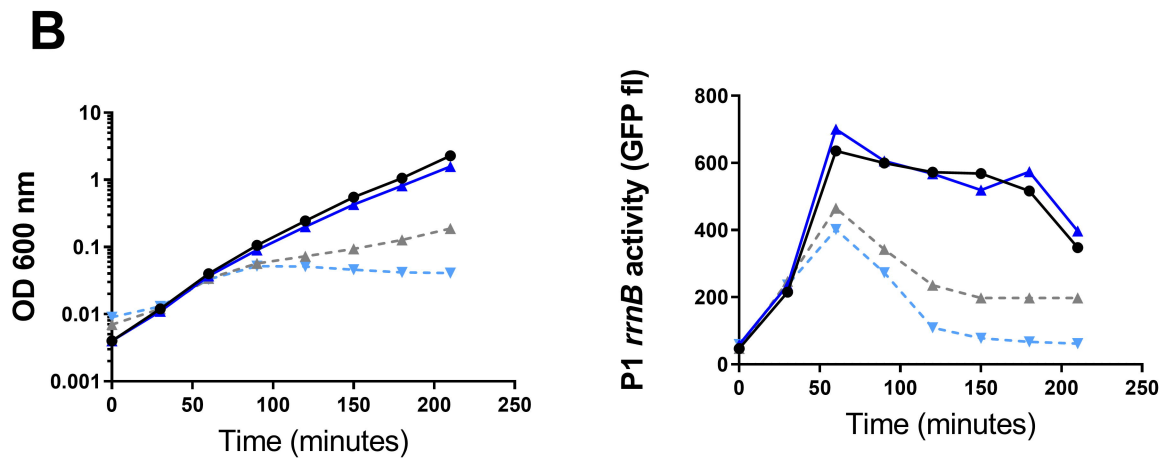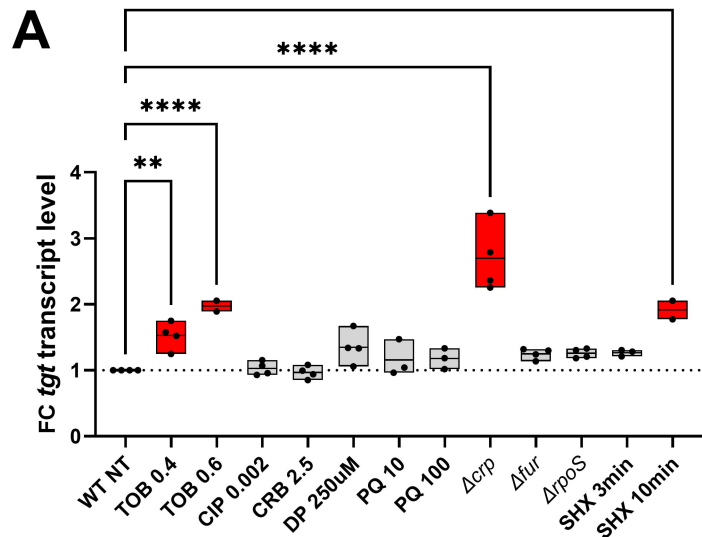
88.   Reback J, M.W., jbrockmendel, den Bossche JV, Augspurger T, Cloud P, et al. (2021) pandas-dev/pandas: Pandas 1.2.4.

89.   Namy, O., Rousset, J.P., Napthine, S. and Brierley, I. (2004) Reprogrammed genetic decoding in cellular gene expression. *Mol Cell*, **13**, 157-168.

90.   Virtanen, P., Gommers, R., Oliphant, T.E., Haberland, M., Reddy, T., Cournapeau, D., Burovski, E., Peterson, P., Weckesser, W., Bright, J. *et al.* (2020) SciPy 1.0: fundamental algorithms for scientific computing in Python. *Nat Methods*, **17**, 261-272.

91.   JD., H. (2007) Matplotlib: A 2D Graphics Environment. . *Computing in Science & Engineering*, **9**, 90--95.

92.   ML, W. (2021) Seaborn: Statistical Data Visualization. *Journal of Open Source Software*, **6**, :3021.

93.   Kluyver T, R.-K.B., Pérez F, Granger B, Bussonnier M, Frederic J, et al. (2016) Jupyter Notebooks -- a publishing format for reproducible computational workflows., **Loizides Fernando, Scmidt Birgit, editors**, 87--90.

94.   Molder, F., Jablonski, K.P., Letcher, B., Hall, M.B., Tomkins-Tinch, C.H., Sochat, V., Forster, J., Lee, S., Twardziok, S.O., Kanitz, A. *et al.* (2021) Sustainable data analysis with Snakemake. *F1000Res*, **10**, 33.

95.   Zhu, X.D. and Sadowski, P.D. (1995) Cleavage-dependent ligation by the FLP recombinase. Characterization of a mutant FLP protein with an alteration in a catalytic amino acid. *J Biol Chem*, **270**, 23044-23054.

A

β-lactamase Tyr103 TAC ⭐

tRNA Tyr^TAC — Tyr

Cognate pairing

AUG Q

mRNA

TAC
tyr

Carb Resistant

Strain with increased mistranslation

β-lactamase Asp GAC ⭐

Carb sensitive

tRNA Asp — Asp

Cognate pairing

CUG

GAC
asp

Faithful translation
Carb sensitive

tRNA Tyr^TAC — Tyr

Near-cognate pairing

AUG Q

GAC
asp

Misincorporation of Tyr at Asp codon. Carb tolerant. Not genetic

WT strain

Strain: increased mistranslation

Sub-population with functional β-lactamase
Transient growth/tolerance?

B

	ASP₁₂₉>TyrTAC	ASP₁₂₉>TyrTAT	Tyr₁₀₃>AspGAC	Tyr₁₀₃>AspGAT

WT / Δtgt (rows) — TOB

C WT CARB100
OD620nm vs MINUTES
Tyr₁₀₃TAC ("wt")
Tyr₁₀₃TAT

E Δtgt CARB100
OD620nm vs MINUTES
Tyr₁₀₃TAC ("wt")
Tyr₁₀₃TAT

D WT CARB100 TOB
OD620nm vs MINUTES
Tyr₁₀₃TAC ("wt")
Tyr₁₀₃TAT

F Δtgt CARB100 TOB
OD620nm vs MINUTES
Tyr₁₀₃TAC ("wt")
Tyr₁₀₃TAT

A Proteome: *Δtgt* TOB vs WT TOB

B
Whole genome (3590, 49% TAT-biased)

More abundant in *Δtgt* TOB vs WT TOB (96, 52% TAT-biased)

More abundant in WT TOB vs *Δtgt* TOB (195, 54% TAT-biased)

C *rsxA* mRNA in *Δtgt* relative to WT

D mean fluorescence — P*rsxA*-gfp

E relative fluorescence *Δtgt*/WT

F relative OD$_{620}$ TOB/MH

A *V. cholerae*

nfo
rnhA
dinG
ruvC
mutTlike
polA
helIV
rep
ruvA
dinB
radD
mutS
→ recR
apaG
ligA
dinG
rnhB
recD
recC
recB
uvrC
recF-like
→ recO
recQ
mutM
ung
alkB
polB
radA
priA
tag
→ recA
pol epsilon
ruvY
mutY
recG
mutT
nth
recN
sbcD
ada
uvrD
mutL
recF
ybjD
mfd
dnaQ
→ lexA

TAC   TAT

49 genes, 71% TAT-biased

B

UV 60J

Survival (relative to WT)

WT   Δtgt

***

C *E. coli*

radA
mutT
→ lexA
ybjD
ligA
rnhB
ung
uvrC
ruvA
alkB
ruvB
recD
rep
nfo
dnaQ
recC
mutM
recQ
dinB
recB
nth
mfd
radD
dinG
polA
dinG
→ recO
sbcD
mutS
polB
→ recR
tag
recN
priA
mutY
mutL
recF
recG
rnhA
ruvC
ada
helD
uvrD
apaG
→ recA

TAC   TAT

45 genes, 51% TAT-biased

D

UV 60J

Survival (relative to WT)

WT   Δtgt

ns